Chemical Exchange in Nuclear Magnetic Resonance

Thesis by

Leonard J. Mueller

In Partial Fulfillment of the Requirements for the Degree of
Doctor of Philosophy

California Institute of Technology
Pasadena, California
1997

(Submitted 10 July 1996)

Acknowledgments

There are many people who have contributed to this thesis, directly and indirectly, over the years I have spent at Caltech. First and foremost, it is with great pleasure that I acknowledge the support and encouragement of my advisor and collaborator, Professor Daniel Weitekamp. Dan's knowledge, enthusiasm and love for science have challenged and inspired me throughout this work and my entire graduate education. I would also like to acknowledge K.D. Kurur and Dan Jones for their contributions to this project. Their critical examination of chemical exchange in nuclear magnetic resonance pointed out experimental and theoretical deficiencies in the traditional theory and motivated this work.

This thesis would never have been completed without the assistance of the entire Weitekamp group. Paul Carson, Jim Kempf, Garett Leskowitz, Lou Madsen, John Marohn and Mike Miller painstakingly proofread and offered constructive criticism on this work. In addition to the current group members, I have benefited through my interactions with many talented individuals in the Weitekamp group over the years. In particular, Pedro Pizarro, Jack Hwang, Steve Buratto, Herman Cho, Dan Jones, K.D. Kurur, Dave Shykind and Margat Werner have all contributed to my graduate education. I feel fortunate to have worked with such a dynamic and intelligent group of colleagues.

Life in the subbasement of Noyes would have been neither as scientifically engaging and diverse, nor socially as enjoyable, were it not for interactions with the members of the Zewail group. These include coffee club members Jen Herek and Dean

Willberg, as well as Søren Pedersen and Chuck Williamson, all of whom deserve special mention for lively discussions, often over the first cup of Peet's in the morning.

I would also like to thank Dr. James Keeler and the University of Cambridge NMR community, especially Jeremy Titman, Steve Wimperis, Helen Geen, Adrian Davis, Lisa McIntyre and David Jones, for first introducing me to graduate research and magnetic resonance. James's abilities, both as a researcher and mentor, and the camaraderie of the lab led to an extremely positive experience that helped coalesce my plans for future graduate studies.

Robert Lee, Tom Dunn, Silvia Cavagnero and Curt Hastings also merit special recognition and gratitude for keeping the spectrometers running and helping the experimental side of this thesis go as smoothly as possible.

My life as a graduate student has been enhanced by the time I have spent as a Resident Associate at Caltech, especially through interactions with the Residence Life staff. In particular I would like to thank Kim West for her support throughout my graduate work and especially these last few months. Were it not for Kim's friendship and greatly appreciated help as a stand-in parent, these last few months would have been much more difficult. The friendship of the other Resident Associates has helped make life in Southern California a lively, exciting, and truly unique experience. I cannot imagine better friends or more supportive colleagues than Ken and Michelle Apperson, Dave and Elizabeth Kaufman, Pedro Pizarro and Monica Kohler, Jim Ostrowski and Liz Price, Doug Yule and Becky McGrew-Yule, Marcia France, Shubba Tole and Sandip Trivedi, Krista and Peo Pettersson, John and Gemma Iannelli, Ashok and Iona Tripathi, and David Wales. Other close friends, Dan and Jacque Pack, Ann and John McCabe, Erik and Laura Bierwagen, Jason Perry, Rob Johnson and Kelly Goodwin, and Tom Lloyd and Benta Kipp, were always there to lend support during difficult moments and to

create the times that I will look back upon so fondly. In addition, life at Caltech would not have been nearly so interesting had I not been a part of life in Dabney House. Through the fun and occasionally combustible times as a Resident Associate and House Member in Dabney, I have appreciated the warmth and friendship of the Darbs.

Much affection and appreciation go to my family, especially to my parents, Ralph and Myrna, for encouragement during both my undergraduate and graduate studies. Arriving when this thesis was less than a draft, my son Evan brought a new joy to my life and welcome distractions from my writing for his 3 A.M. feedings. The wonder and amazement that made his eyes sparkle gave my life perspective and offered much to this thesis. Finally, I would like to acknowledge my wife and best friend Shelley for her love and continual support throughout graduate school and the completion of this thesis. Life together in Southern California has taken us down many new, exciting and occasionally bittersweet paths. Traveling together has given meaning to the journey, and to Shelley, Kenny and Evan, I dedicate this thesis.

Abstract

Nuclear magnetic resonance spectra of molecules undergoing chemical exchange have traditionally been quantified using a theory that combines a quantum-mechanical treatment of the spin dynamics with a kinetic model for the molecular exchange. This implicit factorization of spin and spatial degrees of freedom is without theoretical justification and yet it has been widely relied upon in chemical studies. In this thesis, a quantum-statistical theory of chemical exchange is presented for the calculation of lineshapes in dynamic nuclear magnetic resonance. In this treatment, the rates describing the exchange of spin coherence are shown to be complex valued due to the incomplete cancellation of the imaginary components of the spectral density of purely spatial perturbations. These imaginary components give rise to the previously unrecognized phenomena of exchange shifts, new contributions to the line positions which depend on spatial rates even in the fast-exchange limit. These shifts can be orders of magnitude greater than the experimental resolution. The same purely spatial fluctuations responsible for chemical exchange determine these shifts through a Hilbert-transform relationship.

New measurements on the ^{13}C NMR of methylcyclohexane show that, indeed, the traditional theory fails to relate spectra obtained in the regimes of fast and slow exchange. If interpreted using the traditional theory, the fast-exchange line positions in methylcyclohexane lead to an extracted equilibrium constant with an error of up to 30% and differing between isotopomers by up to 30%. With plausible assumptions on the temperature dependence of the chemical shifts and free energy, an overall fit of the fast- and slow-exchange methylcyclohexane data is unsatisfactory, rigorously excluding the

traditional theory. The exchange-shift theory indicates why additional information is needed to fit the fast-exchange line positions and allows a fit consistent with the observed experimental data on methylcyclohexane using a single conformer free energy difference linear in temperature over the entire experimental range.

Table of Contents

List of Figures

Chapter 2:

Chapter 3:

Appendix B:

List of Tables

1. Introduction

The interpretation of the fine structure in nuclear magnetic resonance (NMR) spectra in terms of the immediate electronic environment surrounding a nuclear spin [1-5] has enabled the development of NMR as a significant analytical tool for chemistry and solid-state physics [6-10]. For chemists, two of the most important components of the fine structure are the chemical shift [1-3] and scalar or J coupling constant [4,5]. Although the *ab initio* calculation of these quantities is now possible [11-13], their empirical correlations with chemical environment have made structural assignments of organic and biological compounds routine.

To the chemist, however imperative the determination of structural properties may be, the ultimate goal is often the elucidation of chemical reactivity and dynamics. NMR is unique in its ability to determine the kinetic and thermodynamic parameters of dynamic systems without the need to perturb chemical equilibrium. For over forty years the interpretation of dynamic NMR experiments has been based on the assumption that the nuclear spins serve merely as isolated probes of the chemical dynamics, having no influence on the kinetics [4,14-38]. In these treatments of dynamic NMR, collectively referred to in this thesis as the traditional theory, there is an implicit factorization of spin and spatial variables, the validity of which has never been established.

In this thesis, both theoretical and experimental evidence are presented that the traditional theory of chemical exchange in NMR is incorrect. Indeed, the traditional theory leads to kinetic equations with rates that cannot be associated with transitions between eigenstates of the full Hamiltonian and do not satisfy detailed balance. An

alternative theory is provided and experimentally supported. Although in certain limits the predictions of the new and traditional theories converge, in most cases they do not. The implications of this work are far reaching, forcing the reinterpretation of many hundreds of dynamic NMR experiments that have been used to provide kinetic and thermodynamic properties for systems ranging from small molecules in solution to large biomolecular reactions. Furthermore, potentials used for molecular mechanics calculations based on thermodynamic and kinetic data from dynamic NMR of small molecules in solution must be appropriately reexamined, as must the conclusions drawn from them. Although the validity of the traditional theory was initally called into question by Jones, Kurur and Weitekamp [39-41], the theoretical interpretation of chemical exchange in NMR presented in this thesis is unrelated to the specific hypothesis proposed by them.

The traditional theory of dynamic NMR is first reviewed in Chapter 2, after which a fully quantum-mechanical theory for chemical exchange in NMR is presented. This quantum theory allows the direct calculation of coherence exchange and shows the generalization of classical exchange rates to be complex valued for coherence exchange due to the incomplete cancellation of imaginary components of the spectral density of purely spatial perturbations. The imaginary components of the resulting exchange superoperator, referred to as exchange shifts, manifest themselves as measurable spectroscopic shifts which if interpreted using the traditional theory would lead to an inaccurate extraction of the thermodynamic properties of the system.

The experimental verification of these shifts, measured as deviations from the traditional theory in the fast-exchange limit, is shown in Chapter 3 for the isomerization reaction of methylcyclohexane. Improved measurements on methylcyclohexane show that the traditional theory of chemical exchange is inconsistent with the experimental data. Although the exchange-shift model presented in Chapter 2 has additional

parameters that are not easily measured, it is shown that the predictions of this model are consistent with the data. If interpreted using the traditional theory, the fast-exchange line positions in methylcyclohexane would lead to an extracted equilibrium constant with an error of up to 30% and that varies by up to 30% between the different carbon sites.

1.1 References

[1] J.T. Arnold, S.S. Dharmatti and M.E. Packard "*Chemical Effects on Nuclear Induction Signals from Organic Compounds*" Journal of Chemical Physics **19**: 507 (1951).

[2] W.C. Dickinson "*Dependence of the F19 Nuclear Resonance Position on Chemical Compound*" Physical Review **77**: 736-737 (1950).

[3] W.G. Proctor and F.C. Yu "*The Dependence of a Nuclear Magnetic Resonance Frequency upon Chemical Compound*" Physical Review **77**: 717 (1950).

[4] E.L. Hahn and D.E. Maxwell "*Spin Echo Measurements of Nuclear Spin Coupling in Molecules*" Physical Review **88**(5): 1070-1084 (1952).

[5] H.S. Gutowsky, D.W. McCall and C.P. Slichter "*Coupling among Nuclear Magnetic Dipoles in Molecules*" Physical Review **84**: 589-590 (1951).

[6] R.R. Ernst, G. Bodenhausen and A. Wokaun Principles of Nuclear Magnetic Resonance in One and Two Dimensions Oxford, Oxford University Press (1991).

[7] J.D. Roberts Nuclear Magnetic Resonance New York, McGraw-Hill (1959).

[8] C.P. Slichter Principles of Magnetic Resonance Berlin, Springer-Verlag (1989).

[9] S. Opella "*Solid-State NMR Structural Studies of Proteins*" Annual Review of Physical Chemistry **45**: 659-683 (1994).

[10] A. Mcdermott, L. Thompson, C. Winkel, M. Farrar, S. Pelletier, J. Lugtenburg, J. Herzfeld and R. Griffin "*Mechanism of Proton Pumping in Bacteriorhodopsin by Solid-State NMR - The Protonation State of Tyrosine in the Light-Adapted and M-States*" Biochemistry **30**(34): 8366-8371 (1991).

[11] R. Ditchfield "*Self-Consistent Perturbation Theory of Diamagnetism. I. A Gauge-Invariant LCAO Method for NMR Chemical Shifts*" Molecular Physics **27**(4): 789-807 (1974).

[12] R. Ditchfield and P. Ellis "*Theory of C-13 Chemical Shifts*" in Topics in Carbon-13 NMR Spectroscopy New York, Wiley-Interscience 1-51 (1976).

[13] E. Oldfield "*Chemical-Shifts and 3-Dimensional Protein Structures*" Journal of Biomolecular NMR **5**(3): 217-225 (1995).

[14] N. Bloembergen, E.M. Purcell and R.V. Pound "*Relaxation Effects in Nuclear Magnetic Resonance Absorption*" Physical Review **73**(7): 679-712 (1948).

[15] H.S. Gutowsky, D.W. McCall and C.P. Slichter "*Nuclear Magnetic Resonance Multiplets in Liquids*" The Journal of Chemical Physics **21**(2): 279 (1953).

[16] H.M. McConnell "*Reaction Rates by Nuclear Magnetic Resonance*" Journal of Chemical Physics **28**(3): 430 (1957).

[17] J.A. Pople "*Nuclear Magnetic Resonance and Rotational Isomerism in Substituted Ethanes*" Molecular Physics **1**: 3-8 (1957).

[18] J.A. Pople, W.G. Schneider and H.J. Bernstein "*The Analysis of Nuclear Magnetic Resonance Spectra. II. Two Pairs of Two Equivalent Nuclei*" Canadian Journal of Chemistry **35**: 1060 (1957).

[19] J.N. Shoolery and B. Crawford, Jr. "*Hindered Rotation and Nonequivalent Nuclear Spin Couplings*" Journal of Molecular Spectroscopy **1**: 270-276 (1957).

[20] J. Kaplan "*Exchange Broadening in Nuclear Magnetic Resonance*" Journal of Chemical Physics **28**(2): 278 (1958).

[21] J.C. Schug, P.E. McMahon and H.S. Gutowsky "*Electron Couplings of Nuclear Spins. IV. Temperature Dependence in Substituted Ethanes*" Journal of Chemical Physics **33**(3): 843 (1960).

[22] R.J. Abraham and H.J. Bernstein "*A Proton Magnetic Resonance Investigation of Rotational Isomerism in 1,1,2,2-Tetrachloro-1-Fluoroethane*" Canadian Journal of Chemistry **39**: 39 (1961).

[23] S. Alexander "*Exchange of Interacting Nuclear Spins in Nuclear Magnetic Resonance. I. Intramolecular Exchange*" The Journal of Chemical Physics **37**(5): 967 (1962).

[24] H.S. Gutowsky, G.G. Belford and P.E. McMahon "*NMR Studies of Conformational Equilibria in Substituted Ethanes*" Journal of Chemical Physics **36**(12): 3353 (1962).

[25] C.S. Johnson "*On the Calculation of Nuclear Magnetic Resonance Spectra for Coupled Nuclear Spins in Intramolecular Reactions*" Journal of Chemical Physics **41**: 3277-3278 (1964).

[26] R.A. Newmark and C.H. Sederholm "*NMR Determinations of Barriers to Internal Rotation in Halogen-Substituted Ethanes*" The Journal of Chemical Physics **43**(2): 602 (1965).

[27] T.D. Alger, H.S. Gutowsky and R.L. Vold "*Internal Rotation in Liquid 1-Fluoro-1,1,2,2-tetrachloroethane*" The Journal of Chemical Physics **47**(9): 3130 (1967).

[28] G. Govil and H.J. Bernstein "*Application of the NMR Method to Rotational Isomerism. Limitations Revealed by Temperature-Dependent Studies on CHBr2-CFBr2*" The Journal of Chemical Physics **47**(8): 2818 (1967).

[29] R.M. Lynden-Bell "*The Calculation of Line Shapes by Density Matrix Methods*" Progress in NMR Spectroscopy **2**: 163 (1967).

[30] G. Binsch "*The Study of Intramolecular Rate Processes by Dynamic Nuclear Magnetic Resonance*" Topics in Stereochemistry **3**: 97 (1968).

[31] G. Binsch "*A Unified Theory of Exchange Effects of Nuclear Magnetic Resonance Line Shapes*" Journal of the American Chemical Society **91**(6): 1304-1309 (1969).

[32] F. Heatley and G. Allen "*An NMR Investigation of Rotational Isomerism in Some Halogenated Ethanes*" Molecular Physics **16**: 77-89 (1969).

[33] W.-C. Lin "*Dependence of Vicinal H-H Coupling Constants in Substituted Ethanes on the Potential Function Characteristics to Internal Rotation. Application to A2B2 PMR Spectrum of Nonsymmetrical 1,2-Disubstituted Ethanes.*" The Journal of Chemical Physics **52**(6): 2805 (1970).

[34] A.J. Vega and D. Fiat "*Relaxation Theory and the Stochastic Liouville Equation*" Journal of Magnetic Resonance **19**: 21 (1974).

[35] S. Szymanski, M. Witanowski and A. Gryff-Keller "*Problems in Theory and Analysis of Dynamic Nuclear Magnetic Resonance Spectra*" Annual Reports on NMR Spectroscopy **8**: 227 (1978).

[36] G. Binsch and H. Kessler "*The Kinetic and Mechanistic Evaluation of NMR Spectra*" Angewandte Chemie **19**(6): 411-494 (1980).

[37] K.G.R. Pachler and P.L. Wessels "*Rotational Isomerism. A Gas-Phase ^1H Nuclear Magnetic Resonance Study of 1-Bromo-2-Chloroethane*" Journal of Molecular Structure **68**: 145-159 (1980).

[38] J. Jeener "*Superoperators in Magnetic Resonance*" Advances in Magnetic Resonance **10**: 1-51 (1982).

[39] D.H. Jones, N.D. Kurur and D.P. Weitekamp "*Stochastic Averaging Revisited*" Bulletin of Magnetic Resonance **14**: 214-219 (1992).

[40] N.D. Kurur "*I. Quantum Mechanical Chemical Exchange II. NMR of Semiconductors*" Ph.D. Thesis, Department of Chemistry, California Institute of Technology (1992).

[41] D.H. Jones "*I. Quantum-Mechanical Chemical Exchange II. Stochastic Averaging in Magnetic Resonance*" Ph.D. Thesis, Department of Chemistry, California Institute of Technology (1993).

2. Chemical Exchange in Nuclear Magnetic Resonance

2.1 Introduction

Chemical exchange in nuclear magnetic resonance refers to any reversible process in which nuclear spins are transported between different chemical environments, so that on the time scale of the NMR experiment they experience a randomly fluctuating spin Hamiltonian. Rotational and conformational isomerization are two examples of intramolecular chemical exchange, while proton exchange with a solvent is an example of intermolecular exchange. The effects of chemical exchange on NMR spectral lines include line broadening, multi-line coalescence and exchange narrowing. These effects are highly state dependent and can provide information on the molecular potentials responsible for kinetic and equilibrium properties. Magnetic resonance is the preeminent tool for the study of chemical exchange, as it discriminates between inequivalent sites in isomers and allows for the extraction of kinetic properties without perturbing chemical equilibrium.

The traditional analysis of chemical exchange, reviewed in Section 2.2, combines a quantum mechanical treatment of the spin dynamics with a kinetic model for the molecular exchange. The implicit factorization of spin and spatial variables leads to kinetic equations with rates that cannot be associated with any transition between exact eigenstates of the full spin and spatial Hamiltonian. In this approximation, which will be referred to as the traditional rate approximation, the exchange rates are independent of spin parameters. The validity of the traditional rate approximation has never been

established. Theoretically, the traditional rate approximation leads to equations of motion that do not establish proper equilibrium, and experimentally, the traditional theory of chemical exchange has not been tested to the accuracy possible. Deviations from the traditional theory have often been attributed to unknown and unmeasured temperature-dependent spectral parameters. In Section 2.3, the theoretical basis for analyzing the effects of chemical exchange in NMR will be addressed. In this section, a weak-collision quantum-mechanical relaxation theory of chemical exchange is presented that allows for the direct calculation of coherence exchange. Approximations familiar in relaxation theory have been revised, so that they can be applied to chemical exchange. The generalization of the classical reaction rates are shown to be real valued for population exchange and complex valued for coherence exchange, leading to measurable deviations of spectroscopic shifts from the predictions of the traditional theory in the fast-exchange limit. If interpreted using the traditional theory, the observed fast-exchange line positions lead to substantial errors in the extracted thermodynamic properties; for the isomerization reaction of methylcyclohexane, errors of up to 30% in the equilibrium constant are obtained as shown in Chapter 3.

2.2 The Traditional Theory of Chemical Exchange

The traditional theory of chemical exchange combines a quantum-mechanical treatment of the spin system with a kinetic theory for the spatial dynamics [1-26]. As an example, consider the two-site exchange of a single, uncoupled nuclear spin illustrated in Figure 2.1. The potential energy surface represents the minimum energy pathway along the reaction coordinate for the exchange of two conformers, A and B, with a Helmholtz energy difference (relevant to constant volume conditions) ΔA. The nuclear spin experiences a conformationally dependent spin Hamiltonian that gives rise to chemical shifts $\omega_A(T)$ and $\omega_B(T)$ in conformers A and B, respectively. In condensed phases, the chemical shift in each conformer cannot be associated with any one rovibrational state,

but represents a thermal average over states, leading, in general, to temperature-dependent spectral parameters.

In the absence of exchange, the NMR spectrum of this system would consist of two lines with chemical shifts $\omega_A(T)$ and $\omega_B(T)$ and with a ratio of amplitudes (line areas) equal to the ratio of the conformer equilibrium populations. In this limit and neglecting relaxation, the equations of motion for the observed complex transverse magnetizations M_{A+} and M_{B+} of sites A and B, respectively, are

$$\frac{\partial}{\partial t}\begin{pmatrix} M_{B+} \\ M_{A+} \end{pmatrix} = \begin{pmatrix} -i\omega_B & 0 \\ 0 & -i\omega_A \end{pmatrix}\begin{pmatrix} M_{B+} \\ M_{A+} \end{pmatrix}. \tag{1}$$

The effect of chemical exchange is to transport conformer A to B at rate k_f and back again

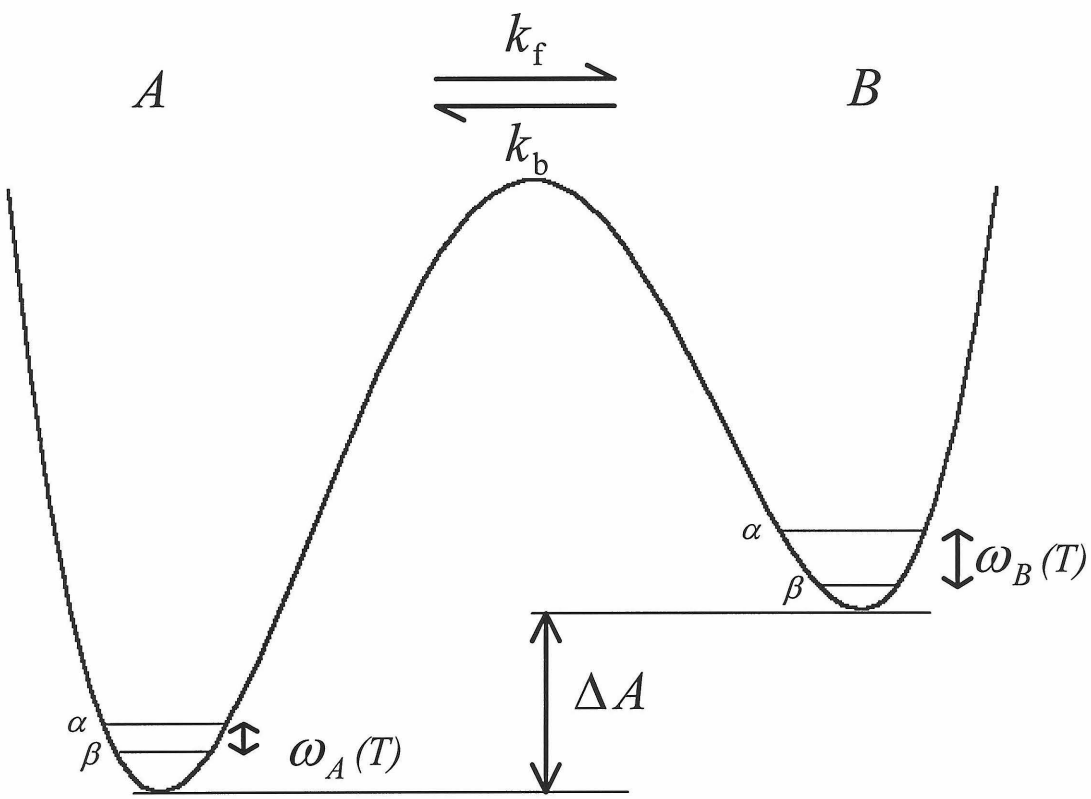

Figure 2.1. Two-site chemical exchange of a single nuclear spin with I=½.

at rate k_b. The normalized populations of the two conformers, p_A and p_B, therefore evolve according to the following kinetic equations,

$$\frac{\partial}{\partial t}\begin{pmatrix} p_B \\ p_A \end{pmatrix} = \begin{pmatrix} -k_b & k_f \\ k_b & -k_f \end{pmatrix}\begin{pmatrix} p_B \\ p_A \end{pmatrix}. \tag{2}$$

Making the traditional rate approximation, in which it is assumed that these kinetic equations also apply to magnetization exchange, the combined evolution and exchange equations of motion for the magnetizations are

$$\frac{\partial}{\partial t}\begin{pmatrix} M_{B+} \\ M_{A+} \end{pmatrix} = \begin{pmatrix} -k_b - i\omega_B & k_f \\ k_b & -k_f - i\omega_A \end{pmatrix}\begin{pmatrix} M_{B+} \\ M_{A+} \end{pmatrix}. \tag{3}$$

This system of coupled linear differential equations is solved using an eigenvalue method [27], giving observed magnetizations M_{i+} of the form

$$M_{i+}(t) = M_{i+}(0)\exp(\lambda_i t), \tag{4}$$

where the λ_i are the eigenvalues of the combined evolution and exchange matrix.

When the exchange rates are slow compared to the difference in the chemical shifts of states A and B, the distinct lines at ω_A and ω_B broaden, but their resonance frequencies remain the same. This broadening is a lifetime effect due to the decay at rates k_f and k_b from the respective states. By the time the molecule returns to its original chemical state, all memory of the phase of its magnetization has been lost. In this limit, the linewidths (full width at half maximum, FWHM) in Hz for the A and B resonances have contributions due to chemical exchange of

$$\begin{aligned} \Delta\nu_A &= \frac{k_f}{\pi}, \\ \Delta\nu_B &= \frac{k_b}{\pi}. \end{aligned} \tag{5}$$

In the limit of fast exchange, where the exchange rates are much faster than the difference between the chemical shifts, there is only one long-lived, exchange-narrowed

peak. The position and width of this peak can be determined by expanding the eigenvalues of the combined exchange and evolution matrix from (3) in powers of $(\omega_A - \omega_B)/2\pi$ and are given in Hz by

$$\begin{aligned} \nu_{\text{av}} &= \frac{k_{\text{f}}\nu_A + k_{\text{b}}\nu_B}{k_{\text{f}} + k_{\text{b}}} = p_A\nu_A + p_B\nu_B, \\ \Delta\nu_{\text{av}} &= \frac{k_{\text{f}}k_{\text{b}}(\nu_A - \nu_B)^2}{\pi(k_{\text{f}} + k_{\text{b}})^3}. \end{aligned} \tag{6}$$

In the fast-exchange limit, the average line position depends only on the normalized equilibrium populations, p_A and p_B, and the linewidth has a contribution $\Delta\nu_{\text{av}}$ due to chemical exchange.

In the intermediate exchange region, the NMR spectral lines continue to broaden relative to slow exchange and their frequencies shift toward each other as the exchange rates increase. Eventually the lines coalesce and, as the rates continue to increase toward the fast exchange limit, this single line sharpens. The linewidths and positions are sensitive functions of exchange rates in this region, allowing for the extraction of kinetic parameters. The simulated NMR spectra shown in Figure 2.2 illustrate the progression from slow to fast exchange as the dimensionless rate $\alpha = k_{\text{f}} / |\omega_A - \omega_B|$ increases.

The above analysis can be generalized to include additional conformers and weak scalar coupling. In the fast-exchange limit, such an analysis predicts average spectral parameters $\langle X \rangle$ that are the probability-weighted sums of separate conformer spectral parameters X_i,

$$\langle X \rangle = \sum_{i=A,B,C\ldots} p_i X_i , \tag{7}$$

where p_i is the equilibrium probability of being in conformer i and X_i is a spin Hamiltonian parameter such as a chemical shift or J coupling constant. Equation (7) has the appearance of a weighted average in equilibrium statistical mechanics. This resemblance is misleading, however, as (7) is not derivable from equilibrium statistical mechanics, but was derived from a kinetic theory that assumes the exchange rate of the coherences was the same as that for the populations and ignores the difference in exchange rate for different spin states. With a nonzero spin Hamiltonian, however, the exchange rate of a population must depend on spin state. This point can be inferred from Figure 2.1, in which the spin energies have been exaggerated. Ignoring these small rate differences does not lead to equilibrium for the combined spatial and spin populations. The quantum-mechanical treatment of chemical exchange presented below avoids the

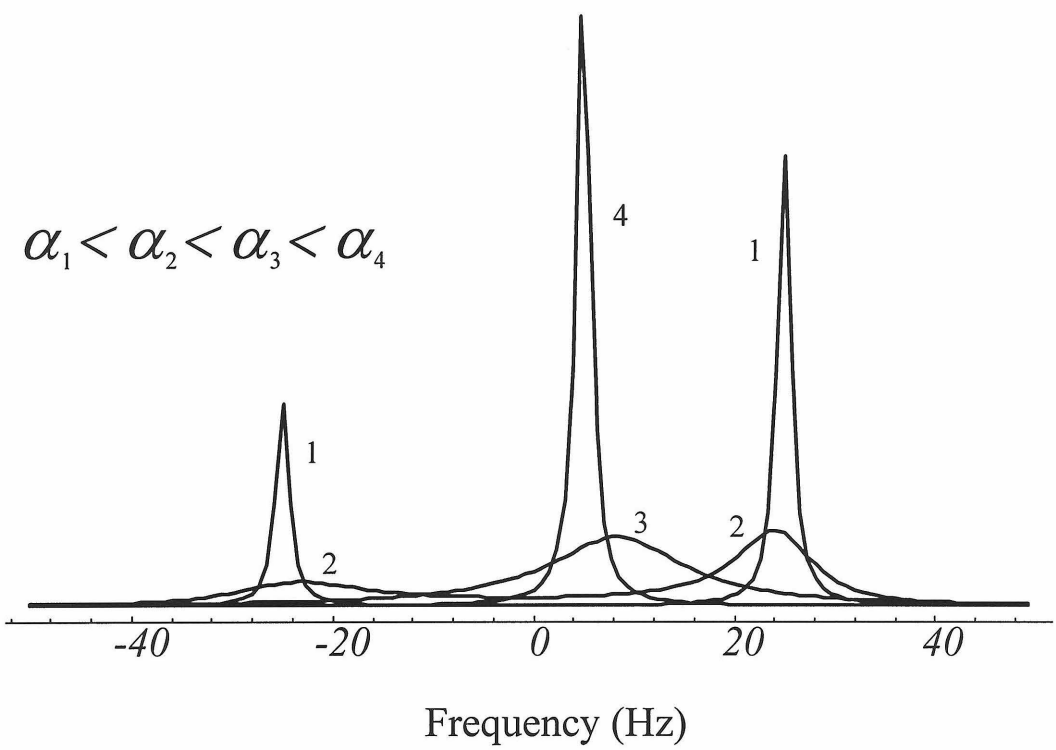

Figure 2.2. Simulated NMR spectra showing the progression from slow to fast exchange.

ambiguities associated with coherence exchange and its relation to population exchange through a direct calculation of coherence exchange.

2.3 Quantum-Mechanical Chemical Exchange

Chemical exchange is a manifestation of the same nonunitary time evolution responsible for all relaxation phenomena. Nonunitary dynamics result when only part of a system is considered and yet its coupling to the rest of the system, or reservoir, is not ignored. In this section, a weak-collision quantum-mechanical relaxation theory (QMRT) of chemical exchange is presented. QMRT [28-32] describes the evolution of a system coupled to a thermodynamic reservoir, treating both the system and reservoir quantum mechanically. Unlike semiclassical relaxation theory [33-37], QMRT satisfies detailed balance, leading to proper equilibrium. More importantly for the present problem, it provides a framework for deriving rate equations for exchange of coherence.

Although the superoperator matrix elements responsible for chemical exchange will be shown to be real valued for population exchange, they are in general complex valued for coherence exchange. This result is related to, but distinct from, the effect of the spin Hamiltonian on the rates between spatial states. The resulting spin dependence of the exchange rates leads in the fast-exchange limit to observable spectroscopic shifts from the predictions of the traditional theory, as will be discussed in Section 2.3.3. Superoperator theory is briefly introduced in Section 2.3.1 and is an important tool for the treatment of the quantum theory of relaxation presented in Section 2.3.2. Although rather technical, Section 2.3.2 provides the theoretical framework that is used here for the novel analysis of chemical exchange in NMR. The principal results of QMRT from Section 2.3.2 are reviewed in Section 2.3.3 before they are applied to chemical exchange.

2.3.1 Superoperator Theory

Superoperators [26,38] are objects that act on operators to give new operators and are ubiquitous in the treatment of relaxation theory. As an example of the use of superoperators, consider the Liouville-von Neumann equation for the unitary evolution of the density operator ρ under a Hamiltonian H,

$$\dot{\rho} = -i[H, \rho], \tag{8}$$

for H in units of radians per second. In superoperator notation the Liouville-von Neumann equation is written as

$$\dot{\rho} = -i\mathcal{L}\rho, \tag{9}$$

where $\mathcal{L} = [H, \ ]$ is the Liouvillian superoperator. Superoperators will be denoted by script letters, with the exception of the chemical exchange and relaxation superoperator, Γ, which is introduced below.

A superoperator requires four Hilbert space (ket) indices to specify a single component, so that the matrix element of an operator produced by the action of a superoperator on another operator is

$$A_{ij} = \sum_{kl} \mathcal{S}_{ijkl} B_{kl}. \tag{10}$$

A formally equivalent description is obtained if a space is considered in which the N×N elements of an operator are arranged in an $N^2 \times 1$ column vector and the N×N×N×N elements of the superoperator are similarly written as an $N^2 \times N^2$ matrix. This operator space is referred to as Liouville space. The mathematics of superoperators acting on operators in Liouville space bears a striking resemblance to that of the action of operators on kets in Hilbert space. In particular, just as eigenstates can be defined for operators, eigenoperators can be defined for superoperators. For example, the level shift operators, $|i\rangle\langle j|$, composed of the eigenbras and eigenkets of the Hamiltonian,

$$H|i\rangle = \omega_i|i\rangle, \tag{11}$$

are eigenoperators of the Liouvillian,

$$\mathcal{L}|i\rangle\langle j| = (\omega_i - \omega_j)|i\rangle\langle j| = \omega_{ij}|i\rangle\langle j|. \tag{12}$$

In Liouville space, the chemical exchange and relaxation superoperator, Γ, is the generalization of the kinetic exchange matrix. As shown in Section 2.3.3, Γ connects only states of the same spin coherence order so that populations exchange with populations and coherences with coherences. The evolution of the density operator is a combination of the unitary time evolution of the Liouvillian and the nonunitary evolution of the chemical exchange and relaxation superoperator, leading to the general equation of motion

$$\dot{\rho} = (-i\mathcal{L} + \Gamma)\rho. \tag{13}$$

The magnetization exchange introduced in Section 2.2 is an example of the application of equation (13). The observable magnetization is given by

$$M_+ = \gamma\hbar\langle I_+\rangle = \gamma\hbar \mathrm{Tr}\{\rho\, I_-\}, \tag{14}$$

where γ is the gyromagnetic ratio and $\hbar$ is Planck's constant, so that the only elements of ρ that give rise to observable magnetization are

$$\begin{aligned} \rho_A &= I_{A+}, \\ \rho_B &= I_{B+}. \end{aligned} \tag{15}$$

In the traditional theory it is assumed that the exchange of coherences follows the same set of kinetic equations as the exchange of populations, giving, in the $\{\rho_A, \rho_B\}$ basis,

$$\Gamma = \begin{pmatrix} -k_\mathrm{b} & k_\mathrm{f} \\ k_\mathrm{b} & -k_\mathrm{f} \end{pmatrix}. \tag{16}$$

In the $\{\rho_A, \rho_B\}$ basis, the Liouvillian is diagonal, as

$$\begin{aligned} \mathcal{L}\rho_A &= [H, \rho_A] = \omega_A \rho_A, \\ \mathcal{L}\rho_B &= [H, \rho_B] = \omega_B \rho_B. \end{aligned} \tag{17}$$

The combined equations of motion for the density operator are therefore

$$\frac{\partial}{\partial t}\begin{pmatrix} \rho_B \\ \rho_A \end{pmatrix} = \begin{pmatrix} -k_b - i\omega_B & k_f \\ k_b & -k_f - i\omega_A \end{pmatrix}\begin{pmatrix} \rho_B \\ \rho_A \end{pmatrix}, \tag{18}$$

which, using equation (14), yields equation (3).

2.3.2 Quantum-Mechanical Relaxation Theory

Quantum-mechanical relaxation theory [28-31] describes the nonunitary evolution of a system coupled to a thermodynamic bath or reservoir in the subspace of the system, treating both the system and reservoir quantum mechanically. Unlike semiclassical relaxation theory [33-37], QMRT satisfies detailed balance, leading to proper equilibrium. Nonunitary dynamics result when only the system Liouville space is considered and yet the coupling to the reservoir Hamiltonian is included. The time evolution under the system Hamiltonian is approximate when couplings to the reservoir are nonzero, in which case the actual evolution under the full Hamiltonian appears as nonunitary evolution of the system, i.e., evolution does not conserve the norm of the system density operator. From a perspective encompassing both the system and reservoir, however, time evolution is still unitary.

Relaxation theory is used to calculate the effect of the system-bath coupling in the restricted space of the system, making it unnecessary to calculate the usually intractable dynamics in the complete space. An example of the separation between system and reservoir is found in NMR, where only the spin Hamiltonian is considered. The Hamiltonians for intramolecular and intermolecular interactions are not considered explicitly, but their couplings to the spin system lead to coherence exchange, decay, and return to spin equilibrium.

The following presentation of QMRT differs from standard treatments with respect to the treatment of spectral densities. It is often assumed that the imaginary components of the spectral density have no effect on the observed NMR spectrum. By treating the reservoir quantum-mechanically, it is shown that imaginary components of the spectral density are manifest as measurable spectroscopic shifts in the fast-exchange region. If the fast-exchange line positions are interpreted using the traditional theory, substantial errors could occur in the extraction of the thermodynamic properties. In addition, the secular approximation is not introduced here in the usual way. The typical application of the secular approximation is incorrect, as pointed out by Goldman in the calculation of nuclear spin cross relaxation [39] and as shown here for chemical exchange. The quantum-mechanical relaxation theory derived in this section will be applied to chemical exchange in Section 2.3.3.

2.3.2.1 Equations of Motion for a System Coupled to a Quantum-Mechanical Reservoir

The total Hamiltonian for a system interacting with a bath or reservoir is

$$\hbar H = \hbar\left(H_{\mathrm{S}} + H_{\mathrm{R}} + V\right), \tag{19}$$

where H_{S} is the system Hamiltonian, H_{R} is the reservoir Hamiltonian and V is the coupling between them, which, in the weak-collision limit assumed here, is small. The Hamiltonians H_{S} and H_{R} contain operators that act solely on the system and reservoir, respectively, and hence commute. Neither, however, is presumed to commute with V.

In general, measurements are performed on the system so that the density operator of interest, σ, is the trace over the reservoir variables of the total density operator ρ,

$$\sigma(t) = \mathrm{Tr}_{\mathrm{R}}\,\rho(t). \tag{20}$$

Similarly, the reservoir density operator, ρ_{R}, is defined by

$$\rho_R(t) = \mathrm{Tr}_S\, \rho(t). \tag{21}$$

The total density operator evolves in time according to the Liouville-von Neumann equation,

$$\dot{\rho}(t) = -i\left[H(t), \rho(t)\right]. \tag{22}$$

The effect of the system-reservoir coupling is solved for by first transforming to an interaction representation in which the effects of both H_R and H_S have been removed. In this Redfield frame the following operators are defined,

$$\begin{aligned} \rho^* &= \exp\left[i(H_R + H_S)t\right]\rho \exp\left[-i(H_R + H_S)t\right], \\ V^* &= \exp\left[i(H_R + H_S)t\right]V \exp\left[-i(H_R + H_S)t\right], \\ \sigma^*(t) &= \mathrm{Tr}_R \rho^*(t), \end{aligned} \tag{23}$$

and the evolution of ρ^*, the density operator in the Redfield frame, is given by

$$\dot{\rho}^*(t) = -i\left[V^*(t), \rho^*(t)\right]. \tag{24}$$

Solving equation (24) iteratively to second order,

$$\dot{\rho}^*(t) = -i\left[V^*(t), \rho^*(0)\right] - \int_0^t dt' \left[V^*(t), \left[V^*(t'), \rho^*(t')\right]\right]. \tag{25}$$

The time evolution of the system is found by performing a trace over the reservoir variables of equation (25),

$$\dot{\sigma}^*(t) = -i\,\mathrm{Tr}_R\left[V^*(t), \rho^*(0)\right] - \int_0^t dt'\, \mathrm{Tr}_R\left[V^*(t), \left[V^*(t'), \rho^*(t')\right]\right]. \tag{26}$$

In applying equation (26) it is presumed that the initial density operator is factorable,

$$\rho(0) = \sigma(0)\, \rho_R(0). \tag{27}$$

In particular, the reservoir is assumed to be in thermal equilibrium initially with

$$\rho_R(0) = \frac{e^{-\beta H_R}}{Z}, \tag{28}$$

where Z is the reservoir partition function, $\beta = \frac{\hbar}{k_B T}$, and k_B is Boltzmann's constant. By construction, V contains only terms that are off diagonal in the bath, or they would have been included in H_R. The trace of V with $\rho_R(0)$ is therefore zero, and the first term on the right hand side of (26) can be discarded. Therefore,

$$\dot{\sigma}^*(t) = -\int_0^t dt' \, \mathrm{Tr}_R \left[V^*(t), \left[V^*(t'), \rho^*(t') \right] \right]. \tag{29}$$

Expanding the double commutator,

$$\begin{aligned} \dot{\sigma}^*(t) = -\int_0^t dt' \, \mathrm{Tr}_R \, \{ & V^*(t) V^*(t') \rho^*(t') - V^*(t) \rho^*(t') V^*(t') - \\ & V^*(t') \rho^*(t') V^*(t) + \rho^*(t') V^*(t') V^*(t) \}, \end{aligned} \tag{30}$$

and letting $\tau = t - t'$,

$$\begin{aligned} \dot{\sigma}^*(t) = -\int_0^t d\tau \, \mathrm{Tr}_R \, \{ & V^*(t) V^*(t-\tau) \rho^*(t-\tau) - V^*(t) \rho^*(t-\tau) V^*(t-\tau) - \\ & V^*(t-\tau) \rho^*(t-\tau) V^*(t) + \rho^*(t-\tau) V^*(t-\tau) V^*(t) \}. \end{aligned} \tag{31}$$

Equation (31) shows that the evolution of the density matrix depends on its history. As the system is damped by the trace over the reservoir variables, the memory of this history is lost. The correlation time, τ_c, is a measure of the memory of the system and, in general, will be much smaller than the evolution time t. The only contribution to the integral in (31), then, will be for short τ on the order of τ_c. This has important implications. First, as the correlation time is small and the weak-collision limit has been assumed, the density operator does not appreciably change between $t - \tau_c$ and t. This allows for the replacement of the argument $t - \tau$ in the density operator on the right-hand side of equation (31) with the argument t and is justified if the dynamics of the system are only considered with time resolution much larger than τ_c. As well, since the only contributions to this integral are from short τ, the limit of the integral may be taken to infinity. This short correlation time approximation, known as the Markoff

approximation, transforms the integro-differential equation (31) into a system of coupled linear first-order differential equations,

$$\dot{\sigma}^*(t) = -\int_0^\infty d\tau \, \mathrm{tr}_R \left\{ V^*(t) V^*(t-\tau) \rho^*(t) - V^*(t) \rho^*(t) V^*(t-\tau) - V^*(t-\tau) \rho^*(t) V^*(t) + \rho^*(t) V^*(t-\tau) V^*(t) \right\}. \tag{32}$$

Although equation (31) is exact, equation (32) is the result of second-order perturbation theory and is valid in the weak collision limit and when the Markoff approximation applies.

The coupling between the system and reservoir allows for the reversible transfer of energy and coherences and the creation of correlations between $\sigma(t)$ and $\rho_R(t)$. As these correlations also decay on the time scale of τ_c and the dynamics are only being considered on time scales much greater than this, the density operator may be factored,

$$\rho(t) = \sigma(t) \, \rho_R(t). \tag{33}$$

Irreversibility is introduced into the equations of motion by assuming that any effect on the reservoir due to the interaction with the system dissipates quickly, so that the reservoir is always in thermal equilibrium. The state of the reservoir will not be affected by the system, then, but the system will be affected by the reservoir. This is the basic condition of irreversibility and allows the total density operator to be written as

$$\rho(t) = \sigma(t) \, \rho_R(0). \tag{34}$$

Considering the dynamics only on a time scale large compared to the correlation time is referred to as coarse graining the dynamics and should be interpreted as an averaging of the equations of motion over a time $\Delta t >> \tau_c$ [29].

Using the density operator (34), the equation of motion (32) may now be written as

$$\dot{\sigma}^*(t) = -\int_0^\infty d\tau \,\mathrm{Tr}_R \left\{ V^*(t)V^*(t-\tau)\sigma^*(t)\rho_R(0) - V^*(t)\sigma^*(t)\rho_R(0)V^*(t-\tau) - V^*(t-\tau)\sigma^*(t)\rho_R(0)V^*(t) + \sigma^*(t)\rho_R(0)V^*(t-\tau)V^*(t) \right\}. \tag{35}$$

The evolution of the $m'm$ reduced density operator matrix element is now calculated. Several of the steps leading to the final equations of motion are detailed below. The combined eigenstates of the system and reservoir are written as $|mM\rangle$, where lower case letters index system eigenstates and upper case letters index reservoir eigenstates,

$$\begin{aligned} H_S|mM\rangle &= \omega_m|mM\rangle, \\ H_R|mM\rangle &= \omega_M|mM\rangle. \end{aligned} \tag{36}$$

Using the definition of trace and the closure relationship,

$$\begin{aligned} \langle m'|\dot{\sigma}^*(t)|m\rangle = -\int_0^\infty d\tau \sum_{n',n,N',N,M} & \left\{ \langle m'M|V^*(t)|n'N'\rangle\langle n'N'|V^*(t-\tau)|nN\rangle\langle nN|\sigma^*(t)\rho_R(0)|mM\rangle - \right. \\ & \langle m'M|V^*(t)|n'N'\rangle\langle n'N'|\sigma^*(t)\rho_R(0)|nN\rangle\langle nN|V^*(t-\tau)|mM\rangle - \\ & \langle m'M|V^*(t-\tau)|n'N'\rangle\langle n'N'|\sigma^*(t)\rho_R(0)|nN\rangle\langle nN|V^*(t)|mM\rangle + \\ & \left. \langle m'M|\sigma^*(t)\rho_R(0)|n'N'\rangle\langle n'N'|V^*(t-\tau)|nN\rangle\langle nN|V^*(t)|mM\rangle \right\}. \end{aligned} \tag{37}$$

From the definitions of the operators in the Redfield frame, (23),

$$\begin{aligned} \langle m'|\dot{\sigma}^*(t)|m\rangle = -\int_0^\infty d\tau \sum_{n',n,N',N,M} & \left\{ \exp\left[i(\omega_{m'n'} + \omega_{n'n})t\right]\exp\left[-i(\omega_{n'n} + \omega_{N'N})\tau\right] \right. \\ & \langle m'M|V|n'N'\rangle\langle n'N'|V|nM\rangle\langle nM|\sigma^*(t)\rho_R(0)|mM\rangle\delta_{MN} - \\ & \exp\left[i(\omega_{m'n'} + \omega_{nm})t\right]\exp\left[-i(\omega_{nm} + \omega_{NM})\tau\right] \\ & \langle m'M|V|n'N\rangle\langle n'N|\sigma^*(t)\rho_R(0)|nN\rangle\langle nN|V|mM\rangle\delta_{NN'} - \\ & \exp\left[i(\omega_{m'n'} + \omega_{nm})t\right]\exp\left[-i(\omega_{m'n'} + \omega_{MN'})\tau\right] \\ & \langle m'M|V|n'N\rangle\langle n'N|\sigma^*(t)\rho_R(0)|nN\rangle\langle nN|V|mM\rangle\delta_{NN'} + \\ & \exp\left[i(\omega_{n'n} + \omega_{nm})t\right]\exp\left[-i(\omega_{n'n} + \omega_{N'N})\tau\right] \\ & \left. \langle m'M|\sigma^*(t)\rho_R(0)|n'M\rangle\langle n'M|V|nN\rangle\langle nN|V|mM\rangle\delta_{MN'} \right\}. \end{aligned} \tag{38}$$

Renaming indices in the first and last terms,

$$\begin{aligned}\langle m'|\dot{\sigma}^*(t)|m\rangle = -\int_0^\infty d\tau \sum_{n',n,N',N} \\ \Big\{ \sum_k \delta_{mn}\exp\Big[i\big(\omega_{m'k}+\omega_{kn'}\big)t\Big]\exp\Big[-i\big(\omega_{kn'}+\omega_{N'N}\big)\tau\Big] \\ \langle m'N|V|kN'\rangle\langle kN'|V|n'N\rangle\langle n'N|\sigma^*(t)\rho_{\mathrm{R}}(0)|nN\rangle - \\ \exp\Big[i\big(\omega_{m'n'}+\omega_{nm}\big)t\Big]\exp\Big[-i\big(\omega_{nm}+\omega_{NN'}\big)\tau\Big] \\ \langle m'N'|V|n'N\rangle\langle n'N|\sigma^*(t)\rho_{\mathrm{R}}(0)|nN\rangle\langle nN|V|mN'\rangle - \\ \exp\Big[i\big(\omega_{m'n'}+\omega_{nm}\big)t\Big]\exp\Big[-i\big(\omega_{m'n'}+\omega_{N'N}\big)\tau\Big] \\ \langle m'N'|V|n'N\rangle\langle n'N|\sigma^*(t)\rho_{\mathrm{R}}(0)|nN\rangle\langle nN|V|mN'\rangle + \\ \sum_k \delta_{m'n'}\exp\Big[i\big(\omega_{nk}+\omega_{km}\big)t\Big]\exp\Big[-i\big(\omega_{nk}+\omega_{NN'}\big)\tau\Big] \\ \langle n'N|\sigma^*(t)\rho_{\mathrm{R}}(0)|nN\rangle\langle nN|V|kN'\rangle\langle kN'|V|mN\rangle \Big\}.\end{aligned} \tag{39}$$

Grouping similar terms in front,

$$\begin{aligned}\langle m'|\dot{\sigma}^*(t)|m\rangle = \sum_{n',n} \langle n'|\sigma^*(t)|n\rangle\exp\Big[i\big(\omega_{m'n'}+\omega_{nm}\big)t\Big] \\ \Big\{ -\delta_{mn}\sum_k \sum_{NN'} \int_0^\infty d\tau\exp\Big[-i\big(\omega_{kn'}+\omega_{N'N}\big)\tau\Big] \\ \langle m'N|V|kN'\rangle\langle kN'|V|n'N\rangle\langle N|\rho_{\mathrm{R}}(0)|N\rangle + \\ \sum_{NN'} \int_0^\infty d\tau\exp\Big[-i\big(\omega_{nm}+\omega_{NN'}\big)\tau\Big] \\ \langle m'N'|V|n'N\rangle\langle nN|V|mN'\rangle\langle N|\rho_{\mathrm{R}}(0)|N\rangle + \\ \sum_{NN'} \int_0^\infty d\tau\exp\Big[-i\big(\omega_{m'n'}+\omega_{N'N}\big)\tau\Big] \\ \langle m'N'|V|n'N\rangle\langle nN|V|mN'\rangle\langle N|\rho_{\mathrm{R}}(0)|N\rangle + \\ -\delta_{m'n'}\sum_k \sum_{NN'} \int_0^\infty d\tau\exp\Big[-i\big(\omega_{nk}+\omega_{NN'}\big)\tau\Big] \\ \langle nN|V|kN'\rangle\langle kN'|V|mN\rangle\langle N|\rho_{\mathrm{R}}(0)|N\rangle \Big\},\end{aligned} \tag{40}$$

and finally rewriting the equation,

$$\begin{aligned}\langle m'|\dot{\sigma}^*(t)|m\rangle = \sum_{n',n} \langle n'|\sigma^*(t)|n\rangle \exp\left[i\left(\omega_{m'n'}+\omega_{nm}\right)t\right] \\ \Big\{ -\delta_{mn}\sum_k \sum_{NN'} \langle m'N|V|kN'\rangle\langle kN'|V|n'N\rangle\langle N|\rho_R(0)|N\rangle \\ \int_0^\infty d\tau \exp\left[-i\left(\omega_{kn'}+\omega_{N'N}\right)\tau\right] + \\ \sum_{NN'} \langle nN|V|mN'\rangle\langle m'N'|V|n'N\rangle\langle N|\rho_R(0)|N\rangle \\ \int_0^\infty d\tau \exp\left[-i\left(\omega_{nm}+\omega_{NN'}\right)\tau\right] + \\ \sum_{NN'} \langle nN|V|mN'\rangle\langle m'N'|V|n'N\rangle\langle N|\rho_R(0)|N\rangle \\ \int_0^\infty d\tau \exp\left[-i\left(\omega_{m'n'}+\omega_{N'N}\right)\tau\right] + \\ -\delta_{m'n'}\sum_k \sum_{NN'} \langle nN|V|kN'\rangle\langle kN'|V|mN\rangle\langle N|\rho_R(0)|N\rangle \\ \int_0^\infty d\tau \exp\left[-i\left(\omega_{nk}+\omega_{NN'}\right)\tau\right] \Big\}.\end{aligned} \tag{41}$$

At this point the secular approximation is often made, in which terms in (41) that oscillate in time are discarded. In the standard application of this approximation, this would exclude all terms for which $\omega_{m'n'}+\omega_{nm}\neq 0$. For chemical exchange in NMR, $\omega_{m'n'}+\omega_{nm}$ takes on the value of the difference between chemical shifts in the exchanging conformers, for appropriate values of the indices. The secular approximation would throw away all exchange between sites with nonequivalent spin Hamiltonians, allowing chemical exchange solely in the trivial case of systems with degenerate NMR parameters. This application of the secular approximation is obviously unphysical and will not be introduced here. In fact, the time dependence of the exponential term in equation (41) is exactly canceled upon returning to the lab frame, where the equations of motion are

$$\langle m'|\dot{\sigma}(t)|m\rangle = -i\langle m'|\big[H_S(t),\sigma(t)\big]|m\rangle +$$
$$\sum_{n',n}\ \langle n'|\sigma(t)|n\rangle$$
$$\Big\{\ -\delta_{mn}\sum_{k}\ \sum_{NN'}\ \langle m'N|V|kN'\rangle\langle kN'|V|n'N\rangle\langle N|\rho_{\mathrm{R}}(0)|N\rangle$$
$$\int_0^\infty d\tau \exp\big[-i\big(\omega_{kn'}+\omega_{N'N}\big)\tau\big] +$$
$$\sum_{NN'}\ \langle nN|V|mN'\rangle\langle m'N'|V|n'N\rangle\langle N|\rho_{\mathrm{R}}(0)|N\rangle$$
$$\int_0^\infty d\tau \exp\big[-i\big(\omega_{nm}+\omega_{NN'}\big)\tau\big] +$$
$$\sum_{NN'}\ \langle nN|V|mN'\rangle\langle m'N'|V|n'N\rangle\langle N|\rho_{\mathrm{R}}(0)|N\rangle$$
$$\int_0^\infty d\tau \exp\big[-i\big(\omega_{m'n'}+\omega_{N'N}\big)\tau\big] +$$
$$-\delta_{m'n'}\sum_{k}\ \sum_{NN'}\ \langle nN|V|kN'\rangle\langle kN'|V|mN\rangle\langle N|\rho_{\mathrm{R}}(0)|N\rangle$$
$$\int_0^\infty d\tau \exp\big[-i\big(\omega_{nk}+\omega_{NN'}\big)\tau\big]\ \Big\}. \tag{42}$$

The equations of motion are written in the final, compact form,

$$\langle m'|\dot{\sigma}(t)|m\rangle = -i\langle m'|\big[H(t),\sigma(t)\big]|m\rangle + \sum_{n',n}\ \Gamma_{m'mn'n}\langle n'|\sigma(t)|n\rangle, \tag{43}$$

where

$$\Gamma_{m'mn'n} = -\delta_{mn}\sum_{k}\ \gamma^{+}_{m'kkn'} - \delta_{m'n'}\sum_{k}\ \gamma^{-}_{nkkm} + \gamma^{+}_{nmm'n'} + \gamma^{-}_{nmm'n'}, \tag{44}$$

and

$$\gamma^{+}_{mkln} = \sum_{NN'}\ \langle mN|V|kN'\rangle\langle lN'|V|nN\rangle\langle N|\rho_{\mathrm{R}}(0)|N\rangle$$
$$\int_0^\infty d\tau \exp\big[-i\big(\omega_{ln}+\omega_{N'N}\big)\tau\big]$$
$$\gamma^{-}_{mkln} = \sum_{NN'}\ \langle mN|V|kN'\rangle\langle lN'|V|nN\rangle\langle N|\rho_{\mathrm{R}}(0)|N\rangle$$
$$\int_0^\infty d\tau \exp\big[-i\big(\omega_{mk}+\omega_{NN'}\big)\tau\big] \tag{45}$$
$$= \sum_{NN'}\ \langle mN|V|kN'\rangle\langle lN'|V|nN\rangle\langle N|\rho_{\mathrm{R}}(0)|N\rangle$$
$$\int_{-\infty}^0 d\tau \exp\big[-i\big(\omega_{km}+\omega_{N'N}\big)\tau\big].$$

Equation (43) is completely general with respect to the type of relaxation process being considered. With the appropriate choice of V, equation (43) can be used to calculate nuclear spin relaxation, chemical exchange, or vibrational dephasing.

2.3.2.2 Quantum-Mechanical Spectral Densities

The one-sided Fourier transforms of equation (45) lead, in general, to complex-valued γ's. Defining J and Δ to be real-valued functions, the γ's can be written as

$$\begin{aligned} \gamma^{+}_{mk\,ln} &= J_{mk\,ln}(\omega_{ln}) + i\Delta_{mk\,ln}(\omega_{ln}), \\ \gamma^{-}_{mk\,ln} &= J_{mk\,ln}(\omega_{km}) - i\Delta_{mk\,ln}(\omega_{km}). \end{aligned} \tag{46}$$

J_{mkln} is the real part of the spectral density and Δ_{mkln} is the imaginary part. J is given by a full Fourier transform while J and Δ are related by a Hilbert transform [40],

$$\begin{aligned} J_{mkln}(\omega) &= \sum_{NN'} \langle mN|V|kN'\rangle\langle lN'|V|nN\rangle\langle N|\rho_{\mathrm{R}}(0)|N\rangle \\ &\qquad \tfrac{1}{2}\int_{-\infty}^{\infty} d\tau \exp\left(-i(\omega+\omega_{N'N})\tau\right), \\ &= \sum_{NN'} \tfrac{1}{2}\delta(\omega+\omega_{N'N})\langle mN|V|kN'\rangle\langle lN'|V|nN\rangle\langle N|\rho_{\mathrm{R}}(0)|N\rangle, \end{aligned} \tag{47}$$

and

$$\Delta_{mkln}(\omega) = \frac{1}{\pi}\mathcal{P}\int_{-\infty}^{\infty} d\omega' \frac{J_{mkln}(\omega')}{\omega'-\omega}, \tag{48}$$

where $\mathcal{P}$ indicates that the principle value integral is to be taken. The opposite signs in front of the Δ term in γ^{+} and γ^{-} reflect the difference in the two one-sided Fourier transforms of equation (45).

In semiclassical relaxation theory, a Lorentzian spectral density is often assumed [33,41], in which

$$J(\omega) = \frac{2\tau_c\langle V^2\rangle}{1+\tau_c^2\omega^2}. \tag{49}$$

This spectral density is symmetric, however, and using equation (47) it can be shown through a termwise comparison that quantum mechanical spectral densities satisfy

$$J_{abba}(\omega_{ba}) = \exp(-\beta\omega_{\mathrm{ba}})J_{baab}(-\omega_{ba}). \tag{50}$$

Combining this result with the Lorentzian spectral density gives

$$J(\omega)=\begin{cases} \dfrac{2\tau_c\langle V^2\rangle}{1+\tau_c^2\omega^2} & \omega<0 \\ \dfrac{2\tau_c\langle V^2\rangle}{1+\tau_c^2\omega^2}\exp(-\beta\omega) & \omega>0. \end{cases} \tag{51}$$

That the Boltzmann weighting should be associated with positive frequencies can be seen in the limit of short correlation times, where V connects all states regardless of the energy splitting between them. In this limit,

$$J(\omega)=\begin{cases} 2\tau_c\langle V^2\rangle & \omega<0 \\ 2\tau_c\langle V^2\rangle\exp(-\beta\omega) & \omega>0. \end{cases} \tag{52}$$

This result is also obtained from the quantum-mechanical expression for the spectral density given in equation (47). When V connects all states regardless of the energy difference between them, $J(\omega)$ is completely determined by the sum over accessible reservoir states.

The imaginary component of the spectral density (51) can be determined analytically by solving the Hilbert transform as shown in Appendix A,

$$\begin{aligned}\Delta(\omega) = \frac{\tau_c\langle V^2\rangle}{\pi(1+\tau_c^2\omega^2)}\Big\{&\Big[-i\pi-\pi\tau_c\omega+\mathrm{Ei}\Big(\tfrac{i\beta}{\tau_c}\Big)-i\tau_c\omega\mathrm{Ei}\Big(\tfrac{i\beta}{\tau_c}\Big)\Big]\exp\Big(-\tfrac{i\beta}{\tau_c}\Big)+\\ &\Big[i\pi-\pi\tau_c\omega+\mathrm{Ei}\Big(\tfrac{-i\beta}{\tau_c}\Big)+i\tau_c\omega\,\mathrm{Ei}\Big(\tfrac{-i\beta}{\tau_c}\Big)\Big]\exp\Big(\tfrac{i\beta}{\tau_c}\Big)+\\ &-\pi\tau_c\omega-2\exp(-\beta\omega)\mathrm{Ei}(\beta\omega)+\ln(\tau_c^2\omega^2)\Big\}.\end{aligned} \tag{53}$$

where $\mathrm{Ei}(x)$ is the exponential integral function [42,43],

$$\mathrm{Ei}(x) = -\mathcal{P}\int_{-x}^{\infty} dt \frac{\exp(-t)}{t}. \tag{54}$$

A plot of the real and imaginary components of the spectral density are shown in Figure 2.3 for a correlation time of 10^{-14} s.

2.3.2.3 Population and Coherence Exchange

The matrix elements of the relaxation and exchange superoperator Γ are comprised of combinations of complex-valued spectral densities, which in general lead to complex-valued matrix elements. Here it is shown that the exchange matrix elements are still real valued for population exchange, but they are complex valued for coherence exchange.

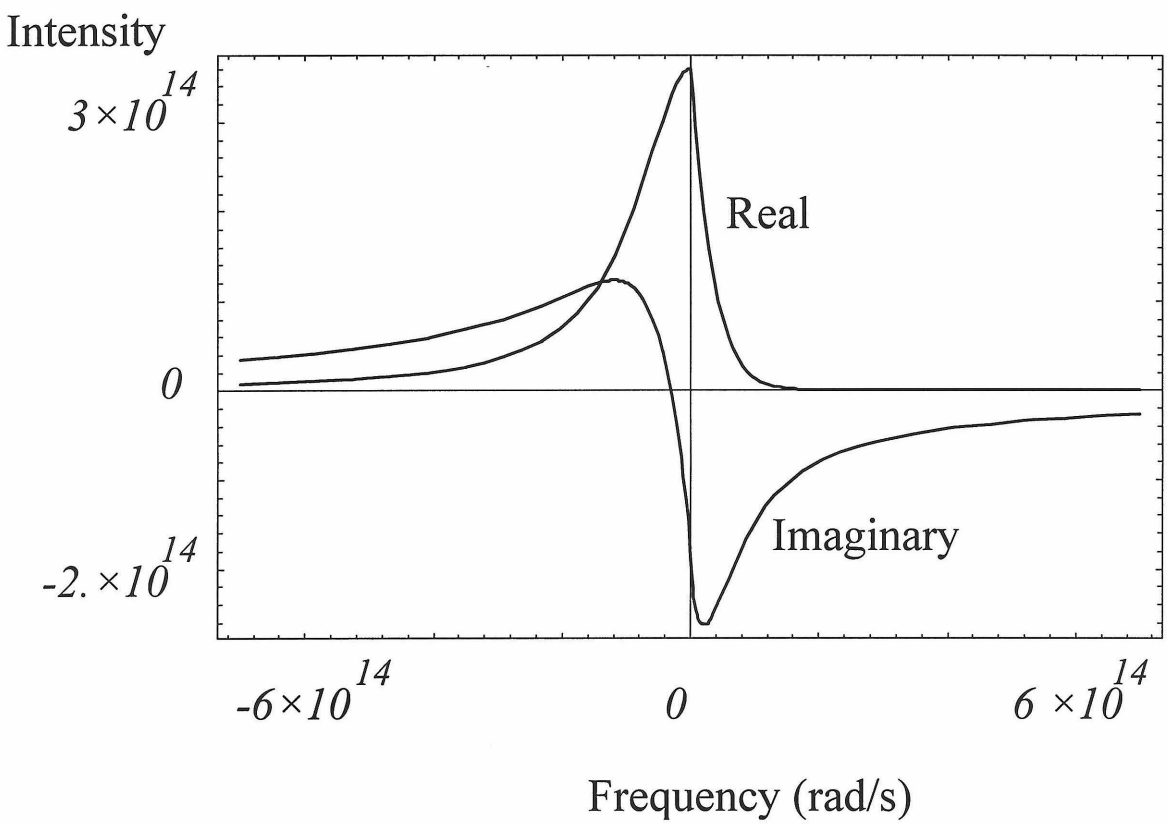

Figure 2.3. The real and imaginary components of the spectral density for a correlation time of 10^{-14} s.

As an example of population exchange, consider a system with 2 states that are coupled through an interaction with a reservoir as shown in Figure 2.4. The equations of motion for the populations of the two states are

$$\begin{aligned}\langle 1|\dot{\sigma}(t)|1\rangle &= -\langle 1|\sigma(t)|1\rangle\left(\gamma^{+}_{1221}+\gamma^{-}_{1221}\right)+\\ &\quad \langle 2|\sigma(t)|2\rangle\left(\gamma^{+}_{2112}+\gamma^{-}_{2112}\right)\\ &= -\langle 1|\sigma(t)|1\rangle\left[2J_{1221}(\omega_{21})+\Delta_{1221}(\omega_{21})-\Delta_{1221}(\omega_{21})\right]+\\ &\quad \langle 2|\sigma(t)|2\rangle\left[2J_{2112}(-\omega_{21})+\Delta_{2112}(-\omega_{21})-\Delta_{2112}(-\omega_{21})\right]\\ &= -\langle 1|\sigma(t)|1\rangle\ 2J_{1221}(\omega_{21})+\langle 2|\sigma(t)|2\rangle\ 2J_{2112}(-\omega_{21}),\end{aligned} \tag{55}$$

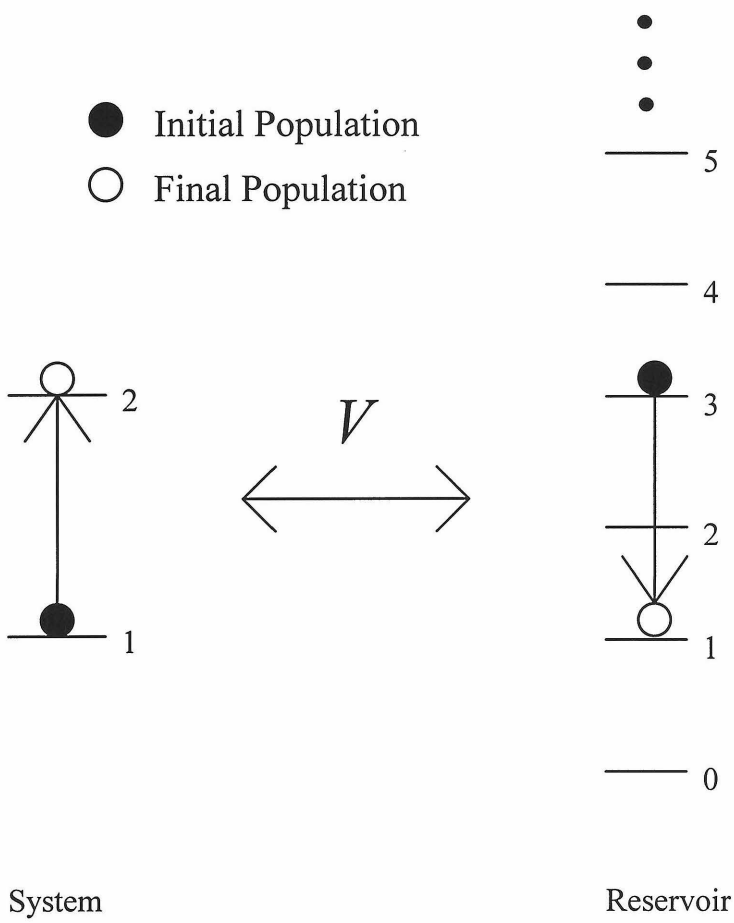

Figure 2.4. Population exchange between two states coupled through an interaction with a reservoir.

and similarly

$$\langle 2|\dot{\sigma}(t)|2\rangle = \langle 1|\sigma(t)|1\rangle\ 2J_{1221}(\omega_{21}) - \langle 2|\sigma(t)|2\rangle\ 2J_{2112}(-\omega_{21}). \tag{56}$$

As

$$J_{1221}(\omega_{21}) = \exp(-\beta\omega_{21})J_{2112}(-\omega_{21}), \tag{57}$$

detailed balance is satisfied,

$$J_{1221}(\omega_{21})\langle 1|\sigma(t)|1\rangle = J_{2112}(-\omega_{21})\langle 2|\sigma(t)|2\rangle, \tag{58}$$

and equilibrium is established in steady state,

$$\langle 2|\sigma_{eq}|2\rangle = \exp(-\beta\omega_{21})\langle 1|\sigma_{eq}|1\rangle. \tag{59}$$

The delta function in the real component of the spectral densities for population exchange denotes a conservation of total energy between the system and reservoir. As the system gains or loses energy, the reservoir compensates (see Figure 2.4).

As an example of coherence exchange, consider a system with 4 states in which V connects state 1 with 3 and state 2 with 4 as shown in Figure 2.5. This can be incorporated into a model for chemical exchange in which spin relaxation is ignored. In

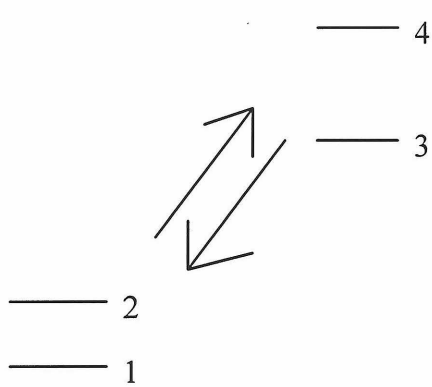

Figure 2.5. Two coherent superpositions undergoing exchange due to a coupling with a reservoir.

the lab frame,

$$\begin{aligned}
&\langle 1|\dot{\sigma}(t)|2\rangle + i\langle 1|\mathcal{L}\sigma(t)|2\rangle \\
&\quad = -\langle 1|\sigma(t)|2\rangle\left(\gamma^{+}_{1331} + \gamma^{-}_{2442} \right) + \\
&\qquad \langle 3|\sigma(t)|4\rangle\left(\gamma^{+}_{4213} + \gamma^{-}_{4213} \right) \\
&\quad = -\langle 1|\sigma(t)|2\rangle\left(J_{1331}(\omega_{31}) + J_{2442}(\omega_{42}) + i\Delta_{1331}(\omega_{31}) - i\Delta_{2442}(\omega_{42}) \right) + \\
&\qquad \langle 3|\sigma(t)|4\rangle\left(J_{4213}(\omega_{13}) + J_{4213}(\omega_{24}) + i\Delta_{4213}(\omega_{13}) - i\Delta_{4213}(\omega_{24}) \right) \\
&\quad = -\langle 1|\sigma(t)|2\rangle\left(J_{1331}(\omega_{31}) + J_{2442}(\omega_{42}) + i\Delta^{24}_{13} \right) + \\
&\qquad \langle 3|\sigma(t)|4\rangle\left(J_{4213}(-\omega_{31}) + J_{4213}(-\omega_{42}) \right),
\end{aligned} \tag{60}$$

and

$$\begin{aligned}
&\langle 3|\dot{\sigma}(t)|4\rangle + i\langle 3|\mathcal{L}\sigma(t)|4\rangle \\
&\quad = -\langle 3|\sigma(t)|4\rangle\left(\gamma^{+}_{3113} + \gamma^{-}_{4224} \right) + \\
&\qquad \langle 1|\sigma(t)|2\rangle\left(\gamma^{+}_{2431} + \gamma^{-}_{2431} \right) \\
&\quad = -\langle 3|\sigma(t)|4\rangle\left(J_{3113}(\omega_{13}) + J_{4224}(\omega_{24}) + i\Delta_{3113}(\omega_{13}) - i\Delta_{4224}(\omega_{24}) \right) + \\
&\qquad \langle 1|\sigma(t)|2\rangle\left(J_{2431}(\omega_{31}) + J_{2431}(\omega_{42}) + i\Delta_{2431}(\omega_{31}) - i\Delta_{2431}(\omega_{42}) \right) \\
&\quad = -\langle 3|\sigma(t)|4\rangle\left(J_{3113}(-\omega_{31}) + J_{4224}(-\omega_{42}) + i\Delta^{42}_{31} \right) + \\
&\qquad \langle 1|\sigma(t)|2\rangle\left(J_{2431}(\omega_{31}) + J_{2431}(\omega_{42}) \right),
\end{aligned} \tag{61}$$

where the exchange shifts,

$$\Delta^{kl}_{ij} = \Delta_{ijji}(\omega_{ji}) - \Delta_{kllk}(\omega_{lk}), \tag{62}$$

are introduced and use is made of the identity provided by Cohen-Tannoudji [29] that

$$\Delta_{2431}(\omega_{31}) = \Delta_{2431}(\omega_{42}). \tag{63}$$

Exchange shifts result for coherence exchange due to an incomplete cancellation of imaginary spectral densities in the decay terms when the frequencies of the coherences are not degenerate. The system-reservoir coupling perturbs the frequency of a coherence and the exchange shift can be viewed as the second-order correction to the energy states of the coherence due to this perturbation. Although having a profound effect on the spin dynamics, this shift is the result of a purely spatial susceptibility and is derivable through

a Hilbert-transform relationship with the very same spatial fluctuations responsible for chemical exchange. These shifts can have an observable consequence as will be shown in the following section for the case of chemical exchange in NMR.

The decay rate of a superposition of two states contains the average of the decay rate for the populations connected by the coherence between the states. The feeding or exchange term is an interference term composed of the scattering amplitudes from both states in superposition. For chemical exchange in NMR, it is expected that these two scattering amplitudes are nearly the same, although for exchange involving electronic transitions they are not [30].

2.3.2.4 Relationship to Dynamic Frequency Shifts

For coherence decay in NMR ($m'=n'$, $m=n$) the imaginary components of the spectral density have been observed as dynamic frequency shifts [44] in quadrupolar nuclei [45] and in spin-½ nuclei [46]. In contrast to exchange shifts, which arise from the imaginary components of the spectral density of purely spatial fluctuations, dynamic frequency shifts result entirely from spin relaxation processes. Dynamic frequency shifts can also be described using the QMRT formalism. As an example, consider the decay of spin coherence between states 1 and 2 when V connects states 1 and 2 as shown in Figure 2.6. For this case,

$$\begin{aligned}
&\langle 1|\dot{\sigma}(t)|2\rangle + i\langle 1|\mathcal{L}\sigma(t)|2\rangle \\
&\quad = -\langle 1|\sigma(t)|2\rangle\left(\gamma^{+}_{1221} + \gamma^{-}_{2112} \right) \\
&\quad = -\langle 1|\sigma(t)|2\rangle\left(J_{1221}(\omega_{21}) + J_{2112}(-\omega_{21}) + i\Delta_{1221}(\omega_{21}) - i\Delta_{2112}(-\omega_{21}) \right).
\end{aligned} \tag{64}$$

As Δ changes sign near the origin as shown in Figure 2.3 the imaginary components can constructively or destructively add depending on ω and the correlation time. For a two-level system these parameters are typically such that the dynamic frequency shifts are smaller than the NMR linewidth and have been ignored [33].

2.3.3 Quantum-Mechanical Chemical Exchange in NMR

In Section 2.3.2, it was shown that the equations of motion for the reduced density operator for a system coupled to a quantum-mechanical reservoir are

$$\langle m'|\dot{\sigma}(t)|m\rangle = -i\langle m'|\big[H(t),\sigma(t)\big]|m\rangle + \sum_{n',n} \Gamma_{m'mn'n}\langle n'|\sigma(t)|n\rangle, \tag{65}$$

where

$$\Gamma_{m'mn'n} = -\delta_{mn}\sum_{k}\gamma^{+}_{m'kkn'} - \delta_{m'n'}\sum_{k}\gamma^{-}_{nkkm} + \gamma^{+}_{nmm'n'} + \gamma^{-}_{nmm'n'}, \tag{66}$$

and

$$\begin{aligned}\gamma^{+}_{mkln} &= J_{mkln}(\omega_{ln}) + i\Delta_{mkln}(\omega_{ln}),\\ \gamma^{-}_{mkln} &= J_{mkln}(\omega_{km}) - i\Delta_{mkln}(\omega_{km}).\end{aligned} \tag{67}$$

J_{mkln} is the real part of the spectral density and Δ_{mkln} is the imaginary part. J is given by a full Fourier transform while J and Δ are related by a Hilbert transform,

$$J_{mkln}(\omega) = \sum_{NN'} \tfrac{1}{2}\delta(\omega+\omega_{N'N})\langle mN|V|kN'\rangle\langle lN'|V|nN\rangle\langle N|\rho_{\mathrm{R}}(0)|N\rangle \tag{68}$$

and

$$\Delta_{mkln}(\omega) = \frac{1}{\pi}\mathcal{P}\int_{-\infty}^{\infty} d\omega' \frac{J_{mkln}(\omega')}{\omega'-\omega}. \tag{69}$$

In these equations, V is the coupling between the system and reservoir, $|mM\rangle$ is an eigenstate of system (lower case variable) and reservoir (upper case variable)

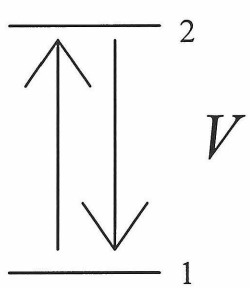

Figure 2.6. The dynamic frequency shift of a two-level system.

Hamiltonians, and ρ_R is the reservoir density operator. Modeling the spectral density as a Boltzmann weighted Lorentzian,

$$J(\omega)=\begin{cases}\dfrac{2\tau_c\langle V^2\rangle}{1+\tau_c^2\omega^2} & \omega<0\\ \dfrac{2\tau_c\langle V^2\rangle}{1+\tau_c^2\omega^2}\exp(-\beta\omega) & \omega>0,\end{cases} \tag{70}$$

and

$$\begin{aligned}\Delta(\omega)=\frac{\tau_c\langle V^2\rangle}{\pi(1+\tau_c^2\omega^2)}\Big\{&\Big[-i\pi-\pi\tau_c\omega+\mathrm{Ei}\Big(\tfrac{i\beta}{\tau_c}\Big)-i\tau_c\omega\mathrm{Ei}\Big(\tfrac{i\beta}{\tau_c}\Big)\Big]\exp\Big(-\tfrac{i\beta}{\tau_c}\Big)+\\ &\Big[i\pi-\pi\tau_c\omega+\mathrm{Ei}\Big(\tfrac{-i\beta}{\tau_c}\Big)+i\tau_c\omega\,\mathrm{Ei}\Big(\tfrac{-i\beta}{\tau_c}\Big)\Big]\exp\Big(\tfrac{i\beta}{\tau_c}\Big)+\\ &-\pi\tau_c\omega-2\exp(-\beta\omega)\mathrm{Ei}(\beta\omega)+\ln(\tau_c^2\omega^2)\Big\}.\end{aligned} \tag{71}$$

For chemical exchange in NMR, equation (65) is often transformed into the rotating frame defined by the frequency ω of the applied radiofrequency excitation pulses. In the rotating frame, the following operators are defined,

$$\begin{aligned}\tilde{\sigma}&=\exp(i\omega I_z t)\sigma\exp(-i\omega I_z t),\\ \tilde{H}_{\mathrm{eff}}&=\exp(i\omega I_z t)H\exp(-i\omega I_z t)-\omega I_z.\end{aligned} \tag{72}$$

For like nuclei in solution,

$$\tilde{H}_{\mathrm{eff}}=\sum_i \Delta\omega_i I_{iz}+\sum_{i<j} J_{ij}I_i\cdot I_j, \tag{73}$$

where $\Delta\omega_i=\omega_i-\omega$ is the relative chemical shift offset of the i^{th} spin and J_{ij} is the scalar coupling constant between spins i and j. In the rotating frame, the equations of motion for an exchanging system are

$$\begin{aligned}\langle m'|\dot{\tilde{\sigma}}(t)|m\rangle=&-i\langle m'|\big[\tilde{H}_{\mathrm{eff}}(t),\tilde{\sigma}(t)\big]|m\rangle+\\ &\sum_{n',n}\exp\big[-i(n_z'-n_z-m_z'+m_z)\omega t\big]\Gamma_{m'mn'n}\langle n'|\tilde{\sigma}\ (t)|n\rangle,\end{aligned} \tag{74}$$

in which m_z', m_z, n_z', and n_z are the I_z quantum numbers of the respective states. By restricting Γ to the connection of density operators of the same coherence order, the time dependence is removed from the sum. Under this restriction, the evolution of the reduced density operator in the rotating frame is

$$\langle m'|\dot{\tilde{\sigma}}(t)|m\rangle = -i\langle m'|\left[\tilde{H}_{\text{eff}}(t), \tilde{\sigma}(t)\right]|m\rangle + \sum_{n',n} \Gamma_{m'mn'n}\langle n'|\tilde{\sigma}\ (t)|n\rangle. \tag{75}$$

In Figure 2.7 a model is given for the "two-site" exchange of NMR coherences of an uncoupled spin-½ nucleus in which the transition state is explicitly considered. Using the results obtained in Section 2.3 for quantum-mechanical chemical exchange, the

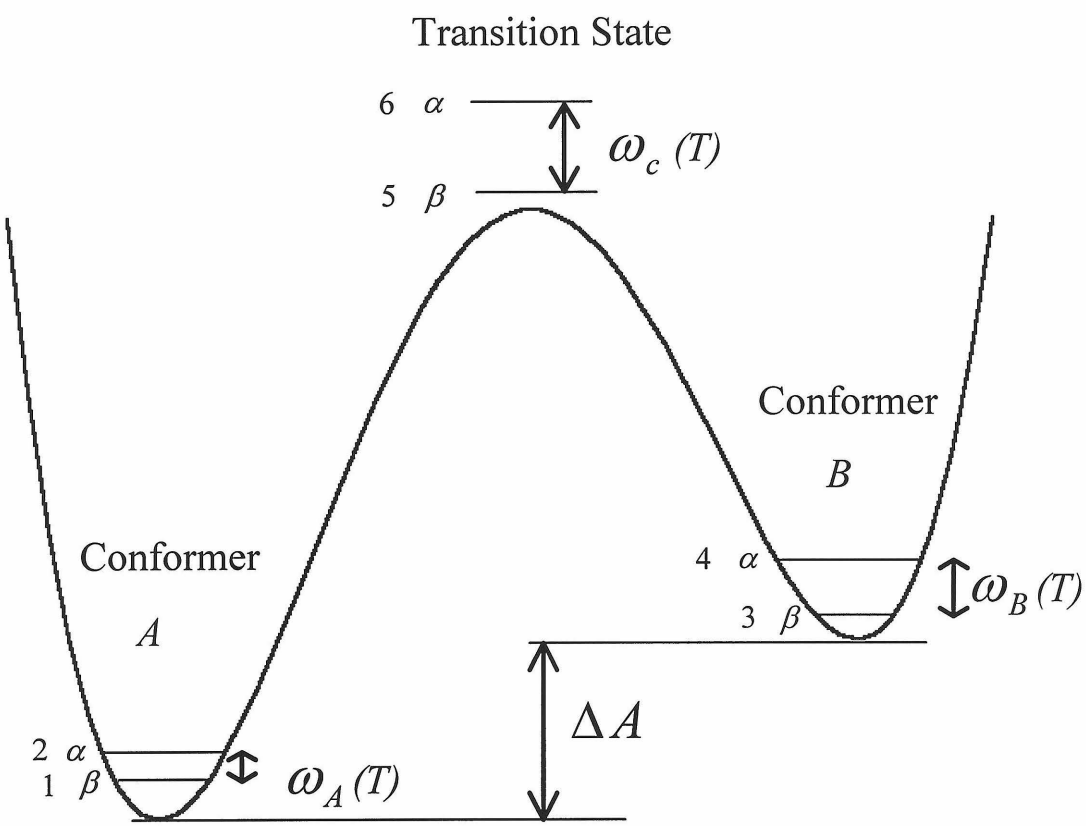

Figure 2.7. A model for two-site chemical exchange of an uncoupled spin-½ nucleus. The states are labeled numerically along with their spin state α and β. In this model the transition state is explicitly considered as state C.

following system of equations describe the evolution of the NMR coherences,

$$\frac{\partial}{\partial t}\begin{pmatrix}\tilde{\sigma}_{56}\\ \tilde{\sigma}_{34}\\ \tilde{\sigma}_{12}\end{pmatrix} = \left(-i\mathcal{L}+\Gamma\right)\begin{pmatrix}\tilde{\sigma}_{56}\\ \tilde{\sigma}_{34}\\ \tilde{\sigma}_{12}\end{pmatrix}$$
$$= \begin{pmatrix}-i\omega_C - k_B^- - k_A^- - i\Delta_C & k_B^+ & k_A^+\\ k_B^- & -i\omega_B - k_B^+ - i\Delta_B & 0\\ k_A^- & 0 & -i\omega_A - k_A^+ - i\Delta_A\end{pmatrix}\begin{pmatrix}\tilde{\sigma}_{56}\\ \tilde{\sigma}_{34}\\ \tilde{\sigma}_{12}\end{pmatrix}, \tag{76}$$

where the exchange shifts are

$$\begin{aligned}\Delta_A &= \Delta_{1551}(\omega_{51}) - \Delta_{2662}(\omega_{62}),\\ \Delta_B &= \Delta_{3553}(\omega_{53}) - \Delta_{4664}(\omega_{64}),\\ \Delta_C &= \Delta_{5115}(-\omega_{51}) - \Delta_{6226}(-\omega_{62}) + \Delta_{5335}(-\omega_{53}) - \Delta_{6446}(-\omega_{64}),\end{aligned} \tag{77}$$

and the approximations

$$\begin{aligned}\frac{k_A^+}{2} &= J_{1551}(\omega_{51}) = J_{2662}(\omega_{62}) = J_{2651}(\omega_{62}) = J_{2651}(\omega_{51}),\\ \frac{k_A^-}{2} &= J_{5115}(-\omega_{51}) = J_{6226}(-\omega_{62}) = J_{6215}(-\omega_{62}) = J_{6215}(-\omega_{51}),\\ \frac{k_B^+}{2} &= J_{3553}(\omega_{53}) = J_{4664}(\omega_{64}) = J_{4652}(\omega_{64}) = J_{4652}(\omega_{53}),\\ \frac{k_B^-}{2} &= J_{5335}(-\omega_{53}) = J_{6446}(-\omega_{64}) = J_{6435}(-\omega_{64}) = J_{6435}(-\omega_{53}),\end{aligned} \tag{78}$$

have been used. As discussed in Section 2.3.2.3, there are no exchange frequency shifts associated with feeding (off-diagonal) terms. Given typical differences in NMR frequencies between spatial conformers of 10^4 rad/s and the large spatial energy differences of $>5\times10^{14}$ rad/s (30 kJ/mol) for transition states in chemical exchange, these approximations are justified. Relaxing these approximations does not affect the results discussed here with respect to exchange shifts. The size of Δ_A, Δ_B and Δ_C, the exchange shifts for sites *A*, *B* and the transition state, can be estimated using equation (53). For a spatial frequency difference of 7.6×10^{14} rad/s, a correlation time of 10^{-14}s, an NMR shift

difference of 10^3 rad/s, and an exchange rate of 2×10^4 rad/s at 300 K, the Δ's are on the order of 10 rad/s.

Equations (76) differ from the corresponding equations for the traditional theory by the inclusion of the imaginary components of the spectral density, appearing as the exchange shifts Δ_A, Δ_B and Δ_C on the diagonal of Γ. These terms result from differences in the imaginary components of the spectral density evaluated at frequencies that differ by the change in the chemical shift between the connected states. The system-reservoir coupling perturbs the frequency of a coherence and the exchange shift can be viewed as the second-order correction to the energy states of the coherence due to this perturbation. Although having a profound effect on the spin dynamics, this shift is the result of a purely spatial susceptibility and is derivable through a Hilbert-transform relationship with the very same spatial fluctuations responsible for chemical exchange.

The exchange shifts depend on exchange rate and are expected to be appreciable only in the fast-exchange limit. The solution of equation (76) is completely analogous to the solution of the equations of motion in the traditional theory in the fast-exchange limit, with the average frequency now equal to the population-weighted sum of the chemical shift and exchange shifts,

$$\langle\omega\rangle = \sum_{i=A,B,C} p_i \left(\omega_i + \Delta_i\right). \tag{79}$$

As the transition state (labeled C here) is assumed to be negligibly populated, it can be excluded from the sum. The transition state is essential, however, in the interpretation of Δ_A and Δ_B.

For multiple-site exchange,

$$\begin{aligned}\langle\omega\rangle &= \sum_{i=A,B,\ldots} p_i\left(\omega_i + \Delta_i\right) \\ &= \sum_{i=A,B,\ldots} p_i\,\omega_i + \sum_{i=A,B,\ldots} p_i\,\Delta_i\,, \\ &= \langle\omega\rangle_{\text{trad}} + \sum_{i=A,B,\ldots} p_i\,\Delta_i\,.\end{aligned} \tag{80}$$

The fast-exchange average may be considered to be the sum of two terms: one equal to the traditional fast-exchange average of the chemical shifts and the other a population-weighted average of the exchange shifts.

From equation (48) it is clear that the exchange shift is zero for a connection between two states with degenerate chemical shifts. For chemical exchange, the net effect of exchange shifts will be zero for any case in which

$$\sum_{i=A,B,C\ldots} p_i\,\Delta_i = 0. \tag{81}$$

One situation in which this would arise is for the exchange of equal energy conformers when the transition state has a chemical shift equal to the average chemical shift of the exchanging conformers.

Chemical shifts decrease linearly with magnetic field, so as zero field is approached there is no exchange shift. The field dependence of the exchange shift is therefore analogous to that of the chemical shift. The exchange shift increases linearly with the difference between the NMR frequency of the transition state and the connected states. Large differences between chemical shifts in the conformer and transition state are expected as molecules in the transition state are typically highly distorted. Although not directly measurable, the chemical shift of the transition state is, in principle, calculable. Recent advances in the *ab initio* calculation of chemical shifts [47-49] could be of considerable use in more detailed modeling of the exchange shifts.

The exact nature of the exchange shift is complicated due to the averaging processes within each of the conformer wells. As previously discussed, the conformer chemical shifts are an average within the manifold of rovibrational states of a particular conformer as depicted in Figure 2.8. Exchange shifts appear at all rovibrational states in the manifold, so again this is not just the traditional average. A more extreme temperature dependence to the chemical shift is indicative of larger differences between chemical shifts within the manifold and thus also of larger exchange shifts in the manifold. A fuller description of chemical exchange would include a multistate model within each conformer well that accurately describes the temperature dependence of the chemical shift within each conformer as well as the averaging between conformers. This complicates the analysis of dynamic NMR data far beyond the traditional analysis, but in principal provides much richer information on the potential energy surface. Further work is needed in this direction, but a few early results from numerical simulations are worth

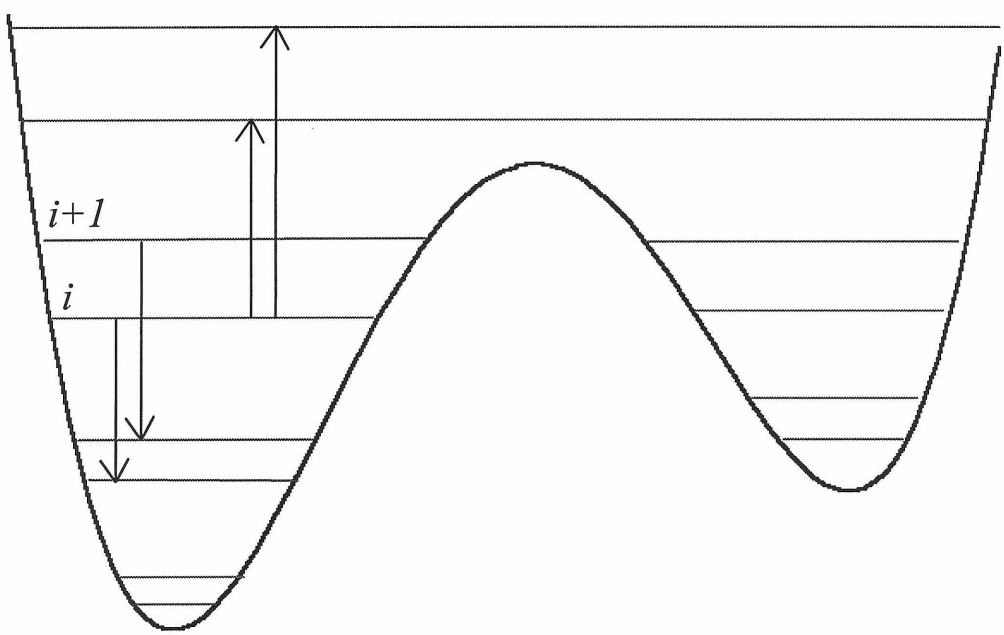

Figure 2.8. A multistate model for chemical exchange in which the rovibrational states within a conformer manifold are explicitly considered.

noting. A model that splits a conformer well into any number of states that linearly increase in chemical shift to the transition state yields predictions similar to those of the single-state-per-conformer model. The net exchange shift at each level consists of a sum of terms for connections to multiple states, some higher and some lower in energy as shown for states i and i+1 in Figure 2.8. The exchange shift is defined to be the sum of the imaginary contributions to the spectral density and for a rovibrational state N composed of spin states i and i+1 it is given by

$$\begin{aligned}\Delta_N = {} & \Delta_{i\,i+2\,i+2\,i}\left(\omega_{i+2\,i}\right) - \Delta_{i+1\,i+3\,i+3\,i+1}\left(\omega_{i+3\,i+1}\right) \\ & + \Delta_{i\,i-2\,i-2\,i}\left(-\omega_{i\,i-2}\right) - \Delta_{i+1\,i-1\,i-1\,i+1}\left(-\omega_{i+1\,i-1}\right).\end{aligned} \tag{82}$$

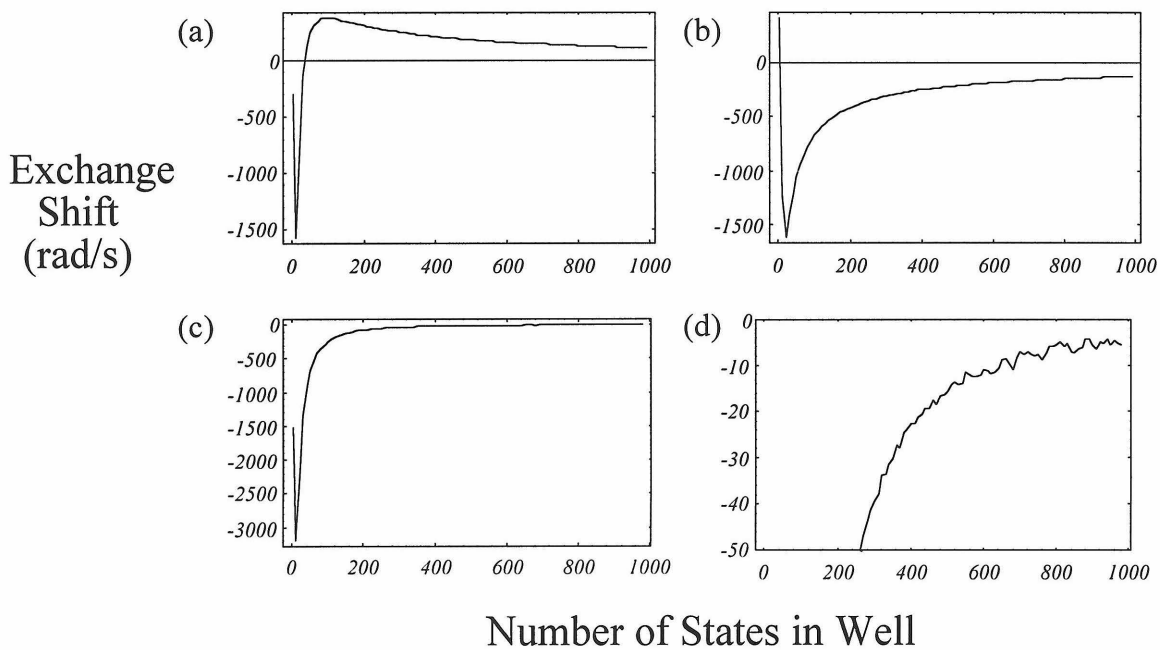

Figure 2.9. The variation of the exchange shift with number of states in the well. The shift is for each level. (a) The contribution to the exchange shift for increasing energy state. (b) The contribution to the exchange shift for decreasing energy in well. (c) The (net) exchange shift is a sum of (a) and (b). (d) An expanded view of (c).

The value of the exchange shift for a rovibrational state is plotted in Figure 2.9 versus the number of equally spaced rovibrational states in a conformer well under the assumption that only nearest-neighbor states are connected. The single-state-per-conformer value has an NMR frequency difference of 10^4 rad/s between the conformer and the transition state, a spatial energy difference of 7.63×10^{14} rad/s (48 kJ/mol), a correlation time of 10^{-14} s and an exchange rate of 2×10^4 rad/s at 300 K. The contribution to the exchange shift for a connection to a higher or lower state changes sign as the energy difference between states decreases, *i.e.*, as the number of states increases, roughly following the derivative of the imaginary component of the spectral density. Even as the number of states in the well increases to 1000, the size of the net exchange shift remains observable. Because of the assumption that the chemical shift varies linearly with energy in the well, the exchange shift is the same for all rovibrational levels within a conformer manifold. The net shift of the spectroscopic line from the traditional theory will in general be equal to the population weighted exchange shift for each conformer manifold.

The correlation time and rate at a given spatial energy splitting and temperature completely specify the kinetic model for the system. Assuming, for the sake of simplicity, a single correlation time independent of temperature, the temperature dependence of the net exchange shift for a level is determined through the use of equation (53). A plot of the net exchange shift vs. temperature is shown in Figure 2.10 for a model of a well with 7 equally spaced states. The single-state-per-conformer value has an NMR frequency difference of 10^3 rad/s, a spatial energy difference of 7.63×10^{14} rad/s (48 kJ/mol), a correlation time of 10^{-14} s and an exchange rate of 2×10^4 /s at 300 K. The net exchange shift first increases in magnitude and then decreases as the temperature increases. In the limit of infinite temperature, the net exchange shift is zero. This model would imply finite exchange shifts even in slow exchange. A more realistic model would

place the bulk of the change in chemical shift near the top of the well, giving no exchange shift in the slow-exchange region.

Exchange shifts also are anticipated in the averaging of other NMR parameters. In the case of scalar couplings, an exchange shift contribution would depend on the difference in J between the conformers and the transition state. For certain molecules, such as the substituted ethanes, continuous parametrizations of J along the reaction coordinate are well established [14], limiting the free parameters in a detailed comparison between theory and experiment. As the range of scalar couplings is typically smaller than the range of chemical shifts, it is expected that the exchange shifts are correspondingly smaller.

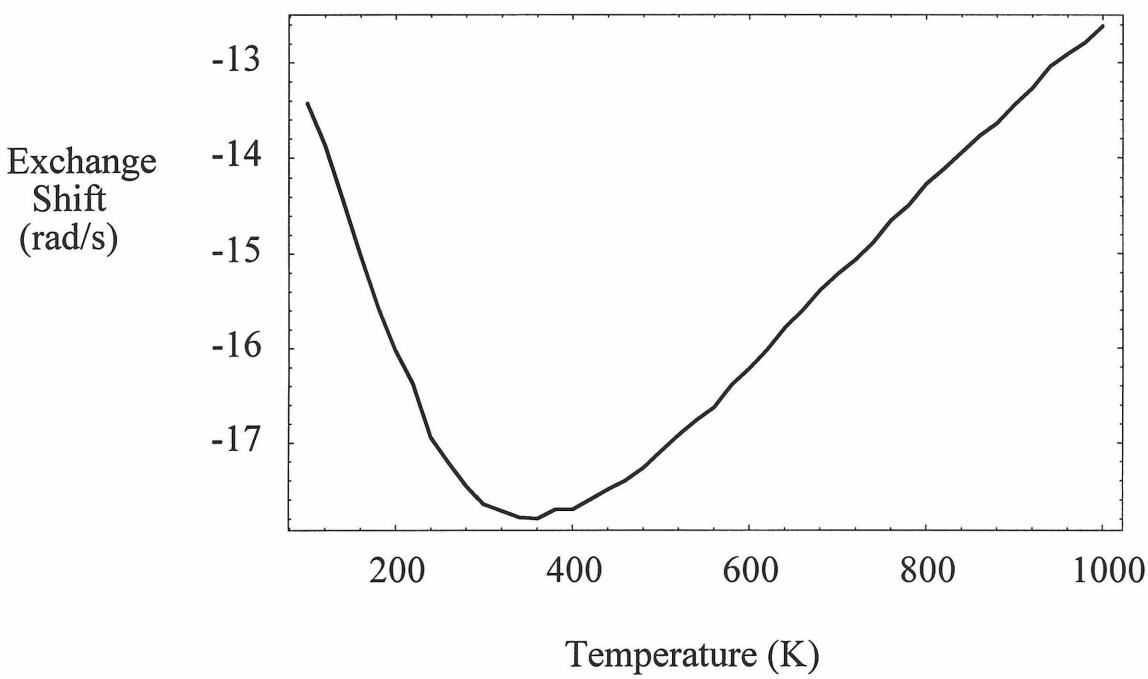

Figure 2.10. The temperature dependence of the exchange shift for one rovibrational state in one of the two conformers.

2.4 Conclusions

Magnetic resonance line positions in the presence of rapid thermal motion have long been interpreted as the spectrum of the time-averaged spin Hamiltonian. One consequence is that the perturbations responsible for the motion have a vanishing effect on the lineshape in the extreme-narrowing limit. In this chapter, a quantum-statistical treatment of chemical exchange between molecular conformations has been presented that is substantially inconsistent with this traditional picture. Previously unsuspected shifts, orders of magnitude greater than the experimental resolution, are found in the average Liouvillian describing fast exchange due to the incomplete cancellation of the imaginary components of the spectral density. The same purely spatial fluctuations responsible for chemical exchange determine these exchange shifts through a Hilbert-transform relationship. Experimental support for this theory is given in Chapter 3.

2.5 References

[1] E.L. Hahn and D.E. Maxwell "*Spin Echo Measurements of Nuclear Spin Coupling in Molecules*" Physical Review **88**(5): 1070-1084 (1952).

[2] N. Bloembergen, E.M. Purcell and R.V. Pound "*Relaxation Effects in Nuclear Magnetic Resonance Absorption*" Physical Review **73**(7): 679-712 (1948).

[3] H.S. Gutowsky, D.W. McCall and C.P. Slichter "*Nuclear Magnetic Resonance Multiplets in Liquids*" The Journal of Chemical Physics **21**(2): 279 (1953).

[4] J.N. Shoolery and B. Crawford, Jr. "*Hindered Rotation and Nonequivalent Nuclear Spin Couplings*" Journal of Molecular Spectroscopy **1**: 270-276 (1957).

[5] J.A. Pople, W.G. Schneider and H.J. Bernstein "*The Analysis of Nuclear Magnetic Resonance Spectra. II. Two Pairs of Two Equivalent Nuclei*" Canadian Journal of Chemistry **35**: 1060 (1957).

[6] J.A. Pople "*Nuclear Magnetic Resonance and Rotational Isomerism in Substituted Ethanes*" Molecular Physics **1**: 3-8 (1957).

[7] H.M. McConnell "*Reaction Rates by Nuclear Magnetic Resonance*" Journal of Chemical Physics **28**(3): 430 (1957).

[8] J. Kaplan "*Exchange Broadening in Nuclear Magnetic Resonance*" Journal of Chemical Physics **28**(2): 278 (1958).

[9] S. Alexander "*Exchange of Interacting Nuclear Spins in Nuclear Magnetic Resonance. I. Intramolecular Exchange*" The Journal of Chemical Physics **37**(5): 967 (1962).

[10] C.S. Johnson "*On the Calculation of Nuclear Magnetic Resonance Spectra for Coupled Nuclear Spins in Intramolecular Reactions*" Journal of Chemical Physics **41**: 3277-3278 (1964).

[11] J.C. Schug, P.E. McMahon and H.S. Gutowsky "*Electron Couplings of Nuclear Spins. IV. Temperature Dependence in Substituted Ethanes*" Journal of Chemical Physics **33**(3): 843 (1960).

[12] R.J. Abraham and H.J. Bernstein "*A Proton Magnetic Resonance Investigation of Rotational Isomerism in 1,1,2,2-Tetrachloro-1-Fluoroethane*" Canadian Journal of Chemistry **39**: 39 (1961).

[13] T.D. Alger, H.S. Gutowsky and R.L. Vold "*Internal Rotation in Liquid 1-Fluoro-1,1,2,2-tetrachloroethane*" The Journal of Chemical Physics **47**(9): 3130 (1967).

[14] H.S. Gutowsky, G.G. Belford and P.E. McMahon "*NMR Studies of Conformational Equilibria in Substituted Ethanes*" Journal of Chemical Physics **36**(12): 3353 (1962).

[15] R.A. Newmark and C.H. Sederholm "*NMR Determinations of Barriers to Internal Rotation in Halogen-Substituted Ethanes*" The Journal of Chemical Physics **43**(2): 602 (1965).

[16] G. Govil and H.J. Bernstein "*Application of the NMR Method to Rotational Isomerism. Limitations Revealed by Temperature-Dependent Studies on CHBr2-CFBr2*" The Journal of Chemical Physics **47**(8): 2818 (1967).

[17] R.M. Lynden-Bell "*The Calculation of Line Shapes by Density Matrix Methods*" Progress in NMR Spectroscopy **2**: 163 (1967).

[18] G. Binsch "*The Study of Intramolecular Rate Processes by Dynamic Nuclear Magnetic Resonance*" Topics in Stereochemistry **3**: 97 (1968).

[19] G. Binsch "*A Unified Theory of Exchange Effects of Nuclear Magnetic Resonance Line Shapes*" Journal of the American Chemical Society **91**(6): 1304-1309 (1969).

[20] F. Heatley and G. Allen "*An NMR Investigation of Rotational Isomerism in Some Halogenated Ethanes*" Molecular Physics **16**: 77-89 (1969).

[21] W.-C. Lin "*Dependence of Vicinal H-H Coupling Constants in Substituted Ethanes on the Potential Function Characteristics to Internal Rotation. Application to A2B2 PMR Spectrum of Nonsymmetrical 1,2-Disubstituted Ethanes.*" The Journal of Chemical Physics **52**(6): 2805 (1970).

[22] A.J. Vega and D. Fiat "*Relaxation Theory and the Stochastic Lioville Equation*" Journal of Magnetic Resonance **19**: 21-30 (1974).

[23] S. Szymanski, M. Witanowski and A. Gryff-Keller "*Problems in Theory and Analysis of Dynamic Nuclear Magnetic Resonance Spectra*" Annual Reports on NMR Spectroscopy **8**: 227 (1978).

[24] G. Binsch and H. Kessler "*The Kinetic and Mechanistic Evaluation of NMR Spectra*" Angewandte Chemie **19**(6): 411-494 (1980).

[25] K.G.R. Pachler and P.L. Wessels "*Rotational Isomerism. A Gas-Phase ^1H Nuclear Magnetic Resonance Study of 1-Bromo-2-Chloroethane*" Journal of Molecular Structure **68**: 145-159 (1980).

[26] J. Jeener "*Superoperators in Magnetic Resonance*" Advances in Magnetic Resonance **10**: 1-51 (1982).

[27] R.G. Gordon and R.P. McGinnis "*Line Shapes in Molecular Spectra*" Journal of Chemical Physics **49**: 2455-2456 (1968).

[28] K. Blum Desity Matrix Theory and Applications New York, Plenum Press (1981).

[29] C. Cohen-Tannoudji "*Atoms in Strong Resonant Fields*" in Frontiers in Laser Spectroscopy Amsterdam, North-Holland Publishing Company First, ed. 3-102 (1977).

[30] P. de Bree and D.A. Wiersma "*Application of Redfield Theory to Optical Dephasing and Line Shape of Electronic Transitions in Molecular Mixed Crystals*" Journal of Chemical Physics **70**(2): 790-801 (1979).

[31] P.H. de Bree "*Optical Relaxation in Organic Impurity Crystals*" Ph.D. Thesis, Department of Physics, University of Groningen (1981).

[32] K.E. O'Hara and C.T. Slichter "*Reexamination of Motional Averaging in Magnetic Resonance*" Journal of Magnetic Resonance, Series A **109**: 74-79 (1994).

[33] A. Abragam Principles of Nuclear Magnetism Oxford, Clarendon Press (1961).

[34] R.A. Hoffman "*Line Shapes in High-Resolution NMR*" Advances in Magnetic Resonance **4**: 87-200 (1970).

[35] A.G. Redfield "*The Theory of Relaxation Processes*" Advances in Magnetic Resonance **1**(1): 1-32 (1965).

[36] S. Szymanski, A.M. Gryff-Keller and G. Binsch "*A Liouville Space Formulation of Wangsness-Bloch-Redfield Theory of Nuclear Spin Relaxation Suitable for Machine Computation. I. Fundamental Aspects*" Journal of Magnetic Resonance **68**: 399-432 (1986).

[37] R.K. Wangsness and F. Bloch "*The Dynamical Theory of Nuclear Induction*" Physical Review **89**(4): 728-739 (1953).

[38] S. Mukamel Principles of Nonlinear Optical Spectroscopy New York, Oxford University Press (1995).

[39] M. Goldman "*Introduction to Some Basic Aspects of NMR*" in Nuclear Magnetic Double Resonance Amsterdam, North-Holland Elsevier Science Publishers B.V. 1st, ed. 1-66 (1993).

[40] G. Arfken Mathematical Methods for Physicists San Diego, Academic Press (1985).

[41] C.P. Slichter Principles of Magnetic Resonance Berlin, Springer-Verlag (1989).

[42] M. Abramowitz and I. Stegun, A. Handbook of Mathematical Functions New York, Dover Publications (1972).

[43] S. Wolfram Mathematica: A System for Doing Mathematics by Computer Reading, Massachusetts, Addison-Wesley Publishing Company (1991).

[44] L. Werbelow and R.E. London "*Dynamic Frequency Shift*" Concepts in Magnetic Resonance **8**(5): 325-328 (1996).

[45] L.G. Werbelow "*NMR Dynamic Frequency Shifts and the Quadrupolar Interaction*" Journal of Chemical Physics **70**: 5381-5383 (1979).

[46] N. Tjandra, S. Grzesiek and A. Bax "*Magnetic Field Dependence of Nitrogen-Proton J Splittings in 15N-Enriched Human Ubiquitin Resulting from Relaxation Interference and Residual Dipolar Coupling*" Journal of the American Chemical Society **118**: 6264-6272 (1996).

[47] R. Ditchfield "*Self-Consistent Perturbation Theory of Diamagnetism. I. A Gauge-Invariant LCAO Method for NMR Chemical Shifts*" Molecular Physics **27**(4): 789-807 (1974).

[48] R. Ditchfield and P. Ellis "*Theory of C-13 Chemical Shifts*" in Topics in Carbon-13 NMR Spectroscopy New York, Wiley-Interscience 1-51 (1976).

[49] E. Oldfield "*Chemical-Shifts and 3-Dimensional Protein Structures*" Journal of Biomolecular NMR **5**(3): 217-225 (1995).

3. An Experimental Test of the Theories for Chemical Exchange In NMR: Methylcyclohexane in Solution

3.1 Introduction

One of the major contributions of nuclear magnetic resonance to molecular physics has been the determination of thermodynamic and kinetic properties of dynamic systems. For such a significant contribution, it is surprising that the traditional theory for extracting this information is not incontestable. A careful examination of the NMR literature shows that the traditional theory relating average line positions to thermodynamic quantities has never been tested to the accuracy possible. Poor agreement with the traditional theory is often plausibly attributed to an unknown temperature dependence of the NMR parameters and, with no alternative theory, has not been further scrutinized. To critically test theories of chemical exchange requires detailed knowledge of the conformer spectral parameters, exchange rates, and equilibrium populations throughout the slow, intermediate and fast-exchange regions. In favorable circumstances, these properties can be extrapolated to fast exchange from the measured slow-exchange spectra, although most often there is incomplete information and a rigorous test of the theory is not possible.

In this chapter, an experimental study of the dynamic averaging of ^{13}C chemical shifts in methylcyclohexane (Figure 3.1) in solution is presented and compared with the traditional and exchange-shift theories. Methylcyclohexane exhibits two-site exchange between the equatorial (major) and axial (minor) conformers shown in Figure 3.2 and is

favorable for the accuracy to which it allows a comparison between theory and experiment. In particular, the measurement of slow-exchange spectra over a 50 degree range of temperatures permits an accurate measurement of the conformer free energy difference and chemical shifts. The measured linear temperature dependence of the chemical shifts, coupled with previous variable-temperature measurements on the model compounds *cis*- and *trans*-1,4-dimethylcyclohexane [1], allow a linear extrapolation of the chemical shifts to the fast-exchange region.

Former studies of chemical exchange in methylcyclohexane [1-4] have too few slow-exchange temperature points to stringently test the traditional theory. The data presented in this chapter are the most extensive to date and rule out the traditional theory with greater than 99.99% confidence limits. This is shown to necessitate considering models with additional parameters. The exchange-shift model presented in Chapter 2 is shown to allow an interpretation consistent with the data.

Section 3.2 begins with a description of the experimental procedures used to collect the variable-temperature ^{13}C NMR spectra. A statistical analysis of these spectra and the extraction of spectral and molecular properties is presented in Section 3.3. A

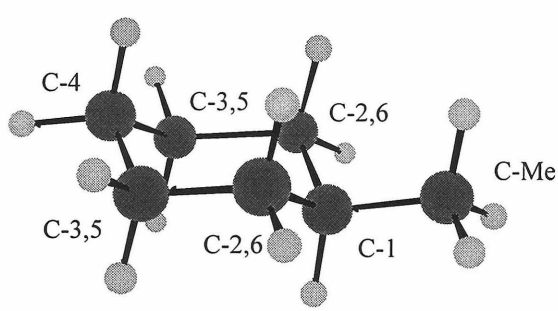

Figure 3.1. Methylcyclohexane with site labels indicated.

comparison between the observed fast-exchange data and the predictions of the traditional and exchange-shift theories is made in Section 3.4, and confidence limits are placed on models based on these theories through a global fit to the experimental results.

3.2 ^{13}C Variable-Temperature NMR Experiments on Methylcyclohexane

3.2.1 Sample Preparation

All key experiments described in this thesis were performed on a single sample consisting of a 2:1:1 mixture by volume of methylcyclohexane (Aldrich), CS_2 (Aldrich), and toluene-d_8 (Aldrich). This sample is approximately 4 M in methylcyclohexane. The NMR tube was sealed under vacuum.

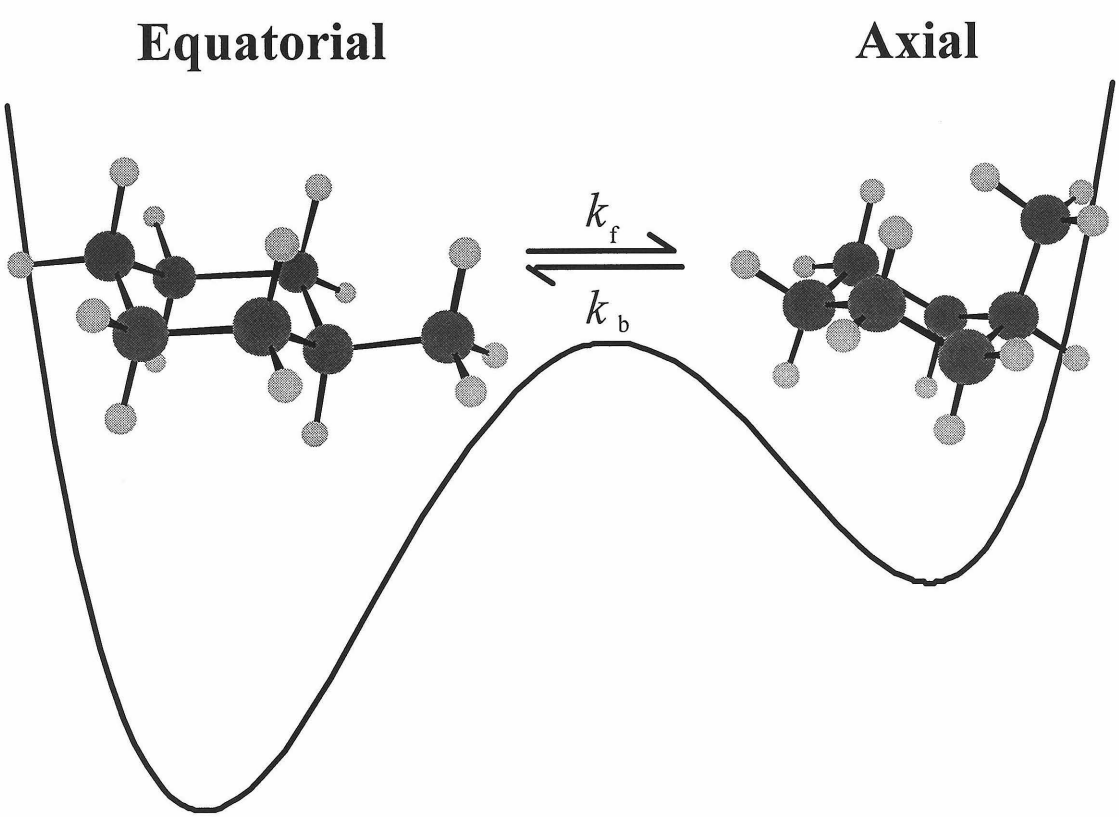

Figure 3.2. Chemical exchange in methylcyclohexane.

3.2.2 Modification of Apparatus

The variable-temperature NMR spectra of methylcyclohexane were collected on a Bruker AMX-500 spectrometer with a ^{13}C frequency of 125.7633 MHz. To observe the full range of chemical-exchange lineshapes, spectra were collected between 150 K and 300 K. In the low-temperature regime, portable glove bags were attached to the magnet,

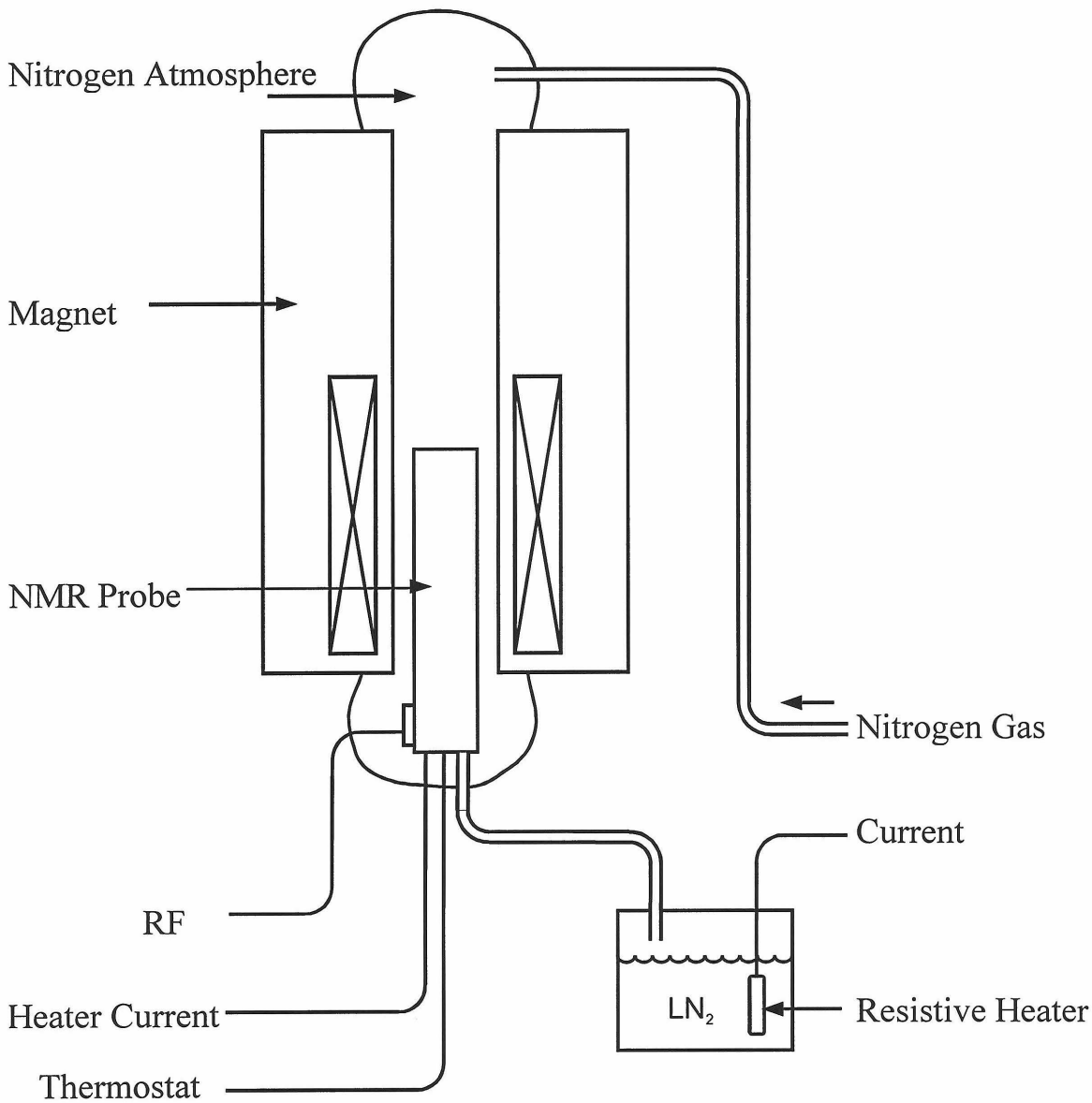

Figure 3.3. Apparatus for low-temperature NMR.

sealing the probe and the top of the bore tube as shown in Figure 3.3. Nitrogen purge gas was continually fed to the bags to prevent the buildup of ice within the bore tube and on the probe. The tuning and matching capacitors for the probe eventually lock due to differential contraction of their components, so, to prevent damage, they were not changed below 240 K.

3.2.3 Temperature Calibration

The temperature of the sample was initially determined with a methanol chemical shift thermometer [5-7] that makes use of a quadratic fit to the temperature dependence of the chemical shift difference between the methyl and hydroxyl protons. For operation at 500 MHz, the relationship between temperature and frequency difference $\Delta\nu$ is

$$T = 406 - 0.0661|\Delta\nu| - \left(\frac{\Delta\nu}{104.66}\right)^2. \tag{83}$$

The chemical shifts of methylcyclohexane were observed to be temperature dependent in

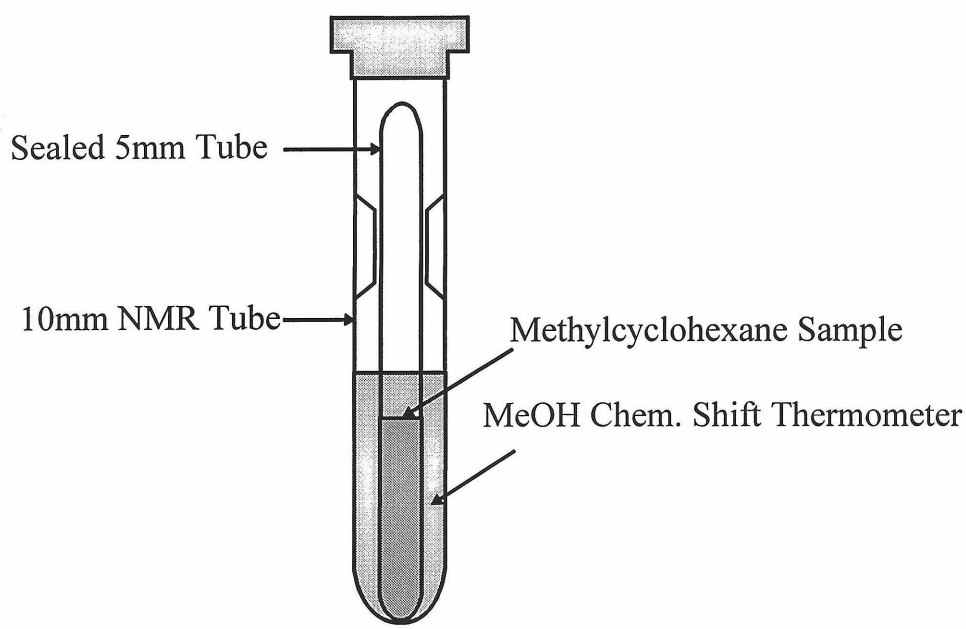

Figure 3.4. Double-tube assembly for NMR temperature calibration.

the slow-exchange region in agreement with earlier observations [1,2]. This temperature dependence was used to provide a convenient internal NMR thermometer. The difference in chemical shift between C-2,6 and C-Me was found to have the greatest temperature dependence and was calibrated using a 10 mm double tube assembly in which the sealed 5 mm methylcyclohexane sample tube sat within an outer tube of methanol as shown in Figure 3.4. The chemical shift difference of C-2,6 and C-Me was then measured as a function of methanol chemical shift difference. A linear fit of the frequency difference of C-2,6 and C-Me to temperature gives

$$T = -1851.29 + 1.34657\,\Delta\nu, \tag{84}$$

with standard errors of 7.50 and 0.004981 for the intercept and slope respectively. The errors are highly correlated, with a covariance of -0.037378, so that at 180 K there is an associated error of only 0.35 K. The fit and residuals are shown in Figure 3.5. The methylcyclohexane chemical shift thermometer was used to measure the temperature of

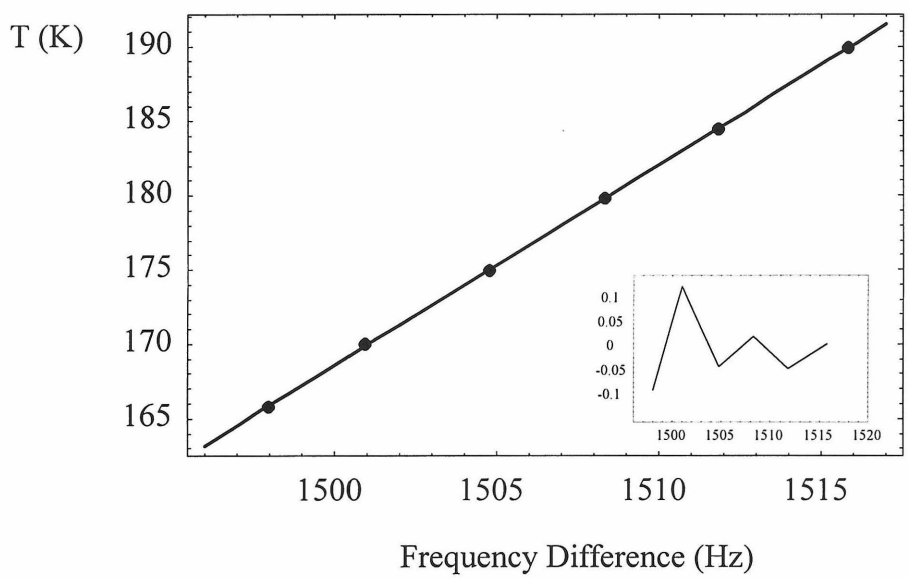

Figure 3.5. Calibration of the methylcyclohexane chemical shift thermometer. The temperature from the methanol chemical shift thermometer is plotted versus the chemical shift difference between C-2,6 and C-Me of the major conformer. Residuals for the fit are shown in the inset.

the methylcyclohexane slow-exchange spectra between 150 K and 190 K. The double-tube assembly was used again to measure the temperature in intermediate and fast exchange.

3.2.4 The DEPT and Interleaved DEPT Experiments

The ^{13}C NMR spectra of methylcyclohexane were measured using the distortionless enhancement of polarization technique (DEPT) to transfer polarization from ^{1}H to ^{13}C [8]. The pulse sequence for the DEPT experiment is shown in Figure 3.6a. Setting the delays between pulses to $1/(2J_{CH})$ maximizes the polarization transfer. J_{CH} was measured to be 124 Hz for all major conformer carbon sites in methylcyclohexane. The dependence of the signal amplitude on the final proton flip angle β is determined by the number of coupled protons as shown in Figure 3.6b. The majority of the experiments reported here were run with $\beta = \pi/4$ for positive intensities for all carbon peaks. In some later experiments β was changed during the experiment between $\pi/4$ and $3\pi/4$ and the free induction decays were saved separately. The free induction decays were later added to give a spectrum with only C-1 and C-Me resonances, and subtracted to give only C-2,6, C-3,5 and C-4 resonances. This interleaved DEPT experiment allows the observation of two minor peaks otherwise obscured by overlap with major peaks; the minor peak of C-1 sits in the base of the major peak of C-3,5, and the minor form of C-3,5 overlaps the residual single protonated solvent peak.

In these experiments, proton decoupling was performed during acquisition using the multiple pulse sequence WALTZ-16 [9,10]. The power of the decoupling pulses was set by an attenuation of the primary amplifier of 15-35 dB, resulting in $\pi/2$ pulses of 24-110 μs for proton. For other parts of the pulse sequence, $\pi/2$ pulses were typically 9 μs for proton and 16 μs for carbon.

3.2.5 ^{13}C and ^{1}H Relaxation Times

The longitudinal relaxation times at several temperatures were measured for the various proton and carbon sites. At 300 K, proton T_1's varied from 3.3 - 3.5 s, while at 180 K they were between 0.3 and 0.55 s. At 143 K they ranged from 0.14 to 0.25 s.

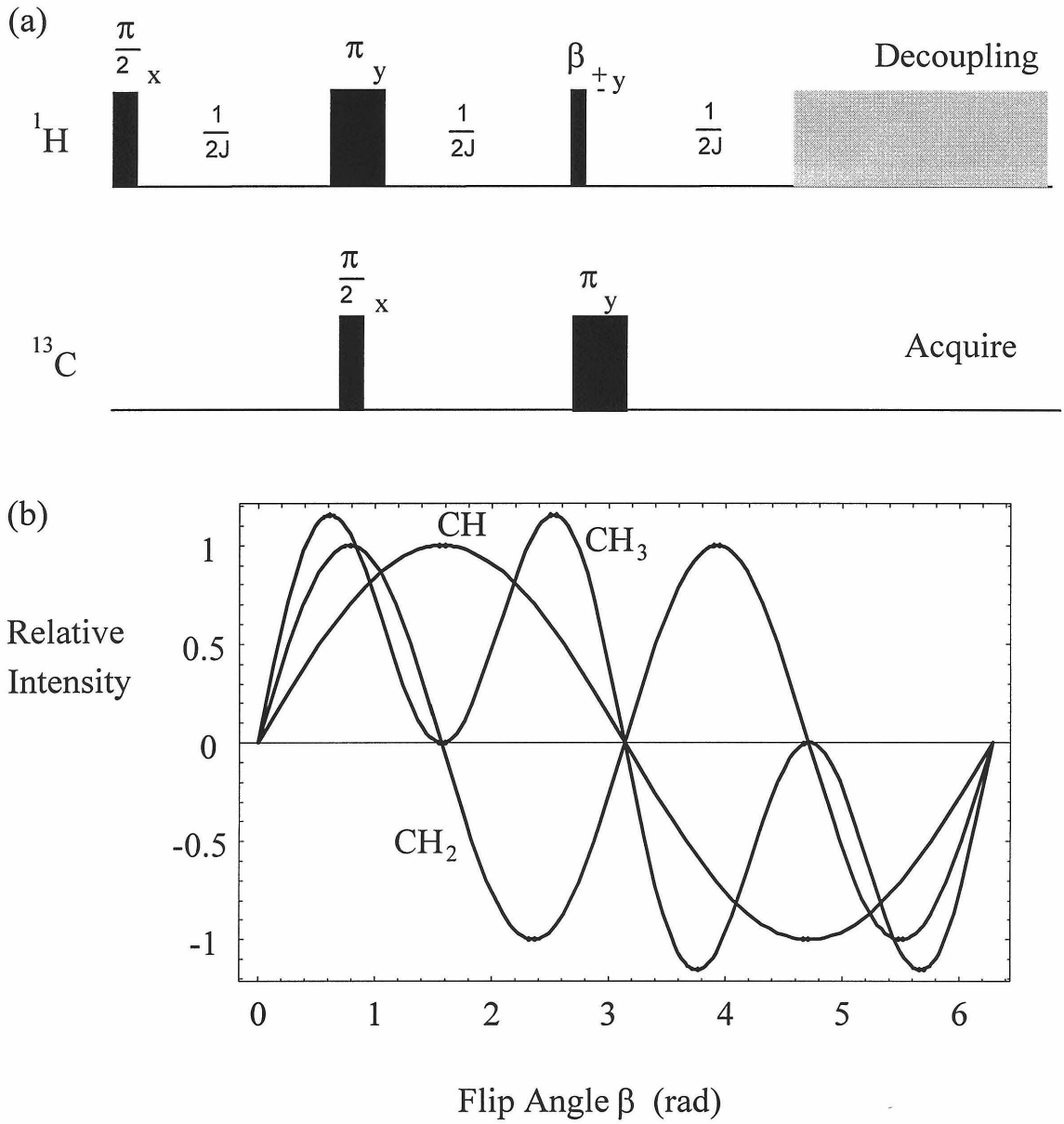

Figure 3.6. The DEPT experiment. (a) Pulse sequence for DEPT polarization transfer. (b) Amplitude dependence on the final proton flip angle for the three carbon groups.

Carbon T_1's varied from 10.8 - 16.1 s at 300 K, 1.2 - 2.4 s at 180 K, and 0.17 s to 0.4 s at 143.5 K. As polarization is transferred to carbon from proton in the DEPT experiment, the observed signal intensities depend on the equilibrium proton magnetization. The relaxation delay between experiments was chosen so that the proton magnetization would recover to equilibrium after the end of the decoupling during acquisition. Typical relaxation delays after the end of decoupling were 2 to 8 s.

3.2.6 Spectrometer and Filter Response

The spectrometer response to input signals of differing size was found to be linear under operating conditions similar to those of the methylcyclohexane slow-exchange experiments. The response was measured using a .05% solution of methylcyclohexane (major conformation) in cyclohexane to give concentrations approximately equal to the major and minor conformers. The falloff of the spectrometer filter was measured and intensity corrections of up to 3% were found for the outermost resonances.

3.3 Chemical Exchange in Methylcyclohexane

The linearity of the temperature dependence of the chemical shifts in the methylcyclohexane conformers allows a convenient extrapolation from slow to fast exchange. This procedure is further justified by the observation that the model compounds *cis*- and *trans*-1,4-dimethylcyclohexane have chemical shifts that are linear in temperature over a 120 K range [1]. In these analogs there are negligible chemical exchange effects on the linewidths over this range. Previous studies of chemical exchange in methylcyclohexane [1-4] have too few measurements of slow-exchange populations to predict fast-exchange averages with sufficient precision. Although recently considered by Anet and Freedburg [2] as consistent with the traditional theory, the study by Anet and Basus [1] allows such large uncertainty in the prediction of the

fast-exchange averages that a more extensive study at higher magnetic field was warranted.

In this section, data and a statistical analysis are presented over the full range of chemical exchange in methylcyclohexane. In Section 3.3.1, the slow-exchange temperature-dependent spectra are analyzed for the conformer chemical shifts and equilibrium populations. In Sections 3.3.2 and 3.3.3, data on intermediate and fast exchange are presented. These data are used in Section 3.4 for a critical test of the traditional and exchange-shift theories for chemical exchange in NMR.

3.3.1 Slow Exchange

In slow exchange, where the rate of interconversion between the axial and equatorial forms of methylcyclohexane is slow compared to the difference in their chemical shifts, sharp spectral lines are observed for both the major and minor conformers as shown in Figure 3.7. As seen in the inset, the axial conformer is present at much lower concentration than the equatorial conformer, with a ratio of peak areas of about 0.5%.

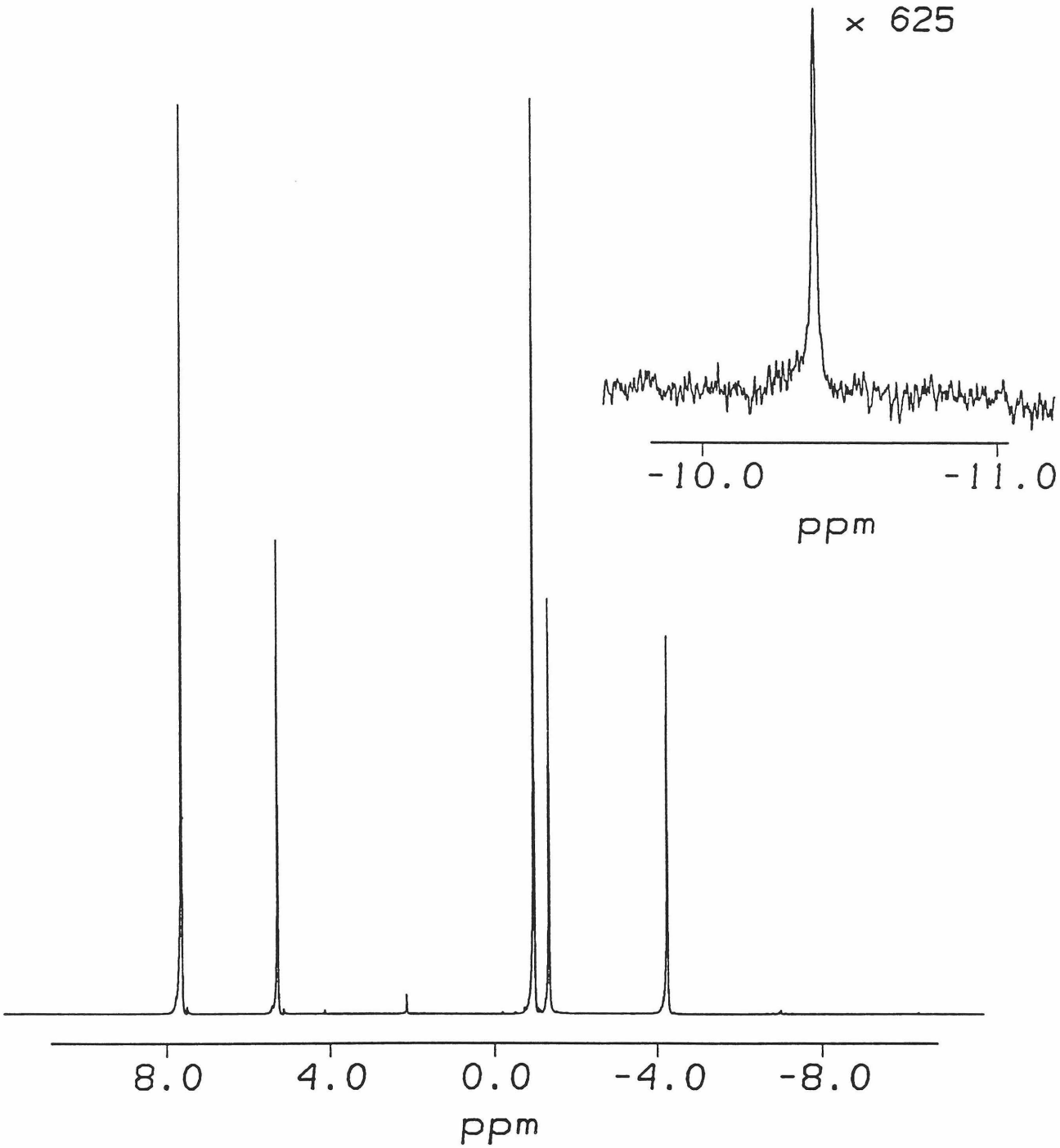

Figure 3.7. The slow exchange ^{13}C spectrum of methylcyclohexane.

To accurately extract the conformer probabilities, chemical shifts and linewidths, a nonlinear least squares fitting procedure was used. In the region of a line, the spectrum was modeled as a composite curve consisting of a linear baseline and a Lorentzian peak. In the case of inhomogeneously broadened NMR lines of different widths, the Monte Carlo simulations discussed in Appendix B show that the lineshape must be corrected first to accurately determine the ratio of the line areas. Since fitting to a composite curve is sensitive to small deviations of the signal from the model [11], the reference deconvolution algorithm of Morris [12] was incorporated. Reference deconvolution uses a reference line within the spectrum to remove global broadening and asymmetric features, such as the effect of magnet inhomogeneity, from the experimental lines. A well isolated, large signal-to-noise peak is first chosen as the reference peak and the remainder of the spectrum is nulled. A best-fit Lorentzian is then found by a least-squares fit to this experimental line with the line position, intensity and width as parameters. A time-domain correction function is produced by dividing the inverse Fourier transform (IFT) of this fit by the IFT of the reference peak. As the fit and experimental free induction decays (FIDs) have both real and imaginary components, the magnitude of the denominator is in practice always finite. The filter is then used to correct all the lines in the spectrum by multiplication with the experimental FID. This is equivalent to deconvoluting the reference lineshape from each line of interest. The algorithm for this procedure was incorporated as a macro into Biosym Corporation's FELIX NMR processing software. As the time-domain filter can become quite large and uncertain near the end of the FID, an exponential apodization was applied to all time-domain signals. In the frequency domain, this corresponded to having convoluted the data with a 1 Hz wide (FWHM) Lorentzian.

In estimating the effect of spectrometer noise on the accuracy of derived quantities, the effect of these manipulations must be taken into account since they lead to

an apparent reduction in noise which does not in fact lead to more accurate line areas. The best estimate of the errors in the fit parameters must in effect be calculated on the unmanipulated data set. This is true for calculating the errors in any least-squares data fit; the errors in the best fit parameters must be extracted from the unmanipulated data set. The fit, however, may be performed on a manipulated data set. Appendix B discusses data manipulation and the processing of NMR spectra, using the technique of Monte Carlo simulation to determine the effect of data manipulations on the standard errors associated with an NMR measurement.

3.3.1.1 Temperature Dependence of the Chemical Shifts

In methylcyclohexane, C-4 has a negligible chemical shift difference between its equatorial and axial forms. Its spectral line remains sharp throughout the entire range of chemical exchange, making it a convenient internal reference for chemical shift. In all subsequent discussion, a shift labeled by another site is in fact a shift in the difference between the resonance position of that site and C-4. The linear least-squares fits of the ^{13}C chemical shifts to temperature for the various sites in methylcyclohexane relative to C-4 are shown in Figure 3.8-Figure 3.11 and summarized in Table 3.1. For each of these spectra, the temperature was measured using the methylcyclohexane chemical shift thermometer of equation (84). For these fits, the errors in the slope and intercept are strongly correlated. Thus, to propagate the error in the fit line position the covariance must be considered. For a general two-parameter fit of a function $G(x)$ to the parameters A and B, the standard error in G is given by the standard errors in A and B, s_A and s_B, respectively, and their covariance s_{AB}^2,

$$s_G^2 = \left(s_A^2 \left(\frac{\partial G}{\partial A} \right)^2 + s_B^2 \left(\frac{\partial G}{\partial B} \right)^2 + s_{AB}^2 \frac{\partial G}{\partial A} \frac{\partial G}{\partial B} \right). \tag{85}$$

Table 3.1 summarizes this analysis. The reduced chi-squared, χ_r^2, values listed suggest that spectrometer noise is largely responsible for the uncertainty in shifts. The standard errors listed are scaled to correspond to $\chi_r^2=1$, thus reflecting the observed scatter and including other possible sources of error.

Table 3.1. Least-Squares fit values for the linear temperature dependence of the carbon chemical shifts in methylcyclohexane. The standard errors and covariance are calculated after a multiplicative factor is used to adjust the standard deviations of each data set to give $\chi_r^2 = 1$.

	Slope	Intercept	Standard Error Slope	Standard Error Intercept	Covariance	χ_r^2
C-Me (eq)	-0.475128	-287.731	0.000512676	0.0881293	-0.0000450228	1.57
C-Me (ax)	-0.243468	-1095.75	0.00114575	0.196282	-0.000224432	0.93
C-1 (eq)	0.00190288	833.708	0.000889973	0.152987	-0.000135675	4.73
C-1 (ax)	-0.0775713	158.21	0.00190638	0.318669	-0.000605909	0.70
C-2,6 (eq)	0.2675	1087.09	0.000512676	0.0881293	-0.0000450228	1.57
C-2,6 (ax)	0.197548	657.654	0.0010507	0.178683	-0.000187296	3.03
C-3,5 (eq)	0.0461793	39.8617	0.000339592	0.058376	-0.0000197542	0.69
C-3,5 (ax)	-0.0202087	-706.924	0.00147978	0.248948	-0.000367432	1.57

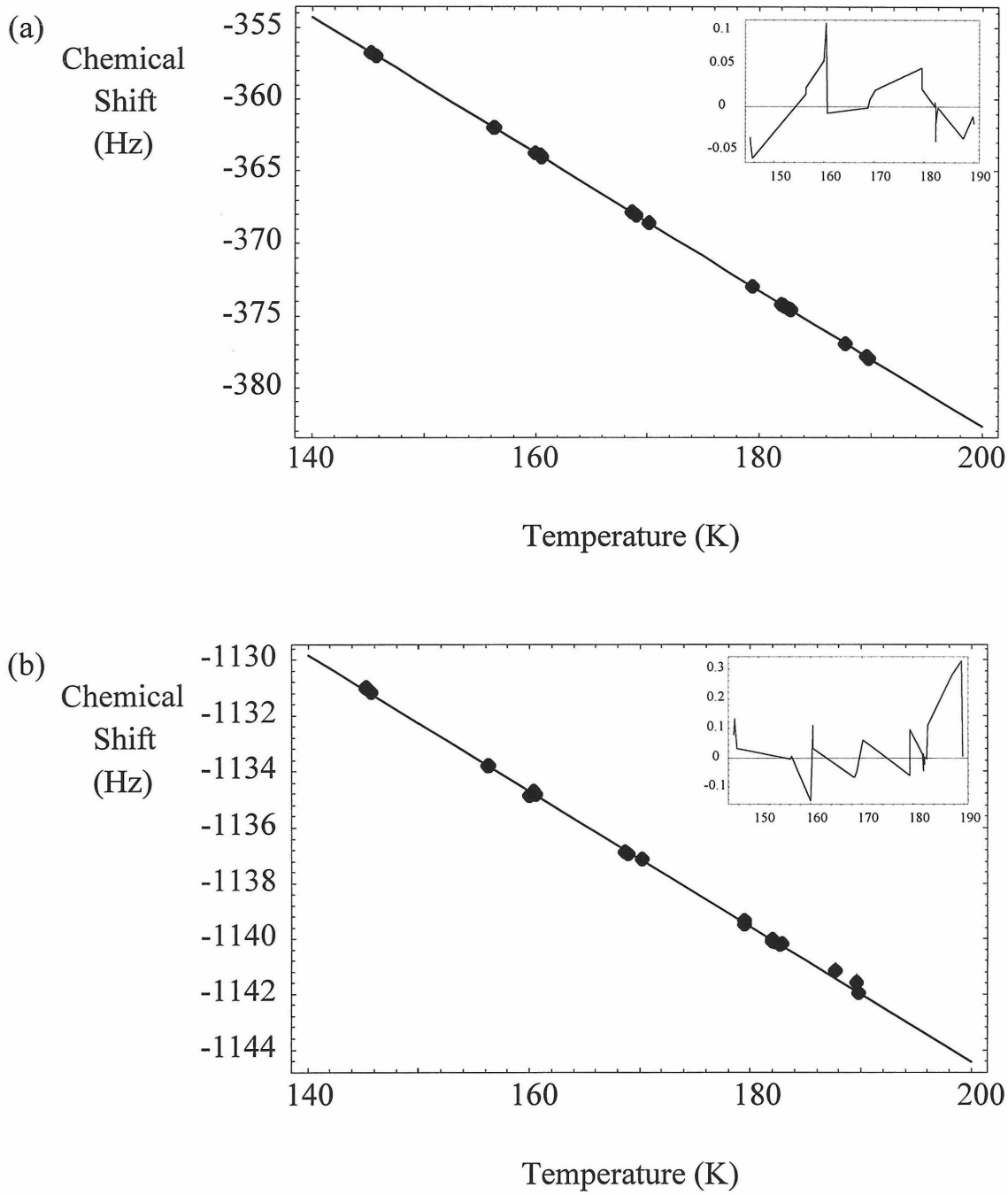

Figure 3.8. Chemical shift of C-Me versus temperature. (a) The major conformer. (b) The minor conformer. The least-squares fit to a straight line is shown and the residuals are given in the inset. Note that the vertical scales differ for the various sites and in Figure 3.8-Figure 3.11.

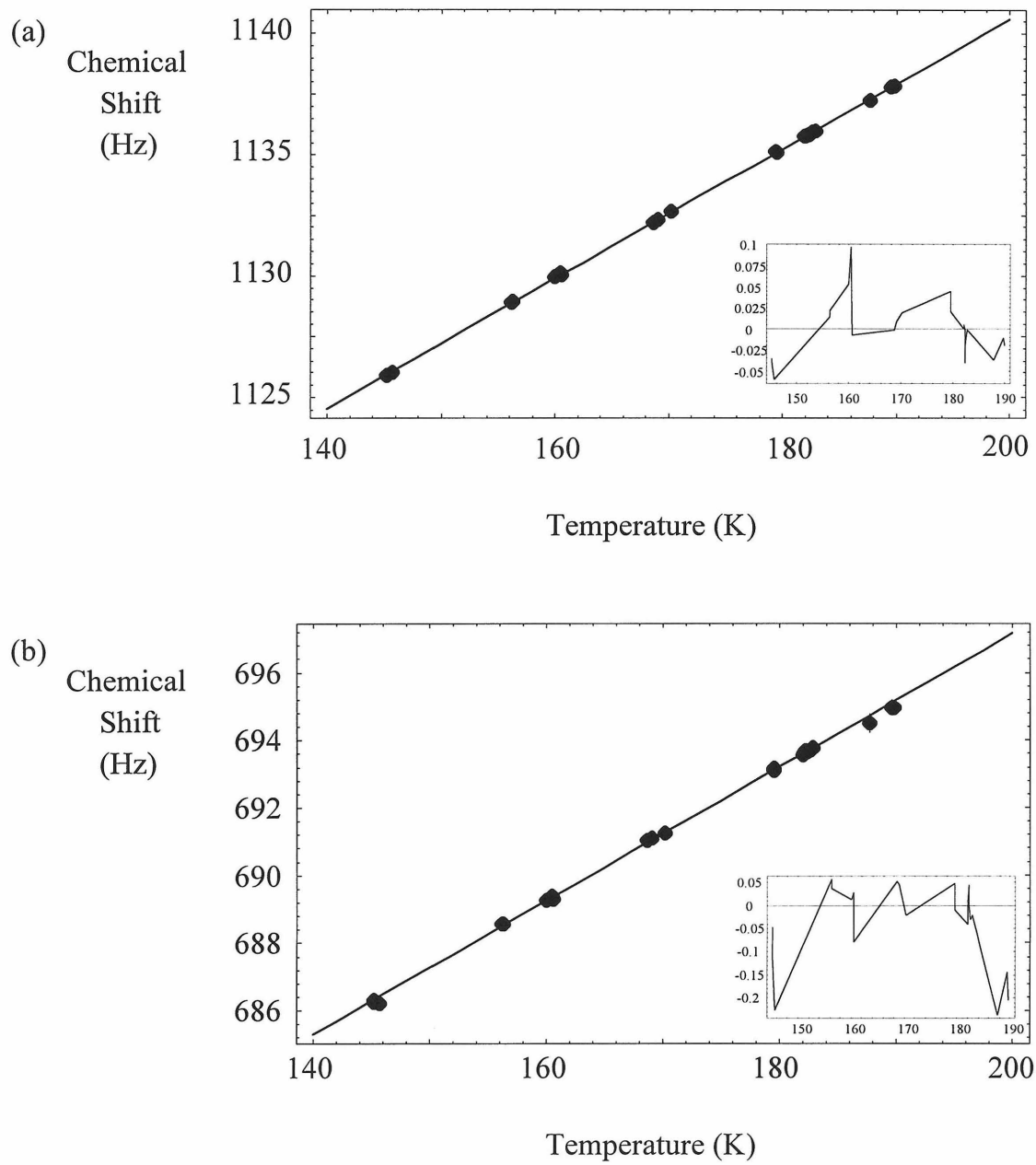

Figure 3.9. Chemical shift of C-2,6 versus temperature. (a) The major conformer. (b) The minor conformer. The least-squares fit to a straight line is shown and the residuals are given in the inset.

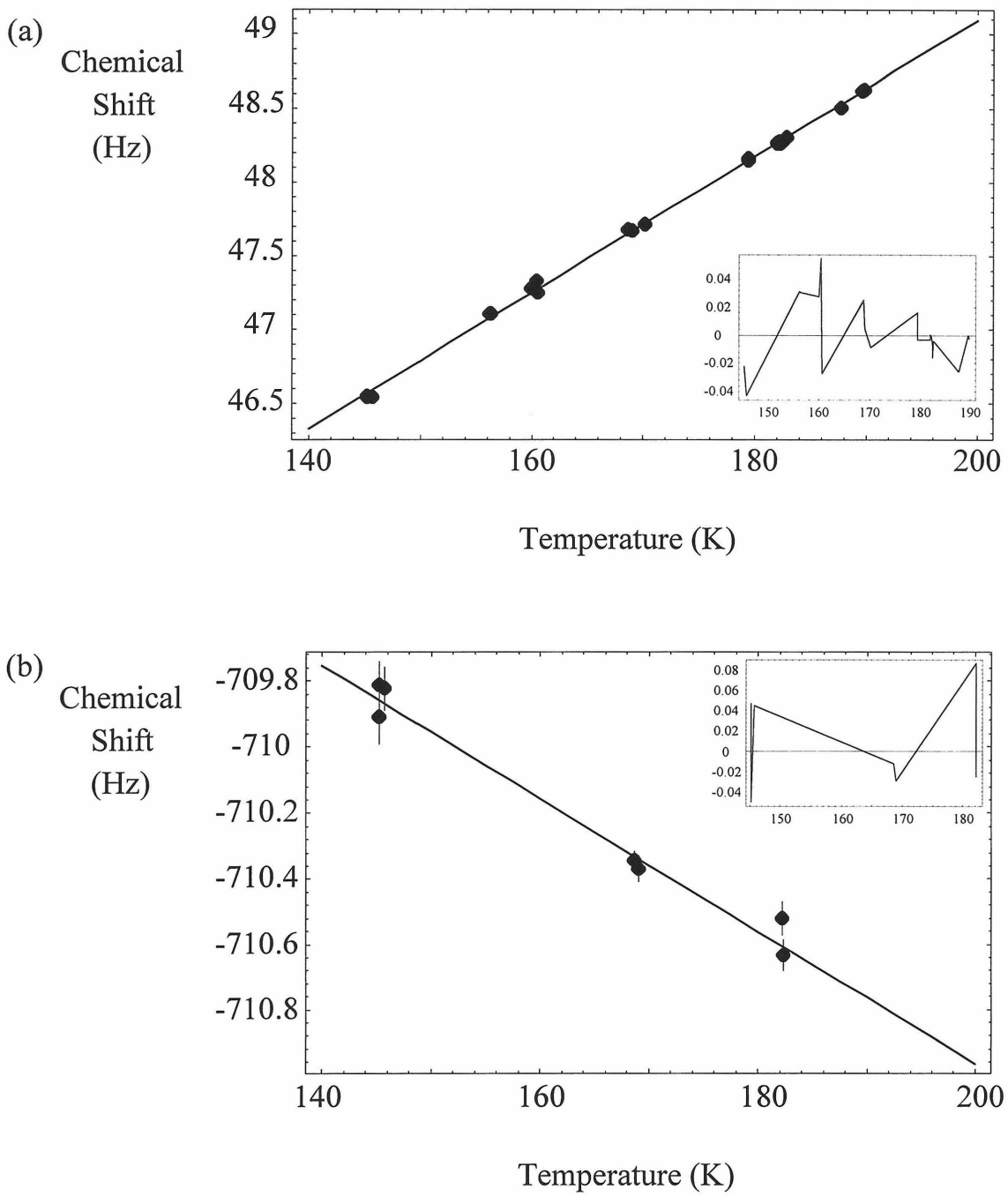

Figure 3.10. Chemical shift of C-3,5 versus temperature. (a) The major conformer. (b) The minor conformer. The least-squares fit to a straight line is shown and the residuals are given in the inset.

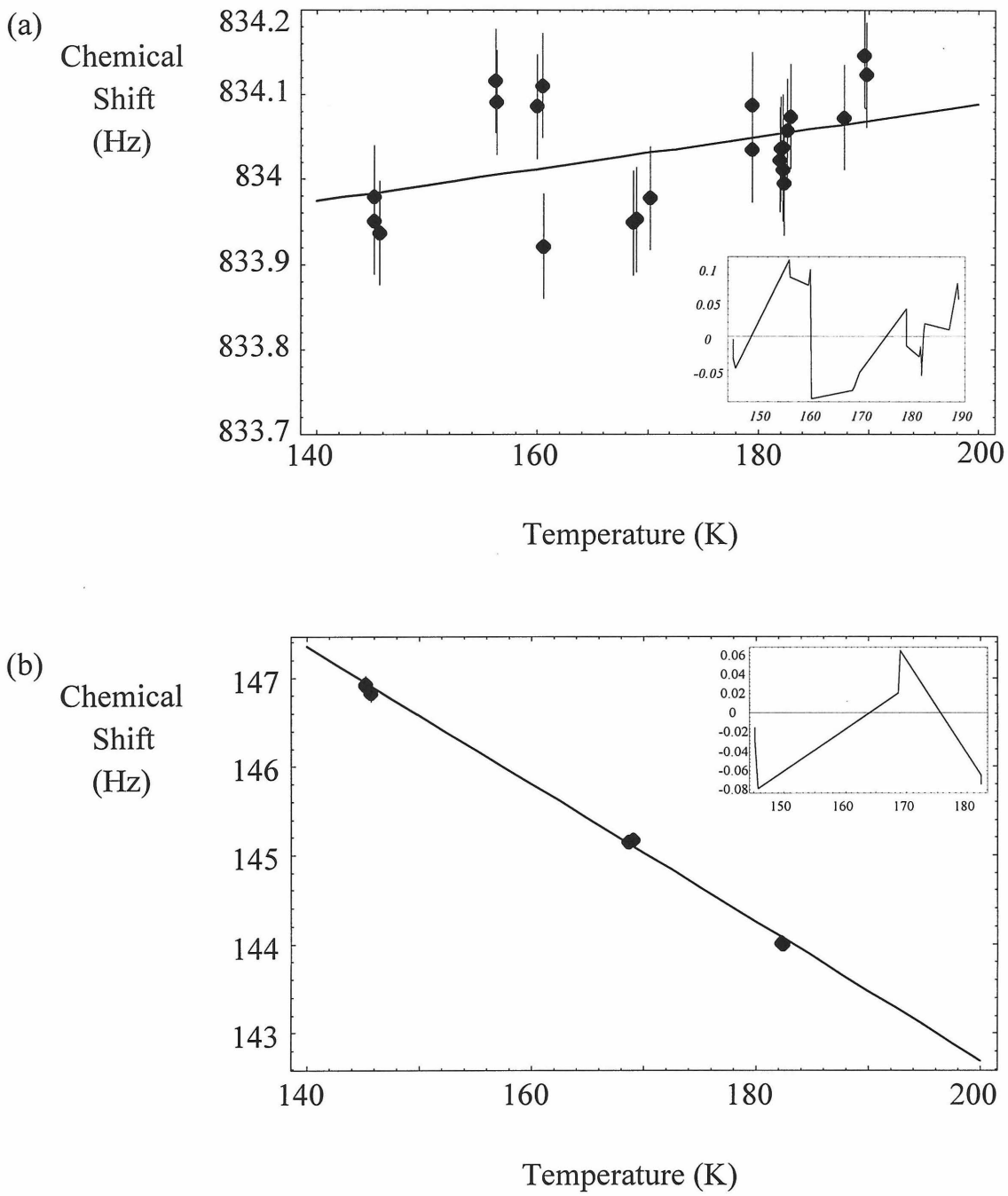

Figure 3.11. Chemical shift of C-1 versus temperature. (a) The major conformer. (b) The minor conformer. The least-squares fit to a straight line is shown and the residuals are given in the inset.

3.3.1.2 Equilibrium Populations and Free Energy Differences

The ratio of equilibrium populations of the minor and major conformers of methylcyclohexane was determined by fitting the slow-exchange spectra and taking the ratio of peak areas. Again, the standard errors for the fit values were calculated using the unmanipulated data sets, while to accurately determine the ratio of peak areas the lineshape correction algorithm was incorporated. Figure 3.12 is a plot of the ratio of conformer populations *vs.* temperature using the data for all resolved carbon sites. A nonlinear least-squares fit of the equilibrium constant to the free energy relationship was performed using a program written in *Mathematica*. The errors in the fit parameters were determined by the standard errors in the ratio of populations. Table 3.2 lists the fit values

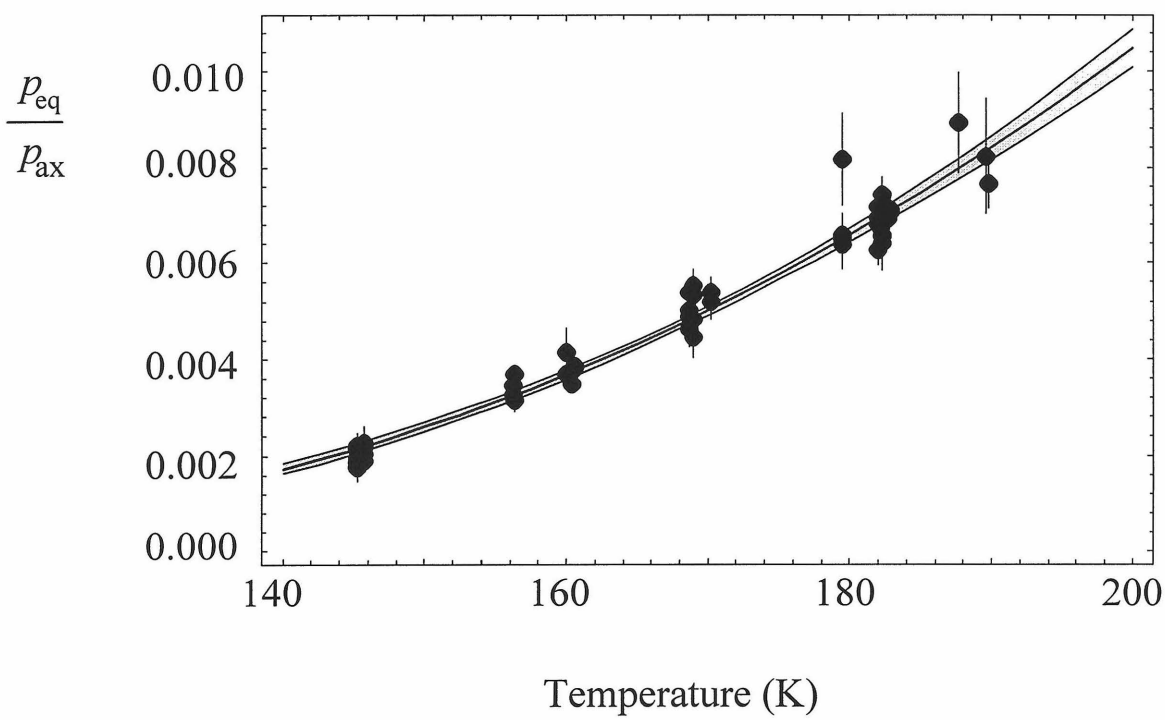

Figure 3.12. The ratio of the equilibrium conformer populations versus temperature. The least-squares fit to a Boltzmann population relationship given by a Helmholtz energy difference between the conformers is shown as the center line. The shaded area depicts the 95% confidence region.

Table 3.2. Least-Squares fit values and standard errors for the Helmholtz energy difference between the axial and equatorial conformers of methylcyclohexane. The standard errors and covariance for C-2,6 are calculated by first scaling the standard errors of the data to give χ_r^2=1.

Fit	ΔE (J/mol)	ΔS (J/mol•K)	Standard Error in ΔE	Standard Error in ΔS	Covariance	χ_r^2
C-Me	6788.0	-4.15	268	1.54	410.287	1.00
C-2,6	6889.5	-3.30	223	1.30	289.311	2.23
C-1, C-3,5	7091.2	-2.59	253	1.50	377.037	1.04
All Carbons	6956.0	-3.12	140	0.81	113.358	1.14

resulting from a fit of the equilibrium constant K_{eq} to a Helmholtz energy difference according to

$$K_{eq} = \frac{p_{ax}}{p_{eq}} = \exp\left(-\frac{\Delta E - T\Delta S}{RT}\right). \tag{86}$$

The fit was performed for sites C-2,6 and C-Me separately and for sites C-1 and C-3,5 together to see if the standard errors in the populations were consistent with the hypothesis that spectrometer noise is the dominant source of error. The χ_r^2 values show that the errors in the data are consistent with this model with the exception of the C-2,6 where the errors appear to be underestimated by a factor of $\sqrt{2.23}$. The standard errors of the data for C-2,6 were scaled up to give χ_r^2=1 before the data were combined with the data for the other carbon sites. The fit of the entire population data to equation (86) gives an internal energy change ΔE of 6956 J/mol and an entropy change of -3.12 J/mol•K. The standard errors are 140 J/mol and 0.81 J/mol•K, respectively, with a covariance of 113.358. Again, these errors are highly correlated, so that at 300 K, the highest fast-exchange temperature studied, the ratio of conformer populations is 0.0422± 0.0018, representing an accuracy of 4%. A plot of the 95% confidence region for the change in

internal energy and change in entropy for the Helmholtz energy difference between the equatorial and axial forms of methylcyclohexane is shown in Figure 3.13. The standard errors define a probability distribution for the actual value of a fit parameter based on limited measurements of it. The ellipse shown encloses 95% of this distribution. Shoemaker and Garland [13] give a table for the change in the reduced chi-squared, χ_r^2, of the original fit for the 95% confidence region of the fit parameter as a function of the number of data points. This is an equivalent description of the confidence region in the fit parameter space. It is important to note that as the standard error of the fit decreases due to a larger sample of data points, more data points will necessarily lie outside the 95% confidence region of the fit, since the population standard deviation is not decreasing along with the standard error of the fit. This is reflected in Figure 3.12. Consider the one-dimensional case for the determination of the mean value of a Gaussian

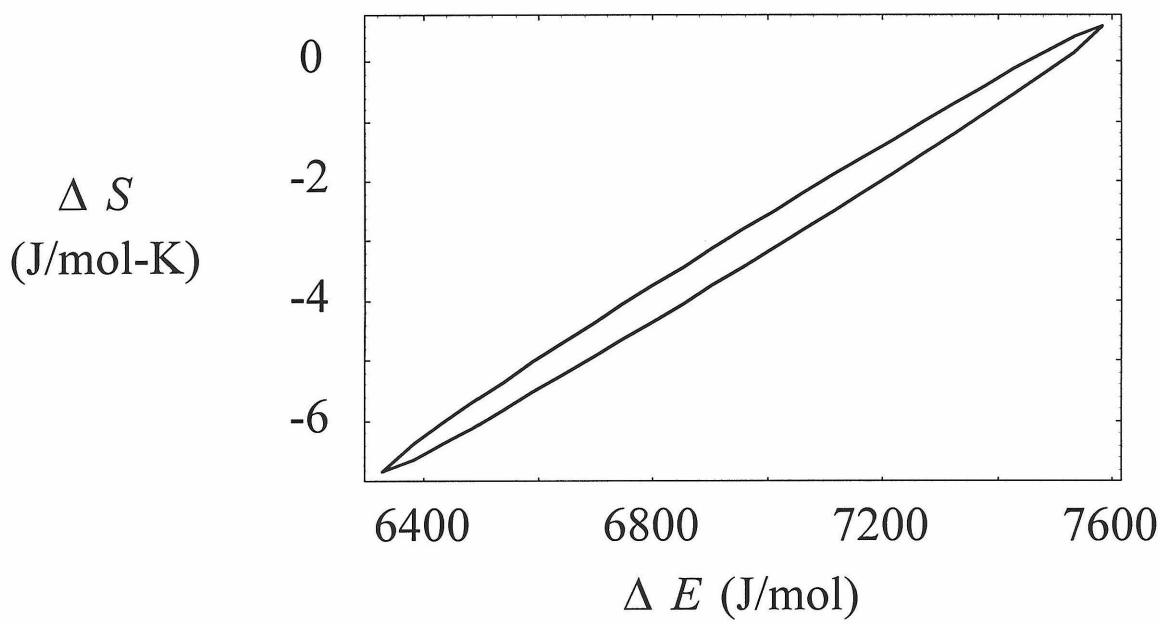

Figure 3.13. 95% confidence region for the Helmholtz energy difference between the equatorial and axial conformers of methylcyclohexane.

distribution with a standard deviation σ. Even though any one point has a finite probability of being x away from the mean value based on σ, when hundreds of samples from the distribution are plotted, the mean value can be determined with great accuracy, *i.e.*, the mean value has a small standard error. Again, the standard error of a fit parameter defines a probability distribution for the actual value of the fit parameter based on limited samplings of the variable.

Anet and Freedburg [2] report the free energy for the isomerization reaction of methylcyclohexane to be $\Delta E = 6317 \pm 837$ J/mol and $\Delta S = -6.7 \pm 5.4$ J/mol•K based on the work of Anet and Basus [1]. These values are consistent with, although less precise, than those presented in this work. The 95% confidence region for Anet and Basus's fit completely enclose the 95% confidence ellipse in Figure 3.13 and is over 4 times larger in

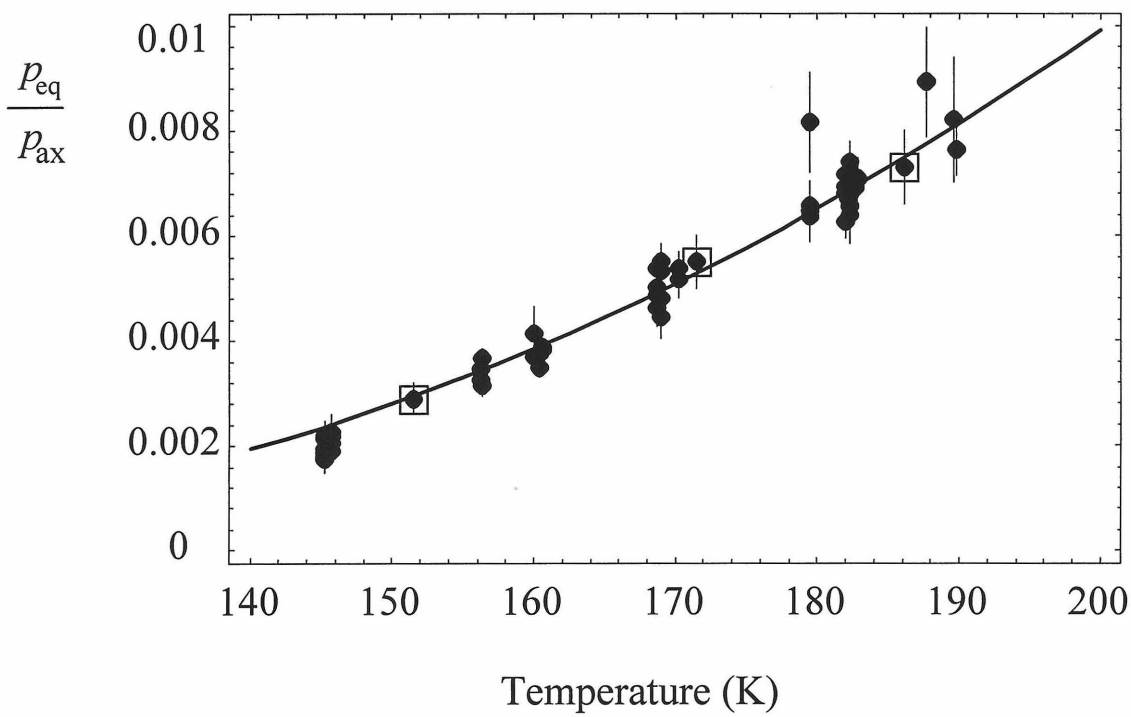

Figure 3.14. Ratio of conformer populations for methylcyclohexane. The boxed data points are from Basus [1,2].

area. The smaller error bars in the present work are a result of the larger number of data points measured. Basus's data are included on the plot of the equilibrium constant shown in Figure 3.14 for the sake of visual comparison with the data from Figure 3.12. Anet and Freedburg also report a free energy difference of $\Delta E = 7113 \pm 209$ J/mol and $\Delta S = +1.25 \pm 0.84$ J/mol•K for methylcyclohexane interconversion using the semi-empirical MM3 potential surface for molecular mechanics. This single-molecule gas-phase molecular free energy differs from the results presented here; neither the best fit value nor any of the 95% confidence region for the MM3 results overlap with the 95% confidence region of this work. This suggests that the use of free energies determined by single-molecule molecular mechanics calculations for a reaction in condensed phases is suspect. Other authors report free energy values from NMR line areas of methylcyclohexane [3,4] consistent with, although less precise than, the value reported here.

3.3.2 Intermediate Exchange

In the intermediate exchange region, the linewidth is a sensitive measure of the chemical exchange rate. The spectra were measured as a function of temperature in this region using the 10 mm dual tube assembly with the methylcyclohexane sample immersed in methanol. The spectra were fit using the *Mathematica* program previously described, although they were not corrected for line-shape distortions. Both the chemical shifts and linewidths are referenced to the sharp C-4 resonance.

3.3.2.1 Chemical Exchange Rates

A *Mathematica* program was written to extract the exchange rates from the linewidths of the spectra in intermediate exchange given a two-site exchange model. In this model, based on the traditional theory, the forward and backward rates are related by the measured slow-exchange free energy and the temperature-dependent chemical shifts

for the sites are extrapolated from slow exchange. A log plot of the exchange rate versus 1/T is shown in Figure 3.15. A fit to the Arrhenius form,

$$k_f = \nu \exp\left(-\frac{\Delta E^{\ddagger} - T\Delta S^{\ddagger}}{RT}\right), \tag{87}$$

gives $\nu = 1.09\times10^{11}$/s, $\Delta E^{\ddagger} = 49964$ J/mol and $\Delta S^{\ddagger} = 34.73$ J/mol•K, where $\Delta E^{\ddagger}$ and $\Delta S^{\ddagger}$ are the differences in energy and entropy, respectively, between the transition state and the major conformer. To achieve a satisfactory fit to this form, data between 220 K and 240 K, where the linewidths are greatest, were excluded. A plot of all the linewidths for the methylcyclohexane carbon sites with the fit parameters for the rates is shown in Figure 3.16. The two-site model for the traditional theory, in conjunction with the Arrhenius form described, misses the maximum broadening by up to 5 Hz for some

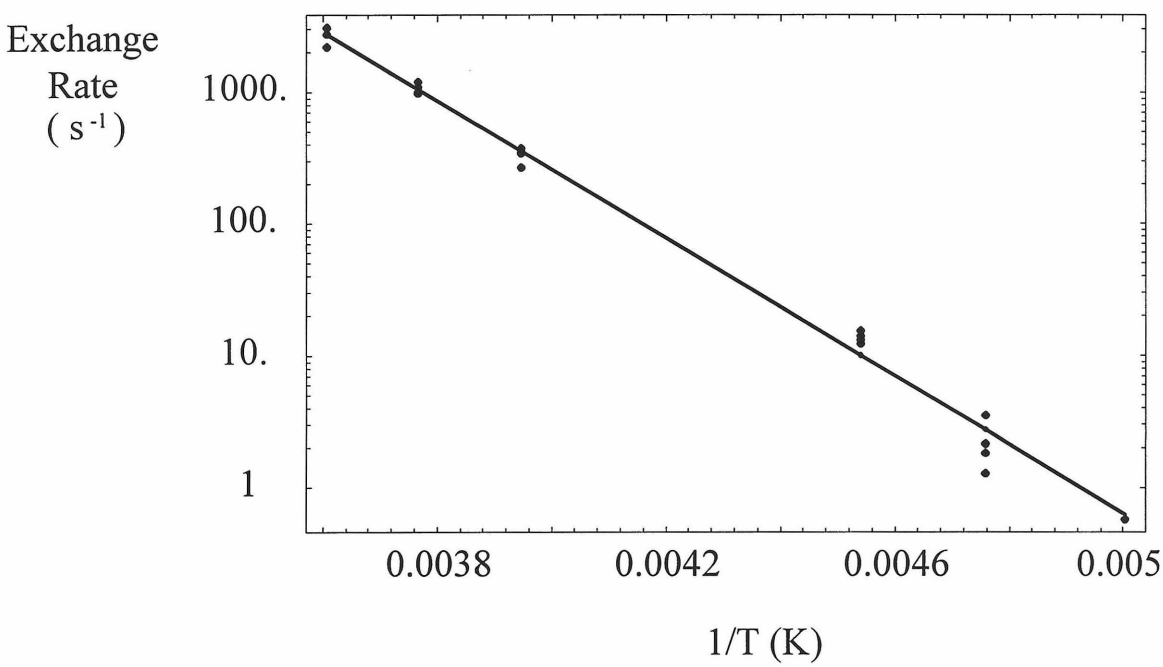

Figure 3.15. Log plot of exchange rate against inverse temperature. The fit to an Arrhenius rate is shown.

carbon sites, but in the absence of independent information on the rate as a function of temperature, it is not strictly possible to conclude whether the lineshape theory or the rate theory is unsatisfactory in the intermediate region.

3.3.3 Fast Exchange

3.3.3.1 Fast-Exchange Averages of Chemical Shifts

The temperature was again measured using the 10 mm dual NMR tube assembly and the methanol chemical shift thermometer described in Section 3.2.3. The chemical shifts and standard errors in the fast-exchange region were determined using the non-linear least-squares program described in Section 3.3.1. These data will be presented in Section 3.4, where the theories for chemical exchange will be critically examined.

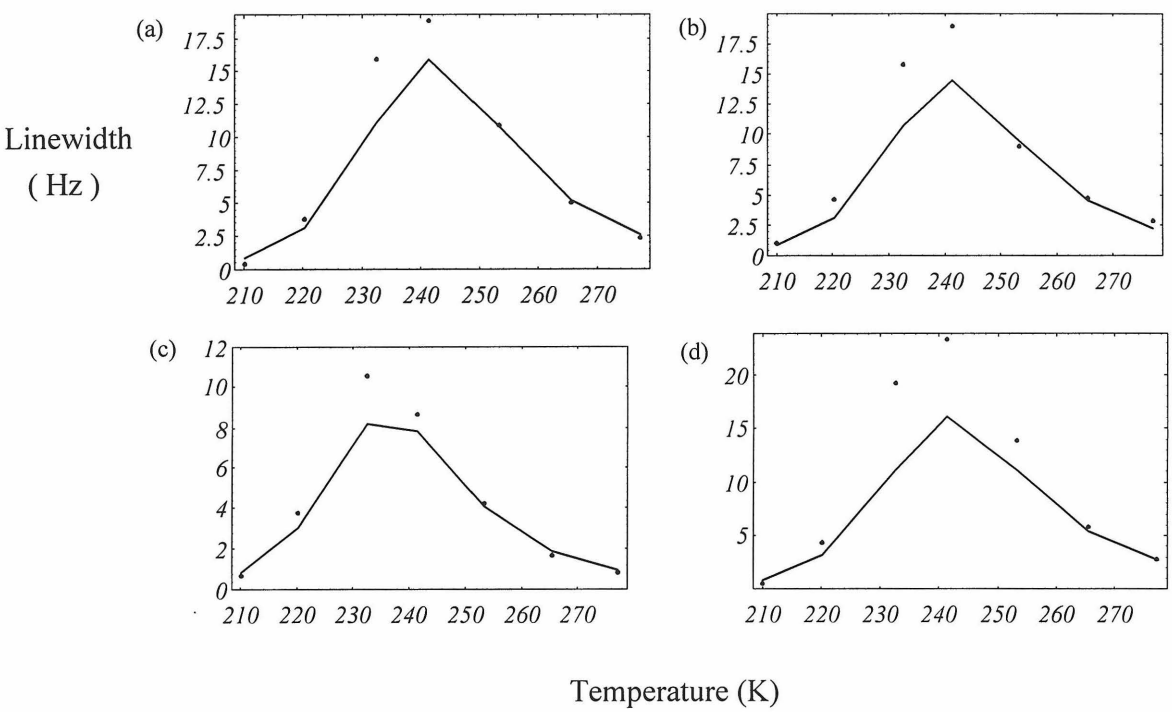

Figure 3.16. Linewidth versus temperature for the carbon sites in methylcyclohexane. The data are given by the points and the lines are the predictions of the traditional theory. (a) C-Me. (b) C-1. (c) C-2,6. (d) C-3,5.

3.4 A Critical Test of Theories for Chemical Exchange

3.4.1 Fast-exchange Deviations from the Traditional Theory

Given the measured slow-exchange parameters, a comparison can now be made between the predictions of the traditional theory and the observed fast-exchange line positions. These comparisons are shown in Figure 3.17, where the shaded region corresponds to 95% confidence limits extracted from the standard errors in slow exchange. The region represents the error range arising from the fit to six parameters, two for the Helmholtz energy, obtained from the slow-exchange data, and four for the linear chemical shifts, taken together. There is only a 5% chance that a random sampling of the distribution of fit parameters with the given standard errors would give a single fast-exchange prediction outside of the error region. The fit to the traditional theory is unsatisfactory for all sites, except possibly C-1, if considered separately. More quantitative statistical arguments are given subsequently for a global fitting procedure. Importantly, there is a lack of consistency between the observed fast-exchange averages and the traditional theory. This is apparent when the observed fast-exchange averages are used to predict the equilibrium constant for the isomerization reaction using the traditional theory and the extrapolated conformer chemical shifts from slow exchange. The extracted equilibrium constants are shown in Figure 3.18. This same lack of consistency between carbon sites in the fast-exchange limit under the traditional theory is apparent in the data of Basus [1], but was not pursued. Given the small error ranges on the extracted equilibrium constants, it is clear that a model consisting of the traditional theory and linear chemical shifts extrapolated from the slow-exchange region can never fit the fast-exchange averages for all four sites simultaneously.

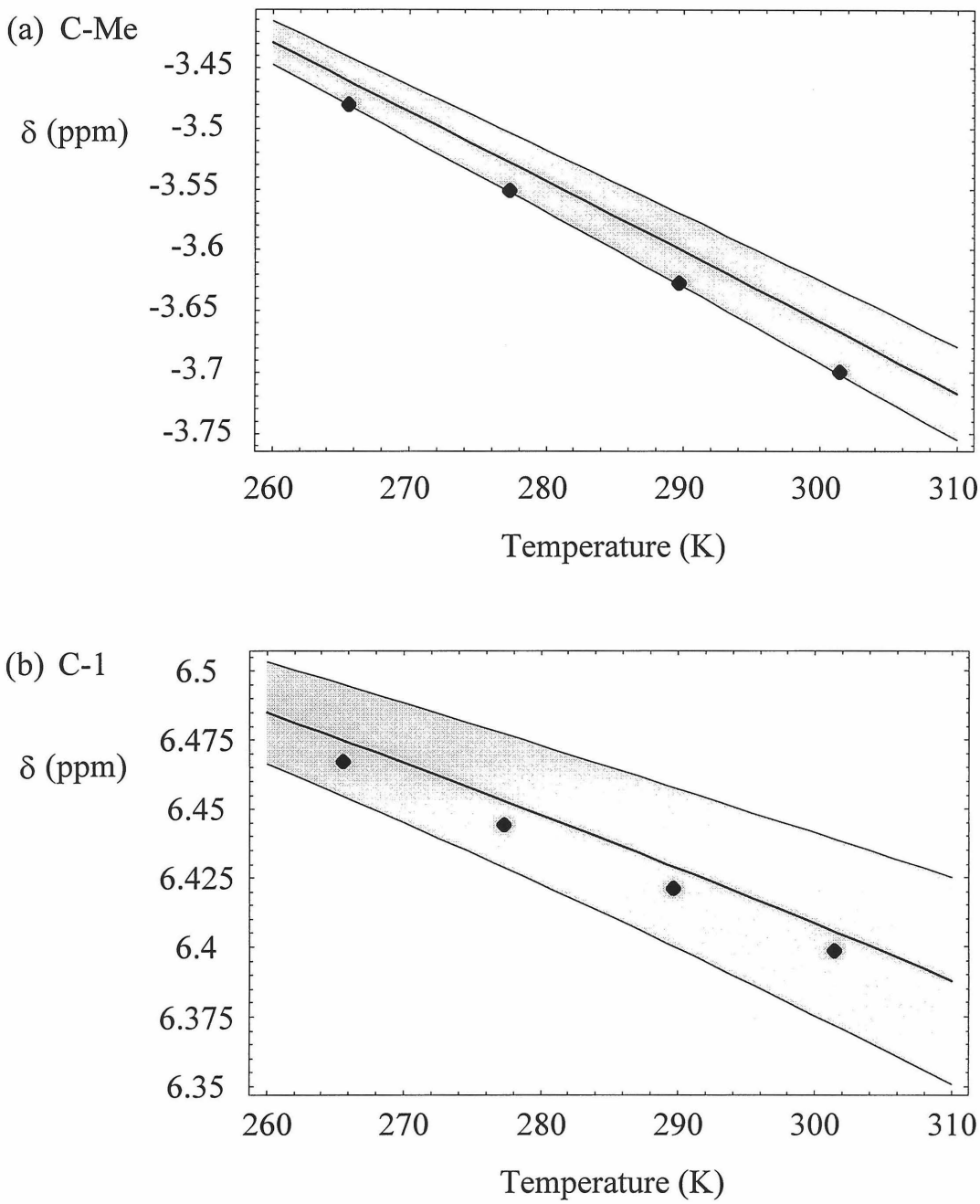

Figure 3.17. Predictions of the traditional theory for fast-exchange chemical shifts based on the parameters measured in slow exchange. The chemical shifts are measured relative to the C_4 chemical shift. The 95% confidence regions (for six variables taken together) are shown as the shaded areas. (a) C-Me. (b) C-1.

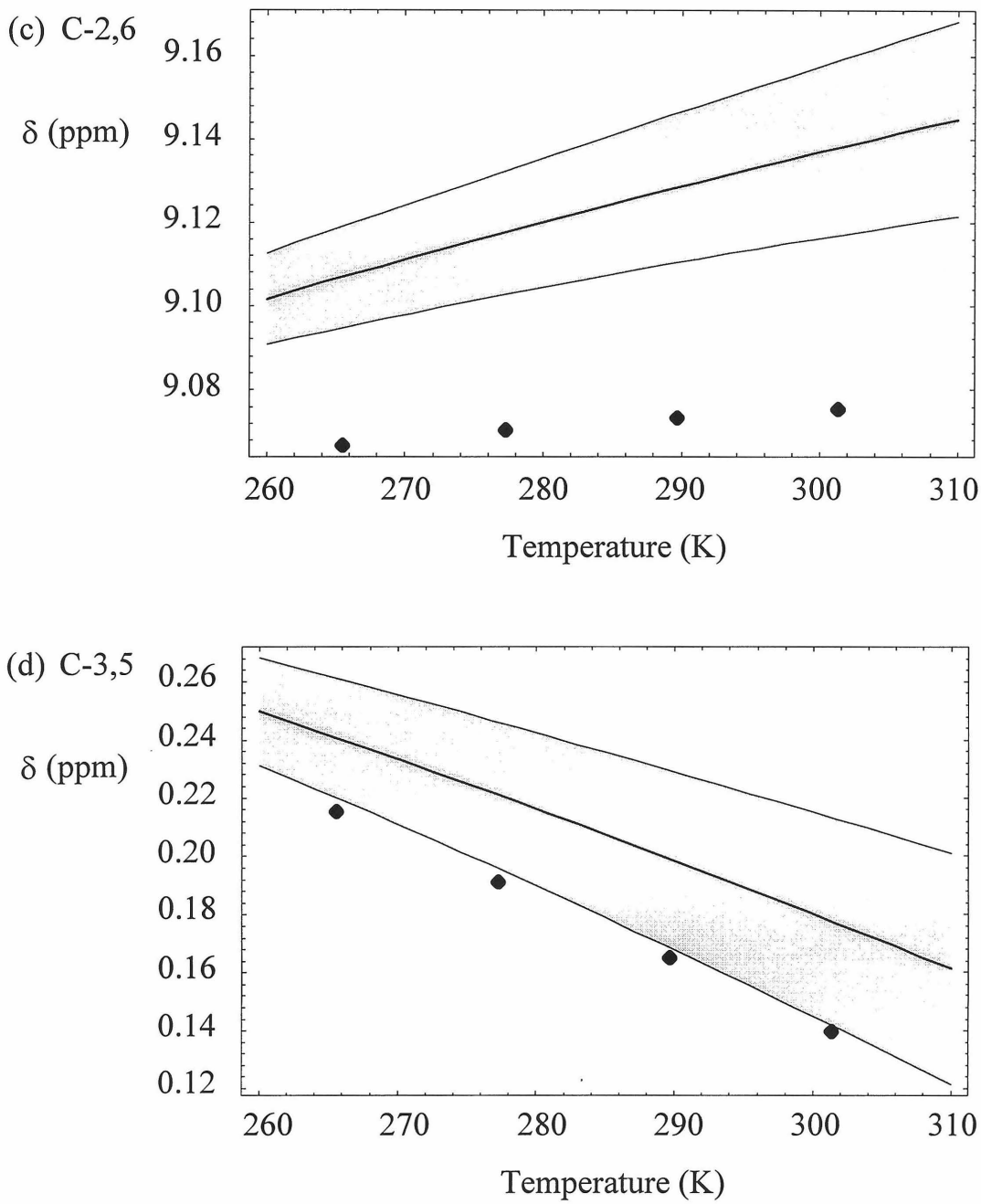

Figure 3.17 (continued). Predictions of the traditional theory for fast-exchange chemical shifts based on the parameters measured in slow exchange. The 95% confidence regions (for six variables taken together) are shown as the shaded areas. (c) C-2,6. (d) C-3,5.

3.4.2 Global Fits to the Traditional Theory

The discrepant equilibrium constants and poor consistency between slow and fast exchange for the carbon sites treated separately indicates that the traditional theory fails. This failure is better quantitated with a global fit including all sites and slow and fast-exchange data together. For a global fit, a χ_r^2 of 1 indicates a fit between the model and experimental data with errors representative of the scatter in the experimental data. A χ_r^2 greater than 1 indicates that the observed deviations from the model are inconsistent with the experimental errors. The significance of χ_r^2 greater than 1 depends on the number of experimental data points and the number of fit parameters. For large numbers of data points, even small deviations of χ_r^2 from 1 indicate low confidence for the model. When

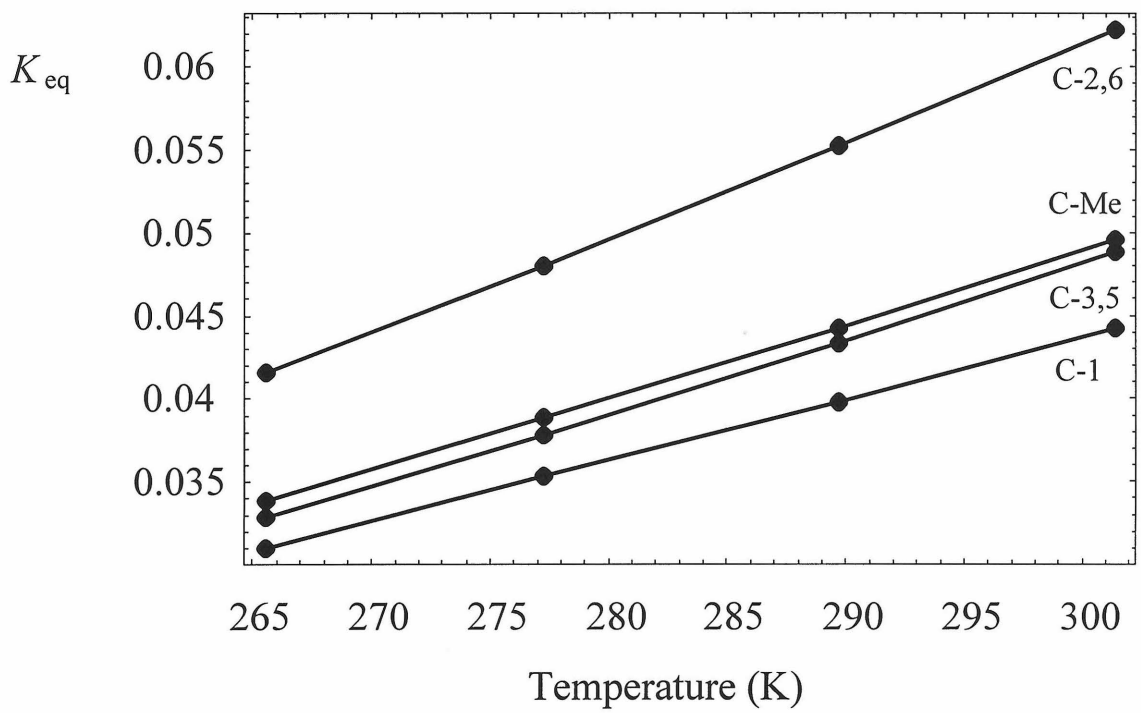

Figure 3.18. The predicted equilibrium constant for the isomerization reaction of methylcyclohexane based on fast-exchange averages, the measured slow-exchange chemical shifts and the traditional theory. The error bars on the data are too small to be seen on this scale but are on the order of 0.5% of the equilibrium constant.

the number of data points in the fit is 120, for example, the 95% confidence region excludes fit parameters that have a χ_r^2 greater than 1.22 [13]. For the global fits presented here, 225 data points are included: 57 for the slow-exchange equilibrium constants, 16 for the fast-exchange averages, and 152 total for the slow-exchange chemical shifts of the major and minor conformers. The standard errors of the data are those determined as described in earlier sections.

Several models are presented below for global fits of the traditional theory to the experimental data. These models have varying constraints on the temperature dependence of the chemical shift and Helmholtz energy.

3.4.2.1 Linear Temperature Dependence of the Chemical Shifts and Cubic Temperature Dependence of the Free Energy Difference

As has already been discussed in Section 3.4.1, there is no value for the equilibrium constant in the fast-exchange region that is consistent with the fast-exchange line positions and linear chemical shifts using the traditional theory, even for models of the Helmholtz energy difference with linear, quadratic, and cubic terms allowed in the temperature dependence. The χ_r^2 for the global fit of such a model to the experimental data is 36, indicating a completely inadequate fit.

3.4.2.2 Cubic Temperature Dependence of the Chemical Shifts and Cubic Temperature Dependence of the Free Energy Difference

For models of the chemical shifts and Helmholtz energy difference with linear, quadratic, and cubic terms allowed in the temperature dependencies, the best fit of the traditional theory to the experimental data has a χ_r^2 of 1.25. This value falls outside of the 95% confidence region for a fit that has 189 data points (225 points minus the 36 fit parameters). For this fit, the chemical shifts of the major conformers have an additional nonlinear temperature dependence of 3-12 Hz per 100 K while the minor conformers have an additional nonlinear temperature dependence of 20-60 Hz per 100 K. This model

questions one of the basic assumptions of this work: the linear temperature dependence of the ^{13}C chemical shifts. The corresponding chemical shifts of the model compounds *trans*-1,4-dimethylcyclohexane and *cis*-1,4-dimethylcyclohexane, however, are far more linear in temperature over their entire measured region (220 K to 370 K for the *trans* compound). Given the extreme similarity of methylcyclohexane to the model compounds it is unlikely that such large nonlinear temperature dependencies would exist for methylcyclohexane. Even ignoring the implausibility of such temperature dependence of the chemical shifts, the χ_r^2 of 1.25 indicates that this model does not adequately fit the experimental data, rigorously excluding the traditional theory.

3.4.3 Global Fit to the Exchange-Shift Theory

The exchange-shift theory predicts that the chemical shift in fast exchange should deviate from the traditional theory by a population-weighted sum of exchange shifts for each rovibrational state within the conformer manifolds. In order to make a simple phenomenological fit incorporating such an effect, it is assumed that the shift can be approximated by a linear function in the fast-exchange region. This function will depend on the carbon site being considered, however, due to the different chemical shifts at each site. This model fits the fast-exchange data as a sum of the traditional theory plus a linear offset and gives an excellent fit to the data with a χ_r^2 of 1.06. Thus it is possible to reconcile all of the data with a linear dependence of the free energy and conformer shifts on temperature. The fast-exchange data are shown in Figure 3.19. with the best fit to this model. The best-fit value for the linear free energy is $\Delta E = 7027.39$ J/mol and $\Delta S = -2.71$ J/mol•K and the best-fit parameters for the exchange and chemical shifts are given in Table 3.3. While a microscopic explanation of these fit parameters along the lines of Chapter 2 would involve modeling rovibrational rates and chemical shifts along the reaction coordinate, it is gratifying from the viewpoint of parsimony that the exchange-shift hypothesis requires only two new parameters per site, while the traditional

Table 3.3. Best-fit parameters in the exchange-shift model for the temperature dependence of the exchange shift and chemical shifts of the equatorial (eq) and axial (ax) sites in methylcyclohexane. Slope has units of Hz/K and intercept has units of Hz.

	slope eq	intercept eq	slope ax	intercept ax	slope exch. shift	intercept exch. shift
C-Me	-0.47513	-287.73	-0.24348	-1095.75	-0.03882	8.27
C-1	0.00189	833.71	0.07756	158.21	0.01276	-4.17
C-2,6	0.26750	1087.09	0.19754	657.66	-0.07446	14.93
C-3.5	0.04618	39.86	-0.02021	-706.92	-0.03444	6.28

theory fails even when four parameters per site are added as was done in considering up to cubic terms in temperature for the chemical shift and free energy.

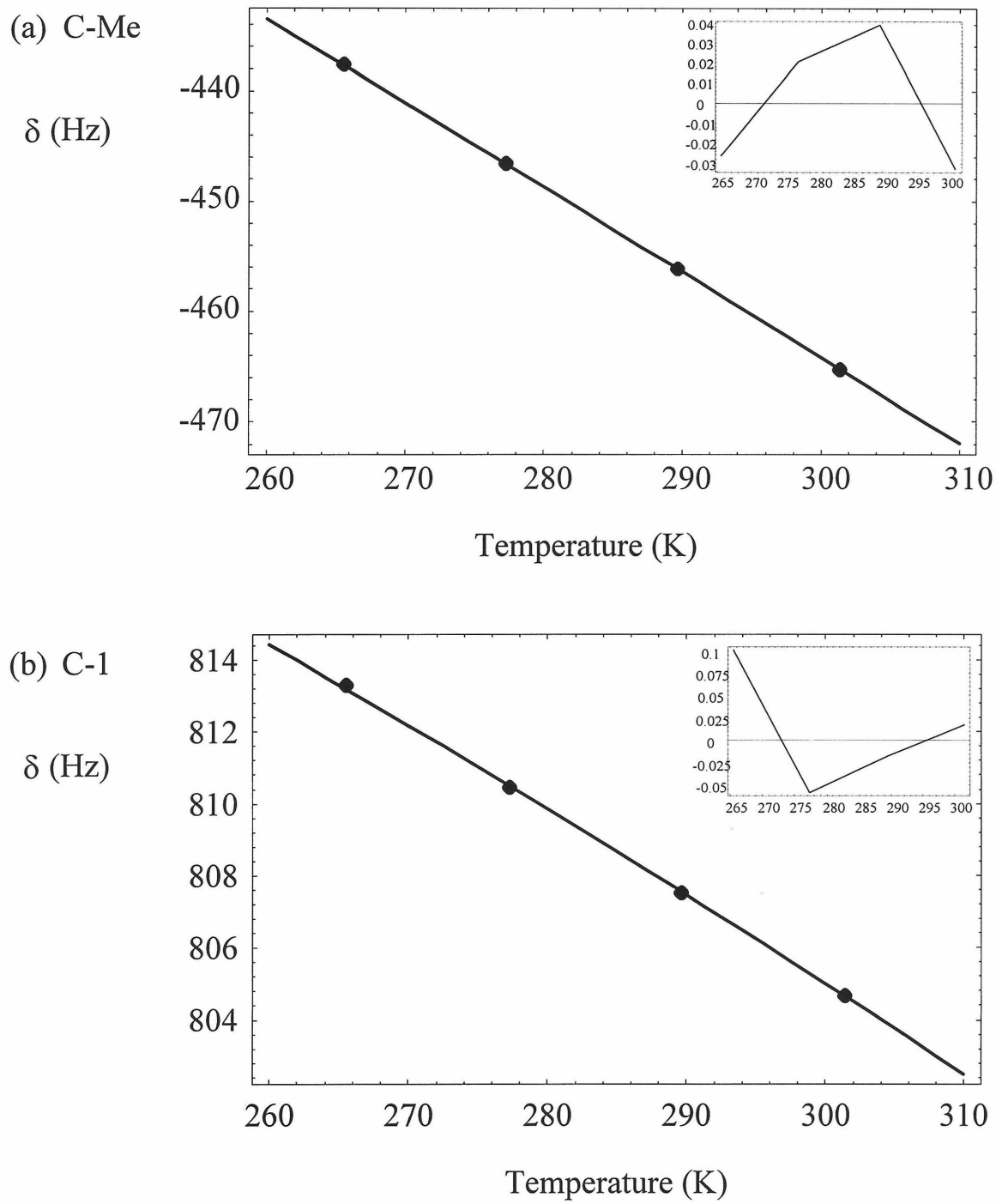

Figure 3.19. Best fit to the fast-exchange region for the exchange-shift theory. (a) C-Me. (b) C-1. Shifts are measured relative to C-4 and the inset shows the residuals.

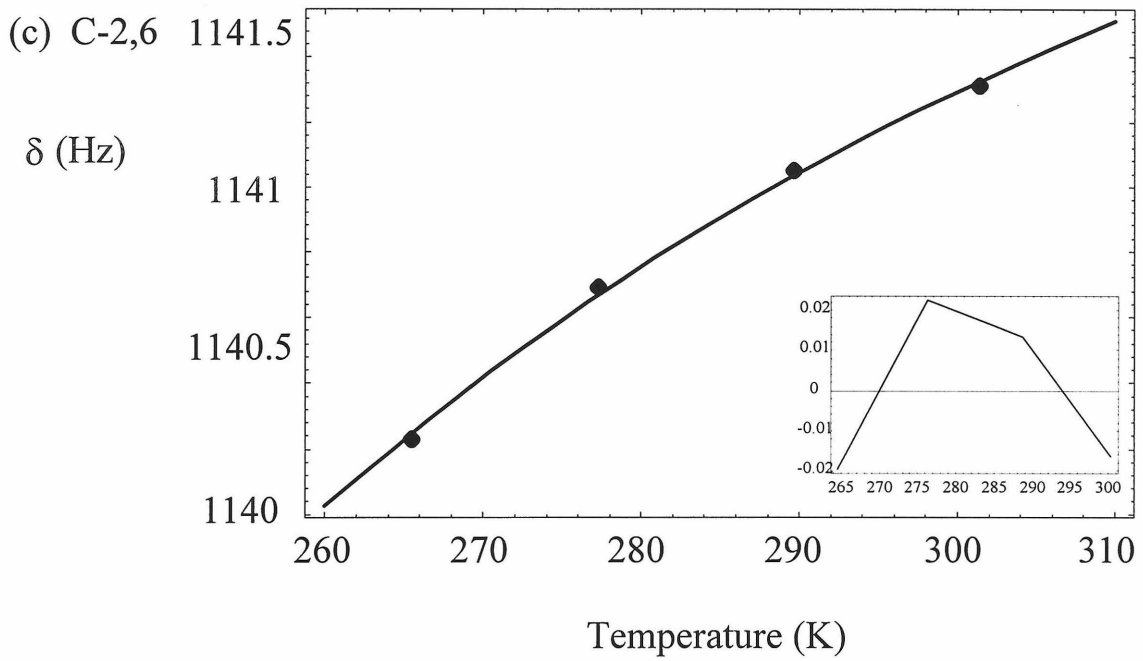

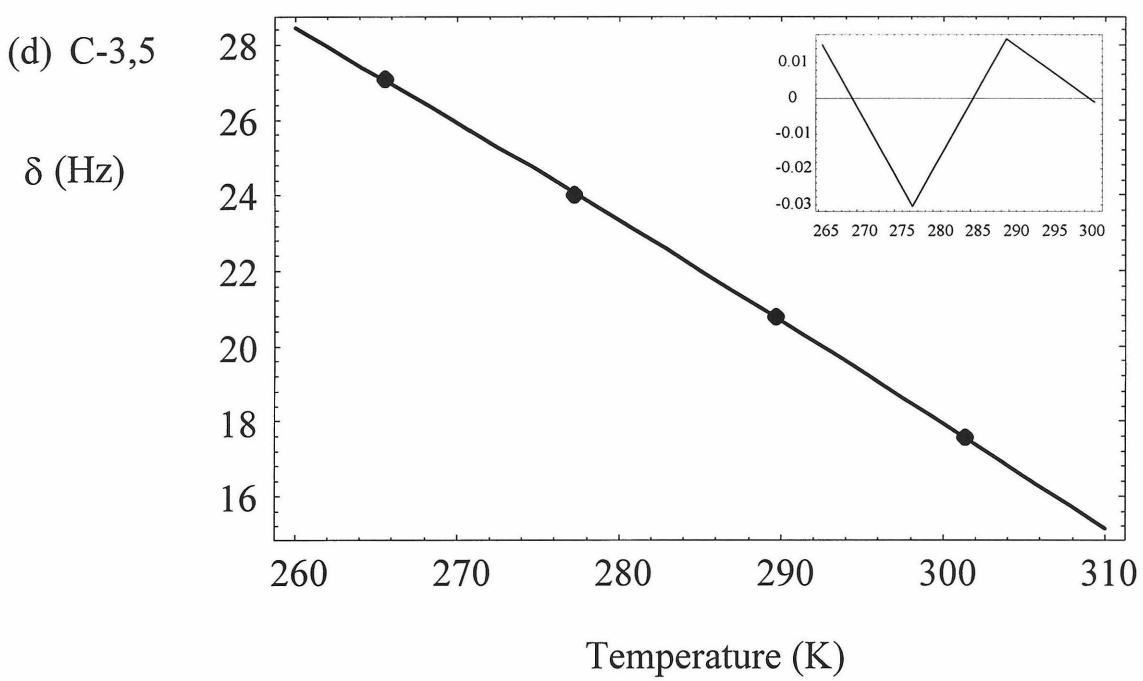

Figure 3.19 (continued). Best fit to the fast-exchange region for the exchange-shift theory. (c) C-2,6. (d) C-3,5.

3.5 Conclusions and Future Directions

The global fit of the traditional theory to the chemical exchange data on methylcyclohexane rules out the traditional theory with plausible assumptions on the temperature dependence of the chemical shift and free energy. Although having adjustable parameters about which no information is available from slow exchange, the model in which additional shifts linear in temperature turn on in fast exchange provides excellent agreement with the observed experimental data for methylcyclohexane. The exchange-shift theory provides an explanation for such shifts.

A more detailed modeling of the exchange shift should now be undertaken. Such a model could involve a slowly changing chemical shift as a function of spatial state among the bottom of the states of the conformer manifold with rapidly changing chemical shift as the transition state is approached so that the exchange shift does not become appreciable until fast exchange is reached. This information could be calculated from *ab initio* theory and thus need not involve free parameters. By comparison with strained ring systems such as cyclopropane [14], where the chemical shift is downfield of TMS, it is currently assumed that the transition state chemical shift is less than that of both the major and minor conformers of methylcyclohexane. This is consistent with the observed sign of the deviation from the traditional theory. The more difficult problem is that a microscopic model would require a plethora of rovibrational rates between quantized states near the transition state. Neither theory nor experiments provide much help in constraining these parameters in solution.

Finally, the validity of the traditional theory and exchange-shift theory for chemical exchange must be reexamined in additional experimental studies. Conclusions based on kinetic and thermodynamic properties extracted through the use of the traditional theory must also be appropriately reconsidered. The exchange-shift theory suggests a previously unsuspected entanglement of dynamic processes in the

interpretation of line positions. A long range goal would be the ability to combine dynamic calculations of molecular motion with *ab initio* NMR parameters and fit the full range of lineshapes observable. In this way, NMR could perhaps achieve the accuracy as a molecular probe that has prematurely been attributed to it.

3.6 References

[1] V.J. Basus "*A High Field Fourier Transform Nuclear Magnetic Resonance Study of Conformational Processes in Cyclohexane, Methylcyclohexane and Cyclooctane*" Ph.D. Thesis, Department of Chemistry, UCLA (1975).

[2] F.A.L. Anet and D.I. Freedberg "*Traditional Averaging of NMR Parameters in the Fast Exchange Limit is Valid!*" Chemical Physics Letters **208**(3, 4): 187-192 (1993).

[3] H. Booth and J.R. Everett "*Conformational Free Energy Difference of the Methyl Group in Methylcyclohexane: An Accurate Determination by the Direct, Low-Temperature Nuclear Magnetic Resonance Method*" Journal of the Chemical Society Chemical Communications : 278-279 (1976).

[4] H. Booth "*The Experimental Determination of the Conformational Free Energy, Enthalpy, and Entropy Differences for Alkyl Groups in Alkylcyclohexanes by Low Temperature Carbon-13 Magnetic Resonance Spectroscopy*" Journal of the Chemical Society Perkins Transactions II : 255-259 (1980).

[5] A.L. Van Geet "*Calibration of the Methanol and Glycol Nuclear Magnetic Resonance Thermometers with a Static Thermistor Probe*" Analytical Chemistry **40**(14): 2227-2229 (1968).

[6] A.L. Van Geet "*Calibration of Methanol Nuclear Magnetic Resonance Thermometer at Low Temperature*" Analytical Chemistry **42**(6): 679-680 (1970).

[7] D.S. Railford, C.L. Fisk and E.D. Becker "*Calibration of Methanol and Ethylene Glycol Nuclear Magnetic Resonance Thermometers*" Analytical Chemistry **51**(12): 2050-2051 (1979).

[8] D.M. Doddrell, D.T. Pegg and M.R. Bendall "*Distortionless Enhancement of NMR Signals by Polarization Transfer*" Journal of Magnetic Resonance **48**: 323-327 (1982).

[9] A.J. Shaka, J. Keeler and R. Freeman "*Evaluation of a New Broadband Decoupling Sequence: Waltz-16*" Journal of Magnetic Resonance **53**: 313-340 (1983).

[10] A.J. Shaka and J. Keeler "*Broadband Spin Decoupling in Isotropic Liquids*" Progress in NMR Spectroscopy **19**: 47-129 (1987).

[11] P. Bevington, R. Data Reduction and Error Analysis for the Physical Sciences New York, McGraw-Hill Book Company (1969).

[12] G.A. Morris "*Compensation of Instrumental Imperfections by Deconvolution Using an Internal Reference Signal*" Journal of Magnetic Resonance **80**: 547-552 (1988).

[13] D.P. Shoemaker, C.W. Garland and J.W. Nibler Experiments in Physical Chemistry New York, McGraw-Hill (1989).

[14] E.D. Becker High Resolution NMR Orlando, Academic Press (1980).

Appendix A: The Imaginary Component of the Lorentzian Spectral Density

The one-sided Fourier transforms of equation (45) lead, in general, to complex-valued spectral densities

$$\begin{aligned}\gamma^{+}(\omega) &= J(\omega) + i\Delta(\omega),\\ \gamma^{-}(\omega) &= J(\omega) - i\Delta(\omega),\end{aligned} \tag{88}$$

where J is the real part of the spectral density and Δ is the imaginary part. J and Δ are related by a Hilbert transform,

$$\Delta(\omega) = \frac{1}{\pi}\mathcal{P}\int_{-\infty}^{\infty} d\omega' \frac{J(\omega')}{\omega' - \omega}\ , \tag{89}$$

where $\mathcal{P}$ indicates that the principle value integral is to be taken.

In this appendix, the imaginary component of the Boltzmann weighted Lorentzian spectral density,

$$J(\omega) = \begin{cases} \dfrac{2\tau_c \langle V^2 \rangle}{1+\tau_c^2\omega^2} & \omega < 0 \\ \dfrac{2\tau_c \langle V^2 \rangle}{1+\tau_c^2\omega^2}\exp(-\beta\omega) & \omega > 0, \end{cases} \tag{90}$$

is calculated analytically by solving the Hilbert transform.

Consider first the case when ω is positive,

$$\Delta(\omega) = \frac{1}{\pi}\mathrm{Lim}_{a\to\infty,\varepsilon\to 0}\left\{\int_{-a}^{0} d\omega' \frac{J(\omega')}{\omega' - \omega} + \int_{0}^{\omega-\varepsilon} d\omega' \frac{J(\omega')}{\omega' - \omega} + \int_{\omega+\varepsilon}^{a} d\omega' \frac{J(\omega')}{\omega' - \omega}\right\}. \tag{91}$$

Using *Mathematica* [1] to evaluate the definite integrals and considering each integral in turn,

$$\frac{1}{\pi}\int_{-a}^{0} d\omega' \frac{J(\omega')}{\omega'-\omega} = \frac{\tau_c\langle V^2\rangle}{\pi\left(1+\tau_c{}^2\omega^2\right)}\Big\{ -2\tau_c\omega\arctan(a\tau_c) + \log\left(1+a^2\tau_c{}^2\right) - 2\log(-a-\omega) + 2\log(-\omega) \Big\}, \tag{92}$$

$$\begin{aligned}\frac{1}{\pi}\int_{0}^{\omega-\varepsilon} d\omega' \frac{J(\omega')}{\omega'-\omega} = \frac{\tau_c\langle V^2\rangle}{\pi\left(1+\tau_c{}^2\omega^2\right)}\Big\{ & \exp\left(\tfrac{i\beta}{\tau_c}\right)\left(1+i\tau_c\omega\right)\mathrm{Ei}\left(-\tfrac{i\beta}{\tau_c}\right) + \\ & \exp\left(-\tfrac{i\beta}{\tau_c}\right)\left(1-i\tau_c\omega\right)\mathrm{Ei}\left(\tfrac{i\beta}{\tau_c}\right) - \\ & \exp\left(\tfrac{i\beta}{\tau_c}\right)\left(1+i\tau_c\omega\right)\mathrm{Ei}\left(\beta\left(\varepsilon-\tfrac{i}{\tau_c}-\omega\right)\right) - \\ & \exp\left(-\tfrac{i\beta}{\tau_c}\right)\left(1-i\tau_c\omega\right)\mathrm{Ei}\left(\beta\left(\varepsilon+\tfrac{i}{\tau_c}-\omega\right)\right) + \\ & 2\exp(-\beta\omega)\left(\mathrm{Ei}(\beta\varepsilon)-\mathrm{Ei}(\beta\omega)\right)\Big\},\end{aligned} \tag{93}$$

and

$$\begin{aligned}\frac{1}{\pi}\int_{\omega+\varepsilon}^{a} d\omega' \frac{J(\omega')}{\omega'-\omega} = \frac{\tau_c\langle V^2\rangle}{\pi\left(1+\tau_c{}^2\omega^2\right)}\Big\{ & -\exp\left(\tfrac{i\beta}{\tau_c}\right)\left(1+i\tau_c\omega\right)\mathrm{Ei}\left(\beta\left(-\tfrac{i}{\tau_c}-a\right)\right) - \\ & \exp\left(-\tfrac{i\beta}{\tau_c}\right)\left(1-i\tau_c\omega\right)\mathrm{Ei}\left(\beta\left(\tfrac{i}{\tau_c}-a\right)\right) + \\ & \exp\left(\tfrac{i\beta}{\tau_c}\right)\left(1+i\tau_c\omega\right)\mathrm{Ei}\left(\beta\left(-\tfrac{i}{\tau_c}-\varepsilon-\omega\right)\right) + \\ & \exp\left(-\tfrac{i\beta}{\tau_c}\right)\left(1-i\tau_c\omega\right)\mathrm{Ei}\left(\beta\left(\tfrac{i}{\tau_c}-\varepsilon-\omega\right)\right) + \\ & 2\exp(-\beta\omega)\left(\mathrm{Ei}(\beta(\omega-a))-\mathrm{Ei}(-\beta\varepsilon)\right)\Big\},\end{aligned} \tag{94}$$

where Ei(x) is the exponential integral function [1,2],

$$\mathrm{Ei}(x) = -\mathcal{P}\int_{-x}^{\infty} dt \frac{\exp(-t)}{t}. \tag{95}$$

Noting the following limits,

$$\lim_{a\to\infty} 2\tau_c\omega\arctan(a\tau_c) = \pi\tau_c\omega, \tag{96}$$

$$\begin{aligned}\lim_{a\to\infty}\ & \log\left(1+a^2\tau_c{}^2\right)-2\log(-a-\omega)+2\log(-\omega)\\ &=\lim_{a\to\infty}\log\left(a^2\right)+\log\left(\tau_c{}^2\right)-2\pi i-\log(a^2)+2\pi i+\log\left(\omega^2\right)\\ &=\log\left(\tau_c{}^2\right)+\log\left(\omega^2\right)\\ &=\log\left(\tau_c{}^2\omega^2\right),\end{aligned} \tag{97}$$

$$\lim_{\varepsilon\to 0}\ \mathrm{Ei}(\varepsilon)-\mathrm{Ei}(-\varepsilon)=0, \tag{98}$$

$$\lim_{a\to\infty}\ \mathrm{Ei}(-a+ib)=i\pi \qquad b>0, \tag{99}$$

$$\lim_{a\to\infty}\ \mathrm{Ei}(-a-ib)=-i\pi \qquad b>0, \tag{100}$$

$$\lim_{a\to\infty}\ \mathrm{Ei}(-a)=0, \tag{101}$$

equation (91) can be written as

$$\begin{aligned}\Delta(\omega)=\frac{\tau_c\left\langle V^2\right\rangle}{\pi\left(1+\tau_c^2\omega^2\right)}\Big\{&\left[-i\pi-\pi\tau_c\omega+\mathrm{Ei}\left(\tfrac{i\beta}{\tau_c}\right)-i\tau_c\omega\mathrm{Ei}\left(\tfrac{i\beta}{\tau_c}\right)\right]\exp\left(-\tfrac{i\beta}{\tau_c}\right)+\\ &\left[i\pi-\pi\tau_c\omega+\mathrm{Ei}\left(\tfrac{-i\beta}{\tau_c}\right)+i\tau_c\omega\,\mathrm{Ei}\left(\tfrac{-i\beta}{\tau_c}\right)\right]\exp\left(\tfrac{i\beta}{\tau_c}\right)+\\ &-\pi\tau_c\omega-2\exp(-\beta\omega)\mathrm{Ei}(\beta\omega)+\ln\left(\tau_c^2\omega^2\right)\Big\}.\end{aligned} \tag{102}$$

A similar calculation for $\omega<0$ yields the same result.

A.1 References

[1] S. Wolfram Mathematica: A System for Doing Mathematics by Computer Reading, Massachusetts, Addison-Wesley Publishing Company (1991).

[2] M. Abramowitz and I. Stegun, A. Handbook of Mathematical Functions New York, Dover Publications (1972).

Appendix B: Monte Carlo Simulations of Data Manipulation in NMR

B.1 Introduction

The interpretation of NMR spectra often relies upon the extraction of spectral parameters such as line position, width, shape and amplitude. In liquid-state NMR the lineshapes are ideally Lorentzian, although in nonisotropic samples they are more complicated but contain considerably more information on local chemical structure [1,2]. In the NMR literature, primary consideration is often given to increasing the signal-to-noise ratio (SNR) of a spectrum, both experimentally and through data manipulation, as a means to more accurately extract spectral parameters. However, increasing the SNR through post-experimental manipulation of the data does not necessarily increase the accuracy with which all parameters may be extracted. In this section, the effect of several common data manipulation techniques on the extraction of NMR spectral parameters from the processed frequency-domain spectra are examined using Monte Carlo simulation. It is shown that some of these, including the matched time-domain filter, do not decrease the standard error with which spectral parameters relevant to chemical exchange can be extracted.

B.2 Monte Carlo Simulation

The technique of Monte Carlo simulation can be used to determine the standard error of a fit parameter when a model for the signal and the noise are provided [3]. Although computationally intensive, this method is conceptually simple. The standard error of a measurement is a measure of the precision of a fit parameter for a given level of

noise in an experiment. Monte Carlo techniques are used to determine this precision by "repeating" the experiment multiple times and keeping track of the best fit parameters. The repetition in Monte Carlo simulations is not a repetition of the actual experiment, but corresponds to a resampling of the noise distribution to determine how the observed level of noise in an experiment affects the fit precision. A flow chart for Monte Carlo simulations is shown in Figure B.1. A least-squares fit of the experimental data to a model is performed to determine the experimental best fit parameters and fit residuals, which are used to characterize the noise. Typically, the model used for the noise distribution is a Gaussian distribution about zero with a given standard deviation. New "data" sets are generated as the sum of the experimental best fit model for the signal plus new noise randomly chosen from the noise distribution. These data sets are again fit to the model and the results stored in an array of simulated best fit parameters. For each fit parameter, the distribution of simulated best fit values is centered about the experimental best fit value. The standard deviation of this distribution is the standard error of the experimentally measured parameter. The larger the number of synthesized data sets analyzed, the more accurately the standard error of the parameters can be determined. If, in contrast, the actual experiment were repeated many times, the distribution of best fit results would have a width identical to that of the Monte Carlo simulations, but the fit parameter would be known to much higher precision than the standard deviation of this distribution. This improved knowledge of the parameter reflects the larger amount of experimental data acquired.

Below, the effect of data manipulation on the standard error associated with a fit variable is determined by manipulating the generated data sets and comparing the standard deviation in the subsequent fit parameter to the standard deviation of the parameter in the absence of data manipulation.

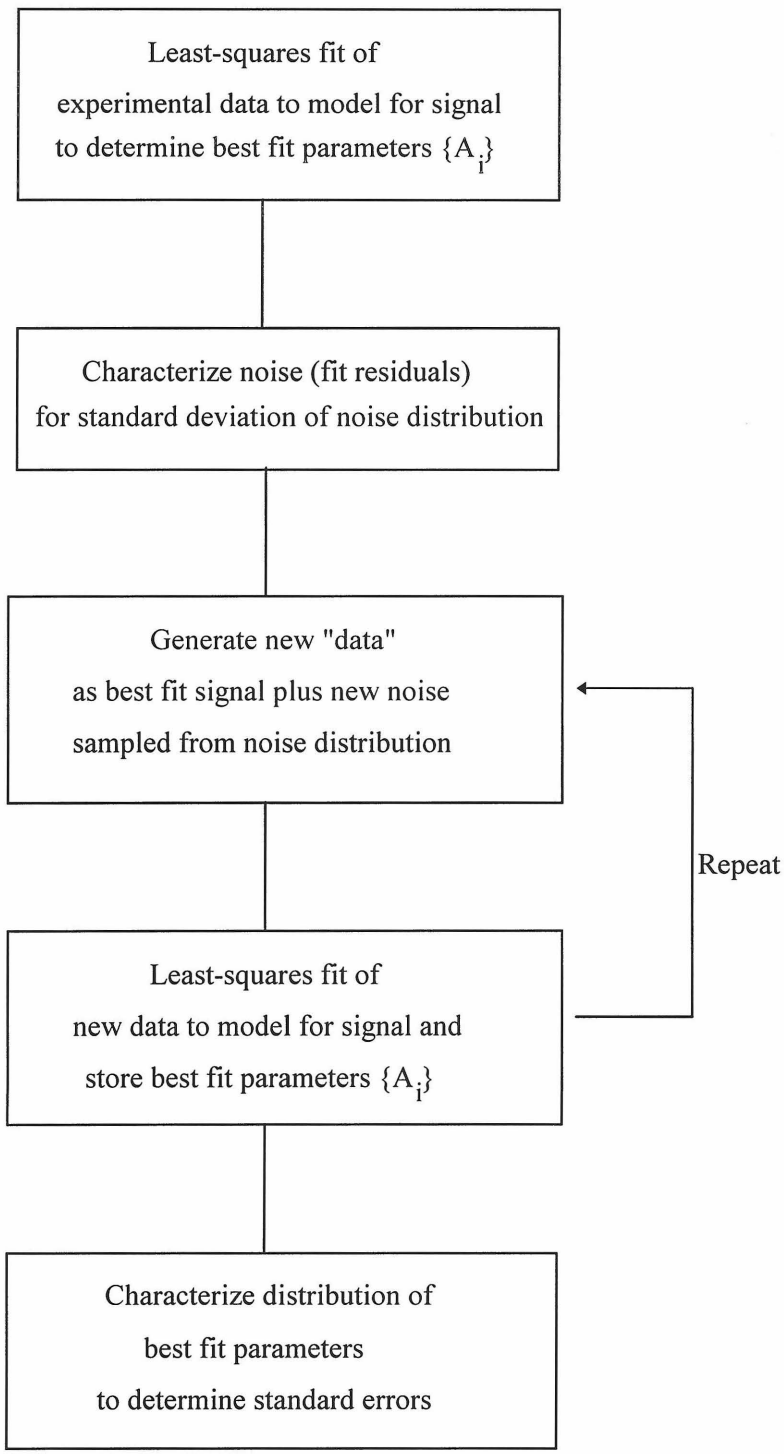

Figure B.1. Flow chart for Monte Carlo determination of standard errors

B.3 The Matched Exponential Filter

Perhaps the most common form of data manipulation in liquid-state NMR is the application of a matched exponential filter to the signal free induction decay (FID) [4,5]. The effect of a matched exponential filter is to increase the SNR in the processed spectrum through the suppression of noise in the tail of the FID where the signal has decayed to a level below that of the noise. To test the efficacy of the matched exponential filter, Monte Carlo simulations are performed in which the signal is modeled in the time domain as an exponentially decaying sinusoid with an amplitude of 1.8, frequency of 20 Hz., and decay constant of 2π (2 Hz. linewidth) and the noise is modeled as a random number chosen from a Gaussian distribution about zero with a standard deviation of 0.15. To see if a matched filter improves the standard error of the extracted spectral parameters in the frequency domain, multiple time-domain FIDs are generated with different noise randomly chosen from the noise distribution. Exponential filters of 0 Hz (no filter), 1 Hz and 2 Hz (matched filter) are applied to each signal, the data sets are zero filled once (see below), and their Fourier transforms are fit in the frequency domain as a Lorentzian with amplitude A, position ν and width (FWHM) $\Delta\nu$. The standard deviation in the set of fit values is shown in Table B.1. The standard errors in the fit parameters show no improvement with either exponential filter, if fact the errors become somewhat larger. While the Fourier transform of the filtered data sets have a better SNR than the unfiltered spectrum, this is deceptive. The exponential filter does not erase the noise, but correlates it in the frequency domain. While increasing the SNR in the frequency domain does improve the ratio of the peak height to the noise level, making it easier to spot a peak by eye, it does not improve the actual precision with which spectral parameters may be determined [4,6]. It should also be noted that when an exponential filter is used and the noise becomes correlated, the fit residuals can no longer be used directly as a measure of the noise distribution. To accurately use analytical forms for the standard error in terms

Table B.1. Best fit values for various time domain exponential filters to 100 simulated data sets.

	No Filter	1 Hz. Exp. Filter	2 Hz. Exp. Filter
Amplitude A	1.795	1.795	1.796
Standard Error in A	0.130	0.140	0.155
Line Position ν	20.004	20.011	20.019
Standard Error in ν	0.068	0.087	0.110
Linewidth $\Delta\nu$	1.992	2.993	3.998
Standard Error in $\Delta\nu$	0.198	0.243	0.328

of the covariance matrix [3,7,8] it is necessary for the residuals of the unmanipulated data to be used (with one zero fill allowed).

B.4 Zero Filling

When only the real part of an NMR spectrum is being fit, there is an advantage to zero filling the data set once before Fourier transformation [9]. In effect, zero filling takes the independent real and imaginary data and noise and combines them so that both parts of the spectrum contain all the information. After zero filling, the two parts are no longer independent and are exactly related by a Hilbert-transform. Monte Carlo simulations show that zero filling the data one time before Fourier transformation decreases the standard error in all spectral parameters by $\sqrt{2}$.

B.5 Length of Data Acquisition

It is a common observation in NMR that if one acquires the FID for too long after the signal has decayed, the quality of the spectrum is worse due to the additional noise that is acquired. While certainly the SNR has decreased, Monte Carlo simulations indicate that the standard errors in the fit parameters are unaffected by the length of data

acquisition (presuming the signal has decayed to near zero in all cases). This appears striking in the frequency domain, where the SNR is much worse with longer acquisition, while in the time domain this effect is obvious as the initial part of the FID remains the same while at longer times the signal contains only random noise centered about zero that does not influence the fitting significantly.

B.6 Reference Deconvolution

In reference deconvolution [10], a reference line within the spectrum is used to remove global broadening and asymmetric features, such as the effect of magnet inhomogeneity, from the experimental lines. In this procedure, a well-isolated, large SNR peak is first chosen as a reference peak, with the remainder of the spectrum nulled. A best-fit Lorentzian is then found by a least-squares fit to this experimental line with the line position, intensity and width as parameters. A time-domain correction function is produced by dividing the inverse Fourier transform (IFT) of this fit by the IFT of the reference peak. As the fit and experimental free induction decays (FID) have both real and imaginary components, the magnitude of the denominator is in practice always finite. The filter is then used to correct all the lines in the spectrum by multiplication with the experimental FID. This is equivalent to deconvoluting the reference lineshape from each line of interest.

In the case of inhomogeneously broadened NMR lines of different widths, Monte Carlo simulations show that the lineshape must first be corrected to accurately determine the ratio of the line areas. For real data, the reference-deconvolution filter can become quite large and uncertain near the end of the FID, so an exponential apodization is applied to all time-domain signals. For typical NMR parameters, the standard errors in the lineshape parameters become worse by approximately a factor of $\sqrt{2}$ with reference deconvolution.

B.7 References

[1] U. Haeberlen, Ed. High Resolution NMR in Solids. Selective Averaging in Advances in Magnetic Resonance, New York, Academic Press (1976).

[2] M. Mehring Principles of High Resolution NMR in Solids Berlin, Springer-Verlag (1983).

[3] W.H. Press, S.A. Teukolsky, W.T. Vetterling and B.P. Flannery Numerical Recipes in C: the Art of Scientific Computing Cambridge, Cambridge University Press (1992).

[4] R.R. Ernst "*Sensitivity Enhancement in Magnetic Resonance*" Advances in Magnetic Resonance **2**: 1-135 (1966).

[5] E.D. Becker, J.A. Ferretti and P.N. Gambhir "*Selection of Optimum Parameters for Pulse Fourier Transform Nuclear Magnetic Resonance*" Analytical Chemistry **51**(9): 1413-1420 (1979).

[6] A.G. Marshall and F.R. Verdun Fourier Transforms in NMR, Optical, and Mass Spectroscopy: A User's Handbook Amsterdam, Elsevier (1990).

[7] P. Bevington, R. Data Reduction and Error Analysis for the Physical Sciences New York, McGraw-Hill Book Company (1969).

[8] B. Roe, P. Probability and Statistics in Experimental Physics New York, Spinger-Verlag (1992).

[9] E. Bartholdi and R.R. Ernst "*Fourier Spectroscopy and the Causality Principle*" Journal of Magnetic Resonance **11**: 9-19 (1973).

[10] G.A. Morris "*Compensation of Instrumental Imperfections by Deconvolution Using an Internal Reference Signal*" Journal of Magnetic Resonance **80**: 547-552 (1988).